remote sensing

MDPI

Review

Exploring Marine Atmospheric Ducts: Current Sensing and Emerging Trends

Jin-Peng Zhang [1], Yu-Jing Li [1], Han-Jie Ji [2,*], Huai-Yun Peng [1], Xiang-Ming Guo [1] and Yu-Sheng Zhang [1]

[1] National Key Laboratory of Electromagnetic Wave Propagation, China Research Institute of Radiowave Propagation, Qingdao 266107, China; zhangjp@crirp.ac.cn (J.-P.Z.); liyujing@stu.xidian.edu.cn (Y.-J.L.); penghy@crirp.ac.cn (H.-Y.P.); guoxm@crirp.ac.cn (X.-M.G.); zhangys@crirp.ac.cn (Y.-S.Z.)
[2] School of Physics, Xidian University, Xi'an 710071, China
* Correspondence: jhjxd@stu.xidian.edu.cn

Highlights

What are the main findings?

- This study presents a comprehensive and well-structured review of atmospheric duct sensing methods, covering recent advances in contact measurement and indirect estimation approaches.
- Indirect estimation methods have emerged as mainstream, accounting for an increasingly significant proportion of current research.

What are the implications of the main findings?

- Deep learning-based atmospheric duct characterization techniques show great potential for typical remote sensing tasks.
- This review provides practical future prospects for atmospheric duct sensing research.

Abstract

Tropospheric refraction significantly impacts the propagation of ultrashort- and microwave-frequency radio waves over marine environments. Atmospheric ducting, the most common super-refractive structure, allows radio waves to travel over the horizon. This holds significant practical value for applications such as maritime communication, remote radar monitoring, and navigation systems. However, atmospheric ducts can also present challenges, especially under unstable meteorological conditions. Atmospheric ducts may cause signal attenuation and even severe interference. Therefore, the detection of atmospheric ducting phenomena is crucial for ensuring the reliability of maritime communication systems and the accuracy of radar monitoring. This paper provides a comprehensive and systematic review of the current state of research on atmospheric duct detection, presenting a detailed analysis of several key methodologies. These include direct measurement techniques, model estimation approaches, numerical forecasting methods, and remote sensing inversion techniques. Additionally, the paper offers an in-depth examination of the strengths and limitations of each method in practical applications, while also highlighting the ongoing challenges within the field. In conclusion, this work aims to provide theoretical foundations and practical guidance for the future development of atmospheric duct detection technologies, fostering further advancements in both theoretical research and technical applications in the field.

Keywords: atmospheric duct; sensing; radio wave propagation; status; emerging trends

Check for updates

Academic Editor: Yukiharu Hisaki

Received: 7 April 2026
Revised: 18 May 2026
Accepted: 21 May 2026
Published: 4 August 2026

Copyright: © 2026 by the authors. Licensee MDPI, Basel, Switzerland. This article is an open access article distributed under the terms and conditions of the Creative Commons Attribution (CC BY) license.

1. Introduction

The troposphere, as the primary sphere of human activities, serves as the operational environment for most EM wave systems. Understanding its impact on EM wave propagation is therefore critical for designing and evaluating radar, satellite, and electronic warfare systems [1]. Beyond absorption and scattering by gas molecules and aerosols, tropospheric effects predominantly manifest through refractive phenomena. Spatial variations in atmospheric refractivity alter EM wave trajectories and energy distribution. Notably, atmospheric ducts emerge when temperature inversions occur or humidity gradients steepen with altitude, creating distinct refractive layers. These structures are characterized by an extremely anomalous vertical decrease in atmospheric refractivity coupled with strong super-refraction, typically occurring within the troposphere—more specifically, in the atmospheric boundary layer. The defining feature of atmospheric ducts lies in their capacity to induce significantly enhanced refraction of EM waves compared to conventional propagation modes. This intensified refraction causes downward bending of waves with a curvature exceeding the Earth's surface curvature, effectively trapping them within a stratified atmospheric layer. Analogous to duct propagation in metallic structures, this phenomenon enables long-distance beyond-line-of-sight (BLOS) transmission of EM energy, particularly valuable for extending the effective range of communication and radar systems in the ultra-high-frequency (UHF)/microwave bands (see Figure 1) [2]. By leveraging atmospheric ducts, EM waves can overcome traditional horizon limitations, achieving BLOS communication, detection, and positioning capabilities—a transformative advancement for modern telecommunications, remote sensing, and military radar systems.

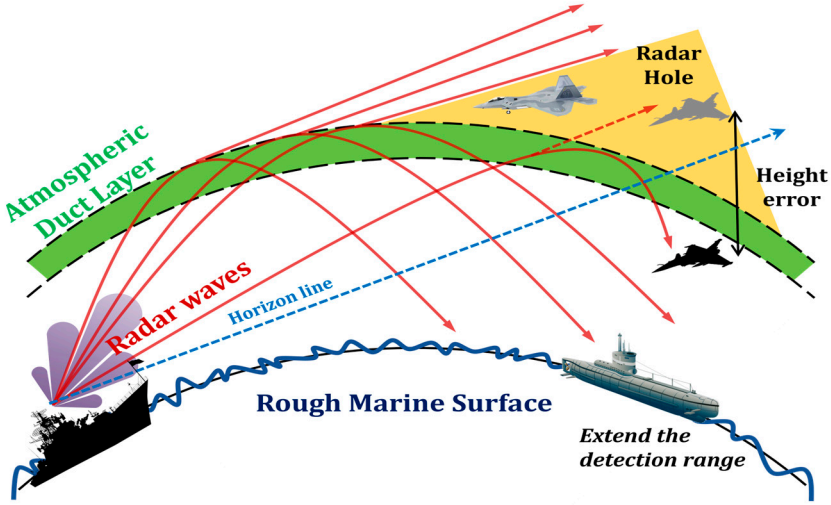


Figure 1. Schematic of atmospheric duct effects on EM waves. This phenomenon extends the operational range of communication systems and enables radar-based BLOS detection of low-altitude targets. Concurrently, the trapping of EM waves within the duct creates an EM shadow zone above the duct layer, where minimal radio energy penetrates due to restricted ray propagation.

The study of atmospheric ducts emerged in the 1930s with radar advancements [3,4], as military aircraft observed anomalous super-horizon signal propagation, sparking global research interest. In 1944, a U.S. Navy experiment linked signal strength to tropospheric inversion layer height, advancing marine duct understanding [5]. British researchers first documented evaporation ducting in 1947 during Irish Sea measurements [6]. By the 1960s, institutions like the Naval Electronics Laboratory Center (NELC) and the University of Hamburg collected global data, with Hamburg's team pioneering large-scale evaporation duct propagation studies. The 1970s saw the Fleet Numerical Oceanography Center (FNOC) and Naval Environmental Prediction Research Facility (NEPRF) develop coupled ocean–

atmosphere models to predict surface duct heights, alongside systems like the Integrated Refractive Effects Prediction System (IREPS) [7] and Engineer's Refractive Effects Prediction System (EREPS) [8] for EM wave propagation analysis. Since the 1980s, the U.S. has advanced duct propagation research in strategic environments like deserts and oceans, with pivotal work by the Naval Research Laboratory (evaporation duct telemetry), L. Ted Rogers (maritime communication [9]), and K.D. Anderson (low-altitude target detection [10]), culminating in tools like AREPS [11]. The Soviet Union contributed extensively through global oceanic experiments, confirming duct-enabled radar ranges up to 1000 km and addressing practical challenges such as over-the-horizon radar reliability and antenna optimization [12]. Similar research expanded globally, involving the UK, France, Australia, the Netherlands, India, Japan, and China [4,13–17]. Since the 1990s, advancements in detection technology and atmospheric science have propelled global research on atmospheric ducts to new heights (see Table 1). Key U.S. institutions include University of California, San Diego [18–32]; Johns Hopkins University [33–44]; Ohio State University [45–48]; Cornell University [49–54]; Coastal Carolina University [28,55–63]; and U.S. Navy divisions [5,11,64–98]. China's contributions are led by Northwestern Polytechnical University [99–125], National University of Defense Technology [126–154], Xidian University [155–194], PLA University of Science and Technology [195–229], Naval University of Engineering [230–247], and China Research Institute of Radiowave Propagation [248–278]. Additionally, active research in this field involves teams from Russia [279–283], India [284–287], Australia [288–290], Germany [291,292], South Korea [293–298], the United Kingdom [2,299–304], Singapore [305–307], France [308–313], Greece [314–316], Ukraine [317–319], Bulgaria [318,320–325], and Turkey [326–329], demonstrating broad international collaboration [330–347].

Table 1. Main countries and institutions for atmospheric duct research.

Country	Main Institution
America	University of California, San Diego
	Johns Hopkins University
	Ohio State University
	Cornell University
	Coastal Carolina University
	Department of the Navy
China	Northwestern Polytechnical University
	National University of Defense Technology
	Xidian University
	PLA University of Science and Technology
	China Research Institute of Radiowave Propagation
	Naval University of Engineering
South Korea	Pohang University of Science
	Hongik University
	Hanwha Systems
	Ajou University
India	National Physical Laboratory
	National Atmospheric Research Laboratory

Table 1. *Cont.*

Country	Main Institution
Singapore	Nanyang Technological University
	Agency for Science, Technology and Research
Australia	Flinders University
	University of Adelaide
Russia	Russian Academy of Sciences
	Pacific Oceanological Institute
Turkey	Middle East Technical University
	Zirve University
	Dogus University
	Istanbul Technical University
Greece	Aristotle University of Thessaloniki
	National Meteorological Service
	Technical University of Crete
France	Polytech Nantes
	Université Paul Sabatier
	Meteo France
Great Britain	University of Leicester
	Meteorological Office
	University of London
Germany	University of Breme
	University of Hamburg
Ukraine	National Academy of Sciences of Ukraine
Bulgaria	Bulgarian Academy of Sciences

Currently, research on atmospheric ducts can be categorized into three primary domains: (1) observational challenges of duct environments, (2) EM wave propagation within ducts, and (3) performance evaluation of radio systems operating under ducting conditions. By integrating duct detection results with tropospheric wave propagation models, accurate assessments of radar and communication system performance become achievable, enabling effective compensation, correction, and enhancement of these systems. Consequently, duct sensing techniques constitute a fundamental and critical component in this research field. This article aims to summarize the latest advancements in the sensing of marine atmospheric ducts, and, based on these developments, to address the challenges faced by radio propagation technologies. Furthermore, it offers a perspective on the future research directions for marine atmospheric duct sensing methods. To achieve this objective, the rest of the article is as follows: Section 2 begins with an overview of marine atmospheric ducts, summarizing the refractive structures, origins, and other characteristics of different categories of atmospheric ducts. Section 3 then provides a detailed overview of the current sensing methods for atmospheric ducts, aiming to establish a comprehensive theoretical foundation for subsequent research. By analyzing the characteristics of various methods, this section seeks to offer valuable guidance for researchers in selecting and applying appropriate techniques. Section 4 then delves into the potential challenges that future marine atmospheric duct sensing methods may encounter, considering the development trends

of emerging technologies, new applications, and evolving scenarios. This section focuses on addressing issues such as limited accuracy, poor real-time capabilities, and insufficient environmental adaptability in current sensing methods. Furthermore, it outlines potential directions for future research and proposes strategies for improvement. Finally, this paper concludes with a summary of the research on marine atmospheric duct observation, aiming to provide a broader perspective for future studies in this field and contribute to the advancement of radio propagation technologies.

Despite extensive field experiments and technological advancements in atmospheric duct observation by global research teams, existing reviews exhibit two critical limitations: (1) inadequate timeliness and systematic integration of emerging observation techniques (e.g., AI-driven remote sensing), and (2) a lack of forward-looking analysis on future directions, hindering strategic guidance for R&D. To address this gap, this review synthesizes over 400 high-relevance publications from SCI/EI databases (1960s–2026s), comprehensively documenting the evolution of in situ sounding, active/passive remote sensing, and theoretical modeling. It stands as the most exhaustive and up-to-date systematic assessment to date, offering actionable insights for future technological and operational development.

2. A Brief Overview of Atmospheric Ducts

2.1. Tropospheric Refraction

Refraction describes the bending of EM waves when they move through the boundary between two different media or a refractive index gradient within a medium [348]. Since this deviation from unity is minimal, it is more practical to represent the phenomenon using refractivity, denoted as N. In the troposphere, refractivity can be determined from [349]:

$$N = (n-1) \times 10^6 = \frac{77.6}{T}\left(p + \frac{4810e}{T}\right) \tag{1}$$

where T is the temperature, p is the pressure, and e is the water vapor pressure. The propagation effects due to Earth's curvature must be considered, typically by adjusting the refractivity. This transformation maps the Earth's spherical stratified medium to a planar one, enabling the modified refractivity (M) profile to be derived using Snell's law:

$$M = N + \frac{h}{a} \times 10^6 \approx N + 0.157h \tag{2}$$

where h is the height above the Earth's surface, and a is the Earth's mean radius. The gradient of M is obtained by differentiating the above equation with respect to height h:

$dM/dh = dN/dh + 0.157$. Tropospheric refraction's impact on EM wave propagation depends on dM/dh or dN/dh. Figure 2 illustrates the classification of atmospheric propagation conditions. When $dM/dh < 0$ or $dN/dh < -0.157$ N-units/m, EM wave rays bend towards the Earth's surface, becoming trapped within a thin atmospheric layer. In this case, the EM wave ray becomes confined within a thin atmospheric layer due to its curvature being greater than that of the Earth's surface. The EM energy undergoes repeated refraction within this layer and propagates forward, resulting in superrefraction. This phenomenon is known as EM duct propagation, and the corresponding atmospheric layer is called the atmospheric duct.

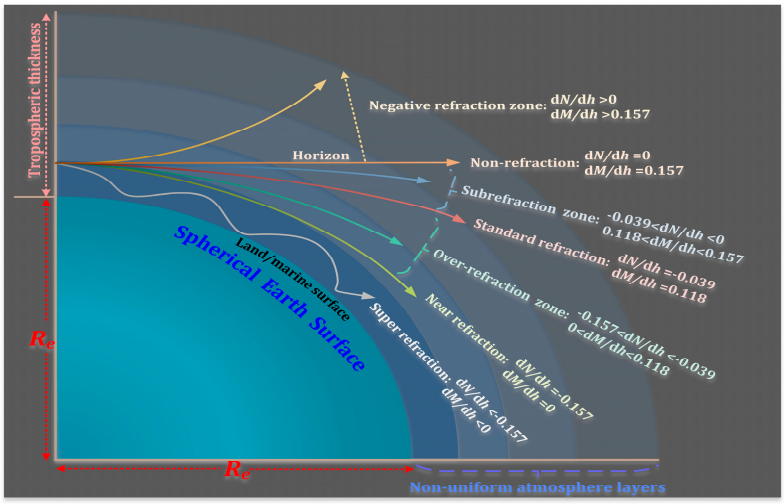


Figure 2. Different tropospheric atmospheric refraction types. The propagation path of EM waves in the troposphere is primarily determined by either dM/dh or dN/dh, enabling the classification of atmospheric refraction characteristics based on these parameters. When $dM/dh < 0$ or $dN/dh < -0.157$ N-units/m, EM wave rays bend towards the Earth's surface, becoming trapped within a thin atmospheric layer.

2.2. Formation Mechanisms and Typology of Atmospheric Ducts

The formation and evolution of atmospheric ducts are closely tied to lower atmospheric parameters such as temperature, humidity, and pressure, with sea surface conditions also playing a key role. Atmospheric ducts can be categorized into several distinct types based on their formation mechanisms. These include evaporation ducts, surface ducts, and elevated ducts (also known as lifting ducts), as shown in Figure 3. The meteorological conditions and occurrence mechanisms that lead to their formation are as follows:

- ***Evaporation ducts:*** Evaporation ducts are surface-hugging ducts formed by the sharp decrease in near-sea surface atmospheric humidity with height due to seawater evaporation. This duct structure typically occurs in the marine atmospheric boundary layer below 40 m, consisting of a relatively thin trapping layer. Since evaporation duct formation primarily depends on the degree of moisture inversion caused by seawater evaporation, the occurrence probability and height vary with geographical region, season, and diurnal cycle. Higher seawater temperature enhances evaporation rates, leading to higher occurrence probability and increased height of evaporation ducts, particularly in low-latitude seas during summer and daytime. For example, the probability of evaporation ducts with heights > 10 m reaches 92% in coastal northern Brazil, compared to only 2% in the Bering Strait [25], and 89% in the southeastern coastal waters of China [171]. The height of evaporation ducts (i.e., the thickness of the trapping layer) generally does not exceed 40 m, with annual averages of 5 m in the North Sea, 10–14 m in the Mediterranean Sea, and ~13 m globally [2]. Due to their weak trapping structure, EM waves with frequencies $\geq$ 1 GHz can be trapped or significantly affected [66].
- ***Surface ducts*:** Surface ducts are relatively high-altitude duct structures with lower boundaries connected to the sea surface. They typically form when dry, warm air masses advect from land over the moist, cold ocean, creating a near-sea surface atmosphere with cold, moist air below and warm, dry air above. There are two types of surface ducts: grounded surface ducts and surface-based ducts. Surface ducts typically occur in the boundary-layer atmosphere below 300 m, with a global average height of ~85 m [350]. Due to their relatively thick trapping stratification,

they significantly affect EM wave propagation. The global annual average occurrence probability is ~15%, with 1% in the North Atlantic, 25% off the southern California coast, and 50% in the Persian Gulf [350]. Surface ducts are not highly sensitive to EM wave frequencies and can support over-the-horizon propagation for radio waves above 100 MHz.

- ***Elevated ducts*:** Elevated ducts are suspended duct structures where the lower boundary is not connected to the sea surface (or ground), generally occurring in the tropospheric atmosphere below 3 km. The meteorological conditions for elevated ducts are the same as those for surface ducts, with the key difference being that the underlying surface of the elevated duct layer is an atmospheric base layer—specifically, the modified refractive index at the top of the duct layer is greater than that at the ground. In coastal environments, surface ducts can evolve into elevated ducts as the slope of the trapping layer decreases. Elevated ducts can reach heights of 600 m off the southern California coast and 1500 m off the Japanese coast [25], with an occurrence probability as high as 50% in many global regions [350].

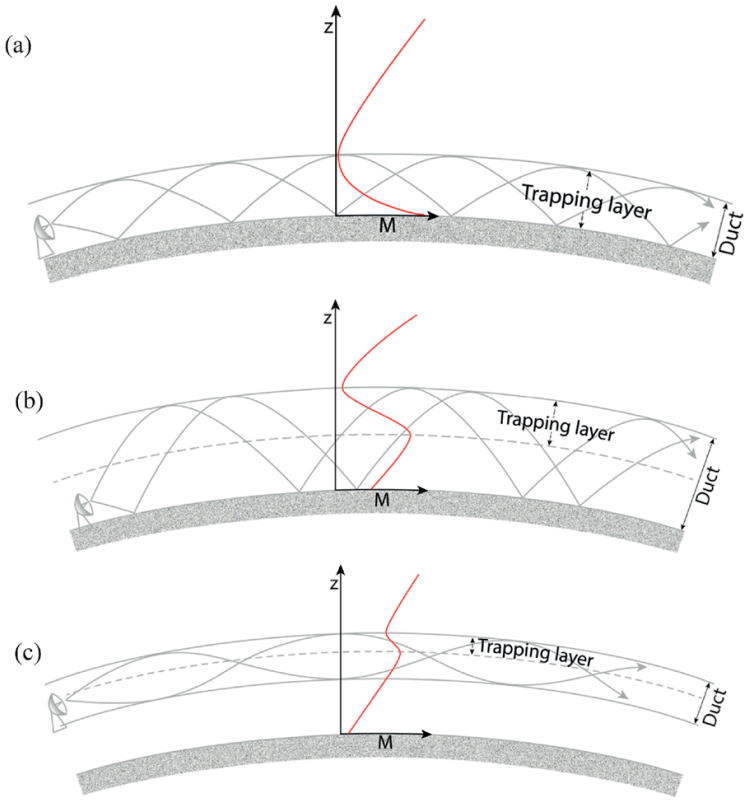


Figure 3. Illustration of the propagation of EM waves from a radar source in various refractive conditions over a distance beyond the line of sight over the Earth. The corresponding vertical *M* profiles are overlaid on the propagation path: (**a**) evaporation duct, (**b**) surface-based duct, and (**c**) elevated duct [65].

Table 2 presents annual statistics on atmospheric duct occurrence probabilities across global regions [25], illustrating significant geographical differences and diurnal variations in tropospheric duct probabilities in major global sea areas. The Persian Gulf and the Gulf of Mexico exhibit the highest daytime occurrence rates of evaporation ducts (>10 m), ranging from 77% to 92%, with the Rio Grande region in the Atlantic Ocean reaching a peak of 92% during the daytime. In stark contrast, the Baltic Sea and Bering Strait have evaporation duct occurrence rates of less than 12%. Surface-based ducts have the highest nighttime occurrence rate in the Persian Gulf (52%), while elevated ducts maintain a high occurrence

level of 38–40% day and night in the Gulf of Mexico. Notably, multiple duct phenomena are prominent in Diego Garcia (Indian Ocean) and the Southern California sea area, with their diurnal average composite occurrence rates reaching 7.3% and 5.6%, respectively. The occurrence rates of various types of ducts in the eastern and western Mediterranean are generally lower than those in other sea areas, among which the eastern Mediterranean has the smallest diurnal difference in elevated ducts (12–16%). The Yellow Sea region exhibits unique duct combination characteristics, with relatively balanced diurnal occurrence rates of surface-based and elevated ducts (13–18%), but the daytime occurrence rate of multiple ducts (7.0%) is significantly higher than that at night (3.4%).

Table 2. Occurrence probability of atmospheric ducts in different regions [25].

Region	Percent Occurrence (Annual Averages)							
	Evaporation Duct > 10 m		Surface-Based Duct		Elevated Duct		Multiple Elevated Ducts	Elevated Duct + Surface-Based Duct
	Day	Night	Day	Night	Day	Night	Diurnal Average	Diurnal Average
Persian Gulf	77	62	36	52	26	33	2.8	4.8
Gulf of Mexico	84	79	9	10	38	40	8.3	2.6
East China Sea	83	76	10	7	15	18	3.4	2.0
Diego Garcia (Indian Ocean)	87	76	34	18	20	37	7.3	3.8
Rio Grande (Atlantic Ocean)	92	87	18	18	24	30	6.8	7.2
East Mediterranean	72	62	13	11	12	16	2.4	2.5
West Mediterranean	58	45	15	14	10	12	1.7	2.6
Yellow Sea	63	56	16	13	17	18	7.0	3.4
Southern California	46	35	23	15	33	38	5.6	3.2
Baltic Sea	12	8	2	3	3	4	0.6	0.4
Bering Strait	2	1	6	5	4	5	1.1	0.8

3. Current Atmospheric Duct Sensing Methods

An atmospheric duct is essentially an anomalous refractive index spatial structure within the lower troposphere. Its vertical structure corresponds to the *M* profile of the duct, while its horizontal structure reflects the spatial heterogeneity of the vertical refractive profile. Thus, the sensing of a tropospheric duct is fundamentally the observation of the refractive distribution in the lower tropospheric atmosphere. Current atmospheric duct detection methods are generally classified into two major categories: contact-based sensing methods, also known as direct observation methods, and indirect estimation methods. The latter includes theoretical estimation, numerical weather forecasting, and remote sensing inversion. The principles, advantages, and disadvantages of each method will be discussed next. Subsequent sections will examine research advancements and distinctive characteristics of each methodology.

3.1. Contact-Based Observation Methods

Contact-based detection methods involve direct interactions with the atmospheric duct, typically using instruments placed in or near the troposphere. These methods often rely on physical sensors, such as radio frequency devices, that can measure atmospheric properties like temperature, humidity, and refractivity in real time, thereby identifying the presence of atmospheric duct structures. Typical direct observation instruments include meteorological towers [343], gradiometers [176], radiosondes [351], rockets [36], balloons, airships [163],

and microwave refractometers [352], among others; the application scenarios of some instruments are shown in Figure 4. The vertical inhomogeneous refractive index profile can be theoretically derived from temperature, humidity, and pressure measurements obtained by radiosondes or sounding rockets. However, the coarse vertical sampling intervals of these measurements may result in low vertical resolution of the calculated refractive index profiles, potentially missing critical trapping layers. Additionally, this method fails to capture horizontally inhomogeneous refractive index structures at varying distances, while the equipment is costly and operationally complex. An alternative approach employs microwave refractometers, which directly measure the atmospheric refractive index by detecting resonant frequency shifts in microwave cavities, currently representing the most accurate technique. Nevertheless, their high cost and single-point observation capability limit their utility for spatial refractive index mapping in the troposphere.



(**a**) (**b**) (**c**) (**d**)

Figure 4. Several atmospheric duct detection instruments: (**a**) meteorological tower [343], (**b**) gradiometer [176], (**c**) rocketsonde, and (**d**) airship.

Beyond the instrumental apparatus essential for observations, the selection of an appropriate observation platform constitutes a critical determinant of data quality and applicability. Identical sensors, when deployed across heterogeneous platforms (e.g., ground-based stations, ship-borne systems, airborne instruments, or satellite constellations), exhibit marked disparities in data acquisition efficiency, measurement accuracy, and scenario-specific suitability. Furthermore, these platforms diverge substantially across four pivotal dimensions: (1) reliability, (2) spatial coverage, (3) operational feasibility, and (4) cost. To delineate these contrasts methodologically, we have systematically tabulated the parametric characteristics of each platform category (see Table 3), thereby enabling comparative analysis for optimized platform selection in diverse observational contexts.

Table 3. Comparative analysis of characteristics across different platforms.

Platform	Reliability	Spatial Coverage	Operational Feasibility	Cost
Ground-based	Moderate	Local	Low	Low
Ship-based	High	Regional	Moderate	Moderate
Airborne	High	Transect	High	High
Satellite	Moderate	Global	Very high	Very high

3.1.1. Evaporation Ducts

Evaporation ducts can be detected using measurement instruments such as microwave refractometers, meteorological gradient meters, and low-altitude radiosondes. While the microwave refractive index meter directly measures atmospheric refractive index parameters, the other instruments infer refractive index by measuring temperature, humidity, and pressure. The detection height typically remains below 40 m. Given the frequent occurrence of evaporation ducts over the sea, numerous institutions globally have conducted extensive observations of this phenomenon. One of the most notable evaporation duct experiments was conducted by the U.S. Naval Ocean Systems Center along the Pacific coastline [88]. Spanning 15 years from 1970 to 1984, the study encompassed a vast range of marine areas, from 40°S to 70°N latitude. Ukraine conducted two meteorological data measurement experiments, one in the Atlantic Ocean in 1983 and another in the Indian Ocean between 1983 and 1984 [317].

In 1998, Australian scholar Kulesza et al. [288], followed by the Naval Surface Warfare Center in 2000 [353], organized measurements of evaporation ducts. Another notable experiment took place from August to September 2001, led by the Space and Naval Warfare Systems Center San Diego. Researchers from four countries participated in the month-long Rough Evaporation Duct (RED) experiment conducted in Hawaiian waters [89]. One of the primary objectives of the RED was to determine the extent to which sea surface roughness affects the vertical distribution of the refractivity. In 2004, German researchers conducted the Validation Measurements for Propagation in the IR and Radar (VAMPIRA) experiment in the Baltic Sea [354]. In 2007, Siddle et al. [301] conducted an analysis of evaporation duct measurements between three islands in the English Channel. Subsequently, to investigate the impact of sea breeze phenomena on radar detection, Sally Garrett conducted the Seabreeze-2009 experiment in New Zealand [355]. In 2012–2013, the Naval Postgraduate School (NPS) conducted measurements of evaporation ducts and elevated ducts in the waters off California, utilizing ships as the primary platform for data collection [82]. In 2017, the Tropical Air–Sea Propagation Study (TAPS) was conducted along the coast of Australia to investigate tropical air–sea wave propagation. In 2015 and 2017, the NPS, in collaboration with multiple research institutions, conducted the Coupled Air–Sea Processes and Electromagnetic Ducting Research (CASPER) experimental program in the waters off the coast of North Carolina [65]. The main platform, ground stations, and towers of CASPER-East are shown in Figure 5. This study aimed to investigate coupled atmospheric–oceanic processes and atmospheric duct phenomena.

3.1.2. Surface Ducts

Surface ducts are detected using both low-altitude and high-altitude detection systems. These systems employ methods such as balloon releases and aircraft flying in spiral patterns at various altitudes to measure parameters such as temperature, humidity, and pressure at different heights, thereby determining the occurrence of surface ducts. The detection heights are typically below 600 m. Between 1985 and 1994, Johns Hopkins University conducted observations using aircraft at Wallops Island, located off the eastern coast of the United States, obtaining extensive surface duct data [43,356]. In 1994, the Navy Radio and Sound Laboratory conducted the Variability of Coastal Atmospheric Refractivity (VOCAR) experiment along the southern coast of California [5]. In March–April 1998, the Navy Surface Warfare Center, in collaboration with the NPS and Johns Hopkins University, conducted a large-scale experiment to collect oceanic meteorological and radar propagation data on Wallops Island, Virginia (Wallops '98) [66]. The Wallops '98 experimental site location is shown in Figure 6. During the experiment, tropospheric refractivity profile data were measured using helicopter-based measurements, while radar wave propagation

data were obtained using the Microwave Propagation Measurement System (MPMS). In 2000, Thompson et al. conducted the Wallops-2000 experiment on Wallops Island, Virginia, where they utilized the experimental data to investigate the influence of sea surface temperature on the surface-based duct [77]. In 1996, the Ship Antisubmarine Warfare Readiness/Effectiveness Measuring (SHAREM-115) experiment was conducted in the Persian Gulf. The authors present the surface duct observation results from this experiment in [26].



Figure 5. CASPER-East: main platforms, ground stations, and towers [65].

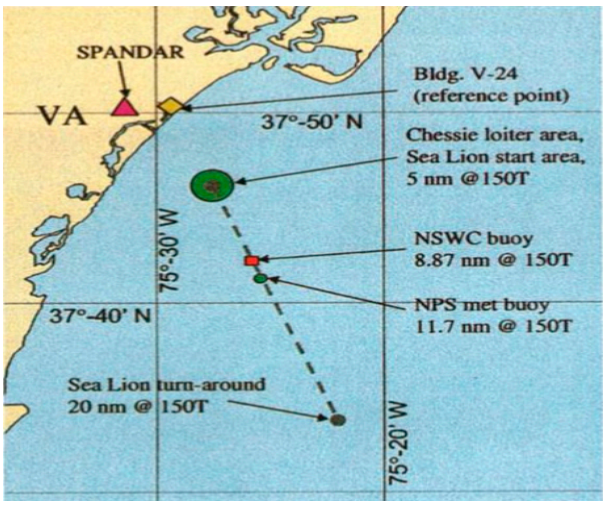


Figure 6. Geographical location of Wallops '98 experimental site [66].

3.1.3. Elevated Ducts

Observation of elevated ducts primarily relies on high-altitude detection systems. Techniques such as balloon releases, meteorological rocket launches, and aircraft performing spiral flights at various altitudes are used to measure parameters such as temperature, humidity, and pressure at different heights [357]. This allows for the identification of

elevated duct occurrences and the acquisition of duct parameters, with detection typically occurring at altitudes below 30 km. For example, elevated duct observation experiments conducted along the west coast of Africa [358] and in Australia, as well as duct measurements based on thrice-daily sounding data from several tropical regions in India, illustrate such methods.

3.2. Indirect Estimation

In addition to directly measuring the atmospheric ducts using meteorological observation equipment, an alternative approach involves developing atmospheric duct diagnostic models based on the atmospheric similarity theory to estimate the atmospheric state. Another method leverages the strong correlation between the meteorological conditions and the spatiotemporal variations in meteorological systems, utilizing numerical forecasting to forecast atmospheric ducts. Additionally, remote sensing retrieval of duct parameters can be performed by analyzing changes in the characteristic physical quantities of radio signals as they propagate through the atmospheric duct.

3.2.1. Theoretical Estimation

In the conventional sense, theoretical estimation of atmospheric ducts refers to diagnosing the atmospheric duct state at a given moment based on observations of certain meteorological parameters. This typically focuses on the diagnosis of evaporation ducts, commonly referred to as predicting. Evaporation duct diagnosis generally relies on diagnostic models. Since the 1970s, researchers have proposed evaporation duct diagnostic models, which are primarily based on the Monin–Obukhov similarity theory for the MABL [359]. These models integrate observational data of atmospheric temperature, humidity, pressure, wind speed, and sea surface temperature to derive refractive index gradient formulas or refractivity profiles for the near-surface atmosphere. Subsequently, the EDH is determined using the critical refractivity gradient. The main existing models for evaporation duct prediction are presented in Table 4.

Table 4. Current primary models for evaporation duct prediction [121].

Time	Prediction Model	Inventor
1973	Jeske model [292]	Jeske
1976	Paulus-Jeske (PJ) model [67]	Paulus and Jeske
1979	Liu-Katsaros-Businger (LKB) model [360]	Liu, Katsaros, and Businger
1984	Naval warfare assessment (NWA) model [361]	NWA Center
1991	Naval Research Laboratory (NRL) model [96]	NRL
1992	Musson-Gauthier-Bruth (MGB) model [313]	Musson, Gauthie, and Bruth
1996	Babin–Young–Carton (BYC) model [38]	Babin, Young, and Carton
2000	NPS model [37]	NPS
2001	Pseudo-refractivity model [168]	Liu, Huang, and Jiang

In 1973, Jeske [292] from Hamburg University proposed an evaporation duct model known as the Jeske model. This model became the earliest evaporation duct prediction tool, gaining widespread use and later being incorporated into the IREPS. The Jeske model utilizes the calculated overall Richardson number to assess the stability conditions of the near-surface atmosphere. Based on the stability results, it then applies a corresponding function derived from the Monin–Obukhov similarity theory to estimate the EDH. Paulus [67] investigated the discrepancies between the observed values and the predictions of the Jeske model, attributing the unrealistic overestimation of EDH to errors in the air–sea temperature difference observations. To address this, a constraint was added to the air–sea temperature difference, limiting the calculated EDH to approximately 20 m. This model

became known as the PJ model. Due to its simplicity and fast computational speed, the PJ model has been widely applied and has been used as an operational model by the U.S. Navy since 1978. In 1992, Musson-Genon et al. [313] introduced the MGB model, which computes the vertical gradient of AP based on fluid statics and the ideal gas law. The model employs scale parameters for potential temperature and specific humidity, along with their corresponding dimensionless gradient functions, to calculate the vertical gradients of AT and WVP. Subsequently, the model estimates the EDH by evaluating the refractivity gradient that gives rise to the duct. Liu, Katsaros, and Businger [360] proposed the LKB model, which utilizes a limited set of meteorological data to compute momentum flux, heat flux, and water vapor flux. This enables the derivation of vertical profiles for AT, specific humidity, and atmospheric pressure. Finally, the model calculates the M profile for the evaporation duct. The introduction of the LKB model provided a crucial foundation for subsequent research on evaporation duct diagnostic models, leading to the development of a class of evaporation duct models built upon the LKB model, including the NWA [361], NRL [96], BYC [38] and NPS [37] models. The NPS model employs the Coupled Ocean–Atmosphere Response Experiment (COARE) [362], an integrated algorithm for air–sea fluxes derived from long-term marine surveys. The NPS model incorporates near-surface measurements of atmospheric temperature (AT), pressure (AP), wind speed (WS), relative humidity (RH), and sea surface temperature (SST) from various altitudes as inputs. Its empirical relationships, derived from marine experiments, demonstrate substantial improvements over the PJ model. Furthermore, with the growing maturity and widespread use of the advanced international COARE3.0 bulk algorithm for air–sea flux calculation, studies [189] have started introducing it into the NPS model to compute key physical quantities, including characteristic scale parameters and sea surface aerodynamic roughness. The NPS model's core computational equations are given by:

$$T(z) = T_0 + \frac{\theta_*}{\kappa}\left[\ln\left(\frac{z}{z_{0\theta}}\right) - \Psi_h(\zeta)\right] - \Gamma_d z \tag{3}$$

$$q(z) = q_0 + \frac{q_*}{\kappa}\left[\ln\left(\frac{z}{z_{0\theta}}\right) - \Psi_h(\zeta)\right] \tag{4}$$

$$P(z_2) = P(z_1)\exp\left(\frac{g(z_1 - z_2)}{R\overline{T}_v}\right) \tag{5}$$

$$e(z) = \frac{q(z)P(z)}{\varepsilon + (1-\varepsilon)q(z)} \tag{6}$$

The key parameters include: T_0 and q_0 representing sea surface AT and specific humidity (SH) respectively; $\zeta = z/L$, L denoting the Monin-Obukhov length; θ_* and q_* as the Monin-Obukhov scaling parameters for potential temperature (PT) and SH; $z_{0\theta}$ and z_{0q} being the roughness lengths for PT and SH; Γ_d as the dry adiabatic lapse rate; κ the von Karman constant; Ψ_h as the temperature correction function; $\overline{T}_v$ as the mean virtual temperature at height z_1 and z_2; and ε being a constant with a value of 6.22. Using vertical profiles of AT, AP, and water vapor pressure from the NPS, the oceanic atmospheric M-profiles can be calculated via Equation (1). Figure 7 presents two evaporation duct refractive index profiles generated from the model's five meteorological parameters, revealing significant environmental dependence. The derived evaporation duct heights (EDHs) were 13.5 m and 27.3 m at corrected refractive indices of 341.3 M and 389.3 M units, respectively, confirming environmental sensitivity. However, under strong stable conditions, the NPS model still exhibits considerable errors in estimating EDH, indicating the need for further refinement and adjustment. For instance, Guo et al. [250] demonstrated an average error of −5.48 m using meteorological gradient tower data. Since 2000, Chinese researchers have undertaken

extensive efforts in the prediction of evaporation ducts. Liu et al. [168] proposed an evaporation duct diagnostic model based on the pseudo-refractivity as a similarity parameter, which is referred to as the pseudo-refractivity model. Ding et al. [199,200] proposed a universal evaporation duct (UED) model based on the COARE algorithm and the NPS model. In 2019, Wang et al. [363] proposed a novel EDH diagnostic method, the ensemble diagnostic approach (Babin_Ens method), based on the Babin model and leveraging numerical weather prediction ensemble forecasting techniques. Compared to the Babin model and the WRF model, this approach effectively improves the mean forecast bias of EDH and EDS.

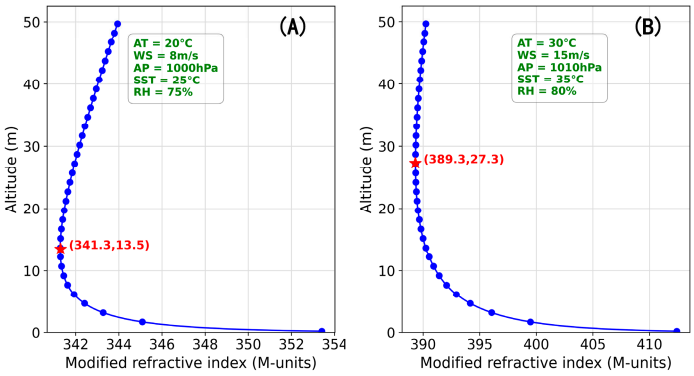


Figure 7. Evaporation duct *M*-profiles for EDH cases: (**A**) 13.5 m and (**B**) 27.3 m [363].

An important aspect of research on evaporation duct prediction models is model validation. Since the 1980s, considerable efforts have been devoted to addressing discrepancies in computational results across different models under identical environmental conditions. These efforts have included numerical simulations, empirical measurements of evaporative ducts, and over-the-horizon propagation experiments, culminating in comparative analyses of various models. Cook [69] investigated the sensitivity of five EDH models to errors in shipborne meteorological data and conducted a comparative analysis of these algorithms. The sensitivity study revealed consistent model responses despite differing frameworks, with sensor-induced errors causing 10–50% uncertainty in duct height calculations. In 1996, Babin et al. [364] employed a method that integrates atmospheric parameters at various heights and SST measurements to determine the atmospheric *M* profile, thereby calculating the EDH. The validation with Wallops Island boat data shows that the confidence level of the model can reach up to 94%. A comparison of the PJ, NPS, Jeske, and BYC models was conducted. Ivanov et al. [317] conducted a comparison of four evaporation duct models using data measured over the ocean. Results show unstable stratification yields duct height estimates of 5–20 m, with ±2.5 m error. In 2009, Cha et al. [238] analyzed the impact of meteorological and hydrological measurement errors on the PJ model, utilizing evaporation duct *M* profiles collected under various meteorological conditions in certain marine areas of China. Experimental results demonstrate the PJ model's superior applicability in Chinese coastal waters with low wind speeds and 75–85% relative humidity. Subsequently, they investigated the applicability of evaporation duct Model A in the maritime regions of China [247]. Results show that with a 0–1 °C air–sea temperature difference under near-neutral stratification, Model A's deviation from measured data averages 1.76 m. Yang et al. [343] present the PJ and NPS models to verify the adaptation of evaporation duct models in the SCS in winter. The PJ model shows an average deviation of 1.03 m, while the NPS model achieves −1.4 m, with superior stability. To enhance the prediction accuracy of evaporation ducts under varying environmental conditions, Qiu et al. [365] proposed a model selection optimization method (MSOM), as shown in Figure 8. The accuracy of this approach was validated using observational data from an offshore platform in the

South China Sea. The results indicated that MSOM significantly improved the prediction accuracy of evaporation duct heights. Under stable and unstable conditions, the median prediction error of MSOM decreased by 0.8 m and 0.6 m, respectively.

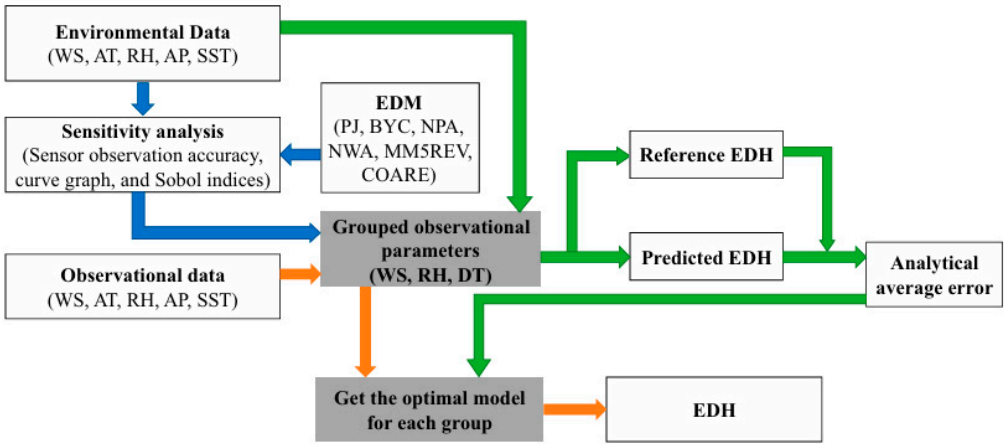


Figure 8. Model selection optimization method (MSOM) [365]. The MSOM comprises three components. In the first module (blue), sensitivity analysis is performed on existing models (PJ, BYC, NPS, NWA, fifth-generation mesoscale revise, and COARE models) against meteorological/hydrological parameters (WS, AT, RH, AP, SST) using sensor accuracy assessments, curve plotting, and Sobol indices. Environmental parameters are then grouped by water temperature, RH, and air–sea temperature difference. The second module (green) derives reference and predicted EDH values for each parameter group, where the model with the lowest mean prediction error per group is selected as optimal. The third module (orange) dynamically assigns new observational data to predefined groups and applies their corresponding optimal models for EDH estimation.

Furthermore, the *M* profiles derived from evaporation duct prediction models are incorporated into EM wave propagation models within the evaporation duct, allowing for the calculation of EM wave propagation loss. Comparing the path loss calculated by the model with the experimentally measured propagation losses provides the most effective means of assessing the predictive accuracy of the evaporation duct models. This method is also employed to investigate discrepancies in the computational results of different models under the same environmental conditions. Subsequently, Babin et al. [37] performed a comparative analysis of the *M* profiles predicted by the NWA, NRL, BYC, and NPS models, taking a propagation modeling approach. Patterson [80] conducted propagation experiments in the Mediterranean region, comparing the results of three evaporation duct models across propagation tests in the L, S, X, KU, and KA frequency bands. Gunashekar et al. [300] conducted a comparative analysis of the PJ and NPS models based on microwave over-the-horizon propagation experiments in the English Channel.

However, the universal functions of these models are derived from empirical generalizations based on the accumulation of extensive data from specific regions, and thus do not possess universally applicable characteristics. This limitation primarily arises because these models rely on macro-scale oceanographic and meteorological observational data, most of which are based on the Monin–Obukhov similarity theory to determine the EDH. These diagnostic models are inherently limited, as they assume the refractive index of the evaporation duct diagnostic model is uniform, which implies that the material and energy exchange between the atmosphere and ocean is in a dynamic equilibrium. In recent years, AI-based diagnostic techniques for EDH have emerged as a promising and novel research direction with broad potential applications. By leveraging AI algorithms, this approach enables the efficient and precise extraction of complex patterns and features from large datasets, facilitating accurate prediction and diagnosis of EDH. Compared to tradi-

tional empirical models, this technique demonstrates superior adaptability and accuracy in handling complex environmental factors and large-scale data. Currently, several studies have begun to explore the use of AI methods to advance the understanding of evaporation duct dynamics. In 2007, Isaakid et al. [315] developed an artificial neural network (ANN) based on Helliniko Airport data to model the evaporation duct. The performance of this ANN model proved to be both effective and successful in predicting EDHs. In 2018, Zhu et al. [130] developed a purely data-driven evaporation duct model based on a Multilayer Perceptron (MLP). The accuracy of the MLP model showed a significant improvement over the PJ model. Yan et al. [99] developed an ANN for evaporation duct prediction using the NPS model and a reanalysis dataset. Comparative analyses of predicted profiles and path loss were conducted under stable/unstable atmospheric conditions.

Zhao et al. have explored a lot of AI models since 2019. They applied the BP neural network to predict EDH [137], and experiments demonstrated that, compared to the traditional PJ model, the BP neural network outperformed simple support vector regression (SVR), offering better precision and regional generalization. In 2019, the gradient-boosted decision tree (GBDT) was first proposed for diagnosing EDH. A purely data-driven GBDT model (PDD_GBR) was introduced, as well as the GBR_PJ and GBR_BYC models, which used GBDT to optimize traditional theoretical models [133], with aerial survey data from five routes used for training and testing. The results indicated that the PDD_GBR model, driven by pure data, exhibited significant advantages in both accuracy and regional generalization over all other models. In 2020, Zhao et al. [131] further explored the application of extreme gradient boosting (XGBoost), which is a theoretically enhanced and efficient implementation of the GBDT algorithm. Its performance in the diagnosis of evaporation duct height was notably effective. Experimental results revealed that the accuracy of the PJ model improved exponentially compared to the traditional theoretical model, and was significantly better than both the MLP and GBR models (the predicted results are shown in Figure 9). In 2021, Zhao et al. [126] utilized the LSTM model, driven by pure data, for predicting EDH. Unlike previous models, LSTM is a recurrent neural network with complex memory capabilities and structure, making it highly effective for time series data prediction. Given the time-sequential nature of the aerial survey data, LSTM was particularly well suited. Experimental results showed that LSTM significantly outperformed the XGBoost model, which had previously shown the best performance, in both accuracy and regional generalization.

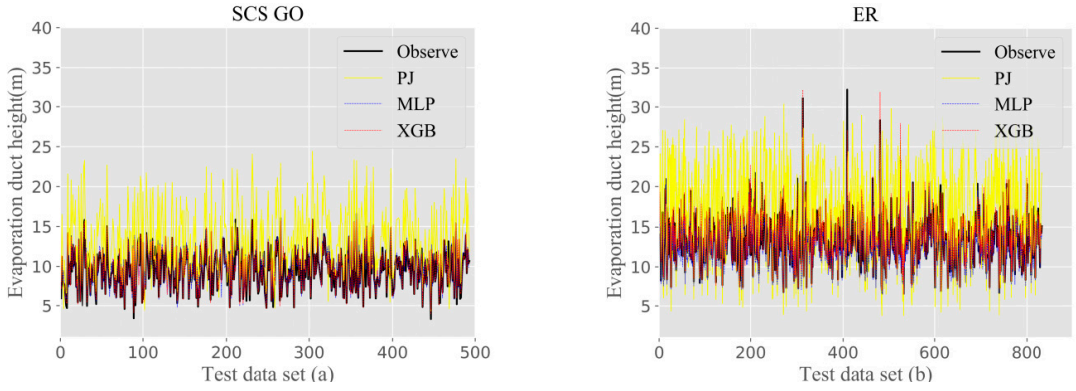


Figure 9. *Cont.*

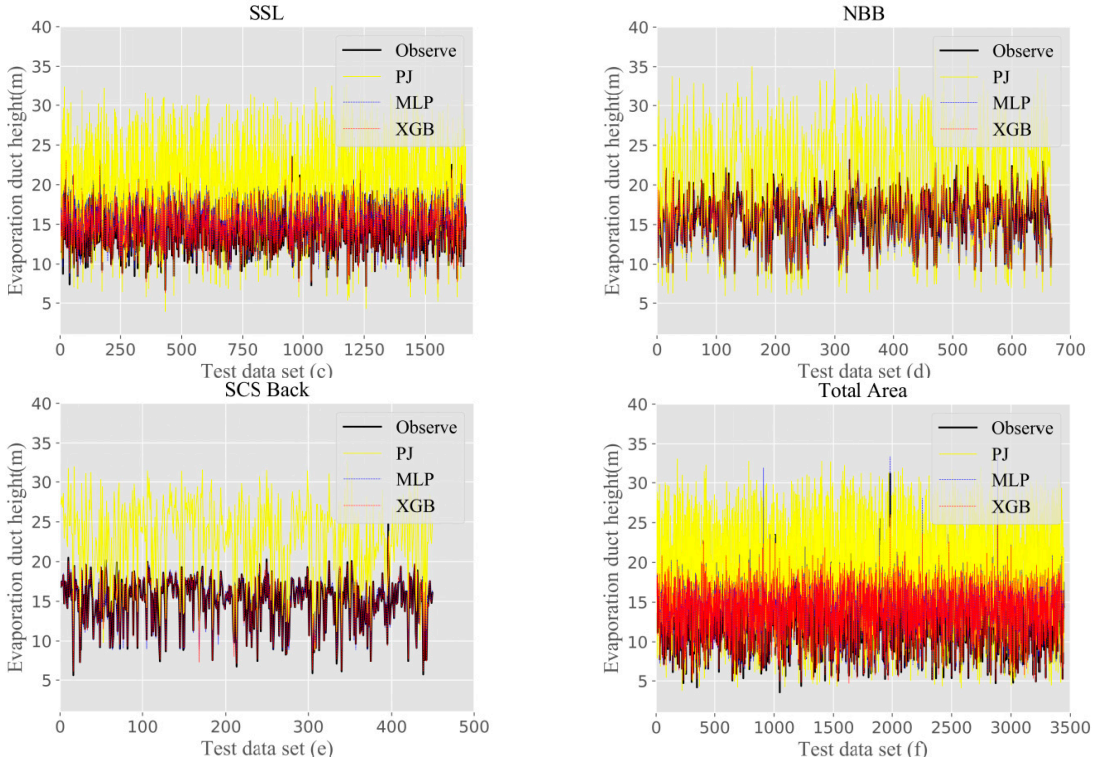


Figure 9. Comparison of predictive curves for different sub-regions (ER: Equator Region, SSL: South of Sri Lanka, NBB: North of the Bay of Bengal), and the total area [131].

3.2.2. Numerical Weather Forecasting

Atmospheric dust forecasting integrates meteorological prediction methods with duct-specific characteristics and atmospheric physics to estimate future duct conditions. Initial approaches relied on synoptic extrapolation (e.g., identifying duct-prone weather patterns like subtropical highs, cold fronts, or typhoons as indicators) [366]. Current research on atmospheric duct forecasting is primarily divided into two categories [253]:

(1) **Forecasting approaches:**

- Synoptic-based forecasting;
- Statistically based forecasting;
- Dynamical forecasting;
- Integrated forecasting.

(2) **Forecasting classification by dimension**

- Classified by service object: including routine forecasting, professional forecasting;
- Classified by forecasting scope: including global forecasting, regional forecasting, site-specific forecasting;
- Classified by forecast lead time: including nowcasting, very short-range forecasting, short-range forecasting, medium-range forecasting, long-range forecasting, etc.

Due to the difficulty in obtaining maritime observational data, particularly high-resolution sounding data—characterized by low daily sampling frequency, fixed timing, and sparse, unevenly distributed observation points—the numerical forecasting methods for atmospheric ducts were developed and have progressively evolved. Atmospheric duct forecasting based on synoptic extrapolation methods generally provides only qualitative predictions, whereas numerical weather prediction (NWP) enables quantitative and regional forecasting solutions. Since the 1970s, the U.S. Navy has conducted research

on the impact of weather patterns on radio wave propagation, leading to the development of the Navy Operational Regional Atmospheric Prediction System (NORAPS) for forecasting atmospheric refractivity [91]. Subsequently, the Navy developed the Coupled Ocean/Atmosphere Mesoscale Prediction System (COAMPS), a higher-resolution system capable of assimilating meteorological data [92]. Subsequently, Burk et al. [75] employed the COAMPS model to analyze the impact of island wake on evaporation ducts and radio wave propagation. Since the 1980s, the rapid development of numerical weather models has led to the widespread application of mesoscale models in atmospheric duct research and forecasting, driving significant advancements. The most widely recognized, well-developed, and representative model is the Fifth-Generation Mesoscale Model (MM5), developed through a collaboration between the National Center for Atmospheric Research (NCAR) and Pennsylvania State University [367]. The Weather Research and Forecasting Model (WRF) [368], a next-generation mesoscale numerical weather prediction model, was developed by NCAR's mesoscale and microscale meteorology division in collaboration with numerous associations and universities (see Figure 10). This model has recently garnered significant attention and played a crucial role in the study of tropospheric ducts.

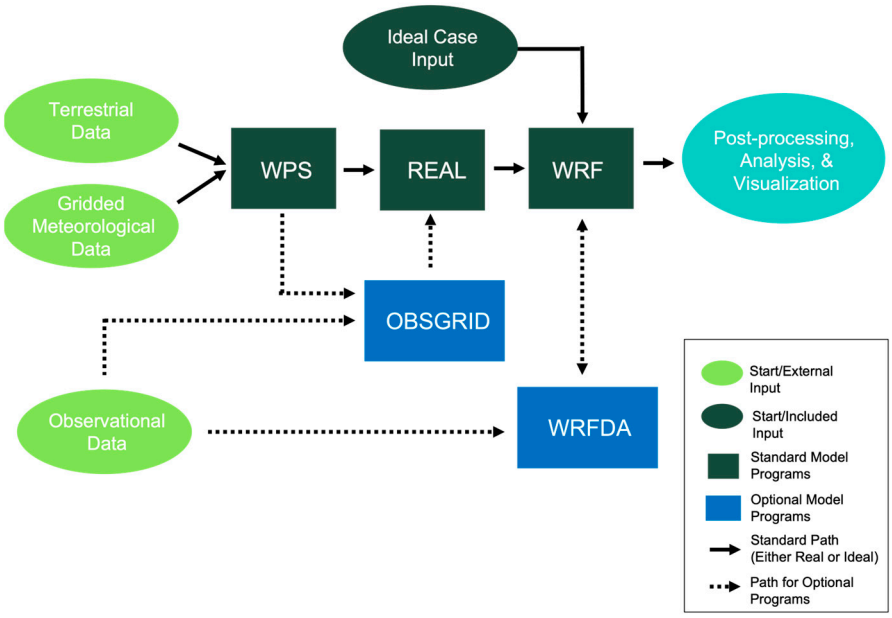


Figure 10. Flow chart of WRF modeling system, where WPS, REAL, OBSGRID and WRFDA denote WRF Preprocessing System, Real Initialization Programs, Observation Grid Module and WRF Data Assimilation, respectively. The step "*Post-processing, Analysis, & Visualization*" in the diagram marks the end of WRF runs, enabling extraction of WRF outputs, variable derivation and visualization, which transform raw data into intuitive charts and useful analytical results.

These high-resolution mesoscale meteorological models not only offer potential for quantitative forecasting of atmospheric ducts but also demonstrate promising applications in the study of atmospheric ducting mechanisms. Atkinson and Zhu [302–304] employed the MM5 atmospheric model to simulate the atmospheric ducts across the entire Persian Gulf region for the year 2002. Using the simulation results, they conducted a detailed analysis of the formation patterns of atmospheric ducts under the influence of sea–land breezes. Chen et al. [259,276] employed MM5 to forecast coastal surface ducts and low-level ducts in the offshore regions of China, presenting statistical characteristics of their occurrence probabilities alongside key parameters. Additionally, they conducted a preliminary investigation into their formation mechanisms and proposed that the variation in the occurrence probability and types of atmospheric ducts in the offshore regions of

China is closely linked to the activity of the East Asian monsoon. Zhang et al. [267] directly applied the atmospheric dynamical equations to the forecasting of atmospheric ducts. They proposed a method for forecasting atmospheric ducts based on moist potential vorticity, given the strong correlation between the moist potential vorticity field and the distribution of atmospheric ducts. Haack et al. [74] subsequently assessed the forecasting capabilities of four mesoscale weather prediction models—COAMPS, the UK Met Office's Unified Model (MetUM), MM5, and Canada's Global Environmental Multiscale Model (GEM)—in predicting atmospheric ducts along the Virginia coastline. They noted that model initialization and STT fields are critical factors influencing forecast accuracy. Zhao et al. [93,94] employed the Ensemble Forecast System developed by the NRL to analyze the occurrence probability, location, intensity, and structure of different types of ducts. Comparison with the Wallops-2000 experimental data revealed that the strong SST gradient formed in spring, due to the cold shelf waters and the warm Gulf stream, significantly influences the formation of duct layers. Ulate et al. [95] analyzed the refractive conditions in the offshore region of Duck, North Carolina, using observational data obtained from the CASPER experiment and COAMPS model. The results show that ducts exhibit more pronounced diurnal variations over land than over the sea, occurring more frequently on land, yet with greater intensity over the sea. Wang et al. [369] proposed a method for ensemble diagnosis of EDH and EDS based on the Babin model and the concept of ensemble forecasting in numerical weather prediction. Compared to WRF, the average improvement rates in forecast bias for EDH and EDS were 14.01% and 16.92%, respectively, significantly enhancing the diagnostic accuracy. Using the WRF model, Liang et al. [146] simulated a strong elevated duct event in the western North Pacific. Their analysis reveals that the persistence of this intense elevated duct was attributed to a robust dry air mass capping the moist MABL, coupled with a subsidence inversion associated with high-pressure systems.

Research on the application of AI technologies in atmospheric duct numerical forecasting remains relatively sparse. Existing studies primarily focus on leveraging traditional diagnostic models and meteorological reanalysis data to derive spatiotemporal distribution datasets of EDH. These datasets typically capture the EDH distribution across large-scale oceanic regions at various temporal intervals. Current research primarily focuses on utilizing these spatiotemporal distribution datasets to develop more accurate EDH prediction models. By employing various machine learning algorithms and deep learning methods, researchers aim to enhance the predictive accuracy and generalization capability of EDH variation forecasts. Chai et al. [128] utilized weather forecast product datasets from the South China Sea region based on the Yin–He global spectral model (YHGSM). A numerical weather prediction product (NWPP) EDH regional forecasting model was developed using a deep learning convolutional neural network (CNN). This represents the first data-driven model for regional EDH prediction. Ji et al. [189] proposed the EDH-STNet model (see Figure 11), based on the Swin-Unet architecture, which integrates multiple environmental information sources. The model employs an encoder–decoder framework utilizing the continuous Swin-Transformer, effectively capturing complex spatial correlations and temporal features. The EDH-STNet model also incorporates various hydrometeorological parameters to model the nonlinear relationships with EDH. By adopting a data-driven approach to integrate these HMPs as prior information, the accuracy and reliability of spatiotemporal predictions are significantly improved.

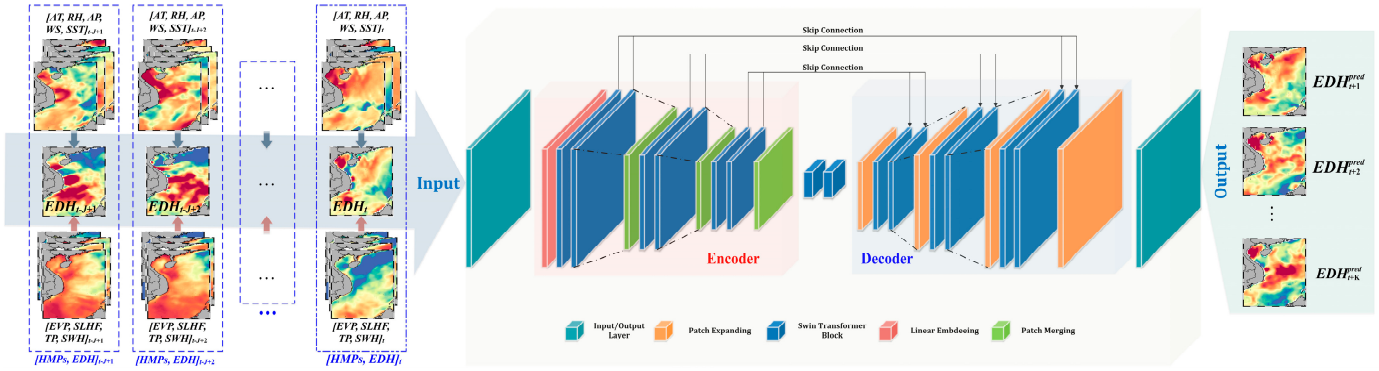


Figure 11. EDH-STNet [189]. This model takes the spatial distribution of EDH at historical times as input and is used to predict the EDH distribution at future times. To improve prediction accuracy, the model also incorporates AT, RH, AP, WS, SST, evaporation (EVP), surface latent heat flux (SLHF), total precipitation (TP), and sufficient wave height (SWH) as supplementary inputs. After the above input is fed into the Swin-Unet model, it is first processed by the encoder: the Swin-Transformer module in the encoder can extract and abstract features from the input data. The above processing module can effectively capture spatial information while deepening the understanding of temporal features. Next, the decoder uses upsampling techniques to gradually reconstruct the advanced features extracted by the encoder, restore detailed information, and ultimately generate an output that is consistent with the original input data. In addition, in the EDH-STNet model, skip connections are used to integrate the features of different levels of the encoder with the features upsampled by the decoder.

3.2.3. Remote Sensing Inversion

The remote sensing inversion method of the atmospheric refractive index refers to the method of indirectly estimating and inverting the atmospheric profile structure by evaluating the degree of influence of the refractive index structure on the characteristic physical quantities of the EM signal. By using different types of EM signals and different affected characteristic physical quantities as detection tools, many specific *M* profile inversion techniques and methods have been proposed [29]. In essence, the rough sea surface can induce reflection and scattering effects on EM waves. Therefore, the reflection and scattering signals from the rough sea surface can be effectively utilized for inversion. The technique of retrieving the *M* profile from sea clutter (referred to as RFC) was first proposed around 1997 by the Space and Naval Warfare Systems Center [29]. The motivation behind this proposal was to develop a method for detecting the marine refractive structure without the need for specialized measurement equipment. RFC technology leverages sea clutter obtained from the normal operation of land-based and shipborne radar systems. Using effective inversion models and algorithms, it inverts the *M* profile parameters within the radar's detection range. This process relies on the close mapping relationship between sea clutter and the atmospheric environment, as sea clutter is influenced by the refractive index conditions (see Figure 12). Fundamentally, the RFC technique constitutes an optimization process that iteratively compares measured radar sea clutter data with forward-modeled clutter simulations. The optimal atmospheric refractivity profile parameters are determined when the highest consistency between these two datasets is achieved. These derived parameters (single or multiple) are then utilized to reconstruct the actual (retrieved) tropospheric refractivity spatial structure through an appropriate refractive index profile model. Richter [90] highlighted the close relationship between the variations in radar echoes and refractivity profiles, while the calculations of radar sea clutter characteristics in atmospheric ducts by Reilly [44] and Pappert [71] further substantiate the feasibility of RFC.

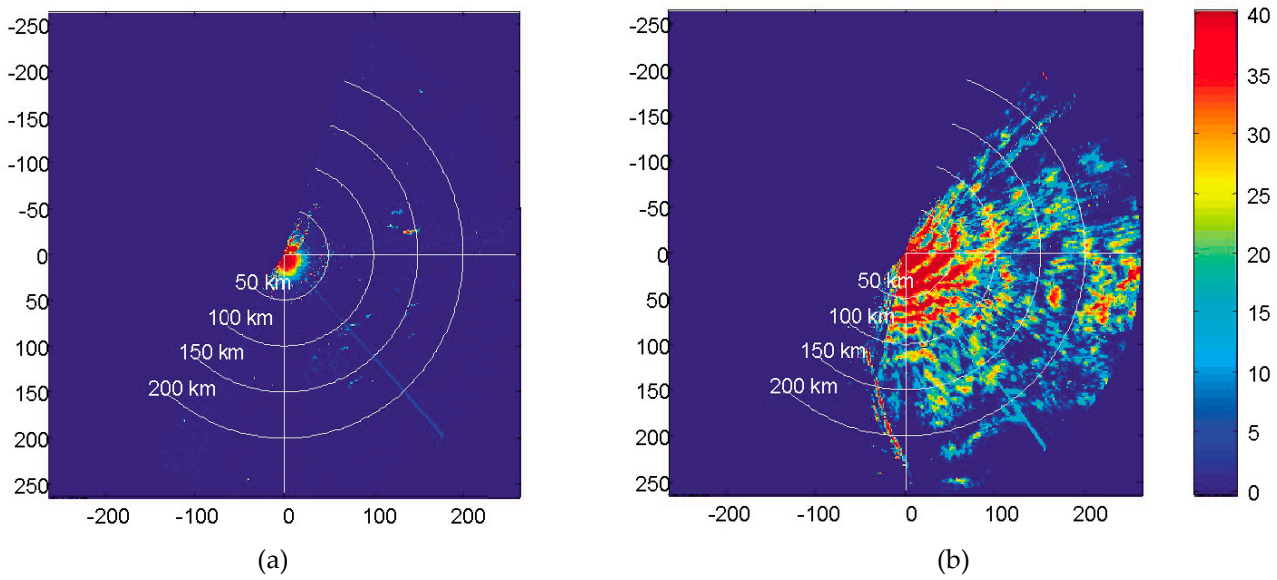


Figure 12. Radar PPI screen showing clutter map (dB) during the 1998 SPANDAR experiment resulting from a (**a**) weak evaporation duct, (**b**) surface-based duct [32].

Compared to direct observations and other indirect methods, RFC offers the following key advantages:

- Beyond sea clutter, RFC does not require additional equipment to measure meteorological data. By establishing an appropriate inversion model, the *M* profile can be retrieved solely from the sea clutter, making the method cost-effective and straightforward.
- The RFC approach can obtain the cumulative refractive effects over the entire detection range and all radar azimuths. In contrast, other methods typically provide vertical *M* profiles at specific locations.
- By modeling regional inhomogeneities, RFC enables the inversion of distance-dependent *M* profiles, providing a spatial distribution of the refractive index across the entire detection space.
- Since the implementation of RFC is generally in real time or near real time, it allows for the dynamic tracking of *M* profiles, capturing temporal and spatial variations.

Due to its advantages, RFC technology has been widely adopted since its introduction, with the fundamental implementation process illustrated in the accompanying Figure 13. Initially, Krolik et al. [370] employed the Maximum A Posteriori (MAP) algorithm to jointly invert the atmospheric refractive index and spatially varying sea surface scattering coefficients. In this approach, the vertical atmospheric refractive index was modeled using two parameters, while the horizontal direction was represented by a single parameter. The primary limitation of this inversion method lies in its capability to retrieve only linearly varying refractive index profile parameters. This Wallops '98 experiment involved the use of helicopters to measure refractive index profiles and the deployment of a Microwave Propagation Measurement System (MPMS) to collect sea clutter data from an S-band Space Range Radar (SPANDAR). The data acquired during this experiment provided significant support for subsequent studies on RFC technology. To comprehensively investigate the feasibility and inversion performance of RFC technology for retrieving actual refractive index profiles, a joint research team comprising the Naval Surface Warfare Center, Dahlgren Division (NSWCDD); the NPS; and the Applied Physics Laboratory of Johns Hopkins University conducted a large-scale field campaign during March–April 1998 at Wallops Island, Virginia [66] (geographic location depicted in Figure 6). The experiment simultaneously acquired (1) tropospheric refractivity profiles via helicopter-borne sensors, and (2) radar

propagation data using the S-band Space Range Radar (SPANDAR) integrated with the Microwave Propagation Measurement System (MPMS). The collected meteorological and EM propagation datasets were specifically designed for RFC inversion algorithm validation. This foundational experiment subsequently catalyzed international efforts to refine RFC implementation methodologies, with numerous research institutions advancing its operational frameworks [19,23,25,29,31,32,73,371–377].

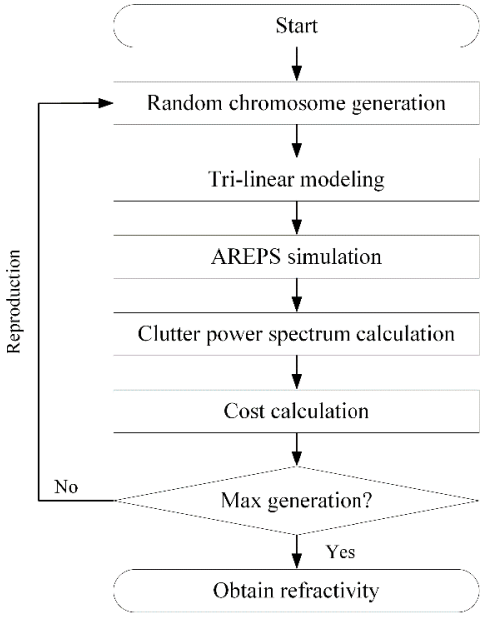


Figure 13. GA process for estimating atmospheric refractivity [378].

Following initial developments, researchers have further investigated the methods of implementing RFC [190]. They have employed various techniques to invert *M* profiles, including (1) intelligent optimization algorithms, such as least squares optimization [66,105,159,162], simulated annealing [31,209,379], genetic algorithms [31,55,63,210,211,215,221], particle swarm optimization [158,164,180,184,261,379–383], the artificial bee colony algorithm [384], the immune algorithm [235], the cuckoo search algorithm [225], and colony optimization [385], as well as improved algorithms based on these methods [114,134,138,142,145,148,157,212,222,224,225,261,386–389] and hybrid algorithms [232,390]; (2) statistical methods, including sequence importance sampling [372], Gaussian process regression [50], particle filtering algorithms [195,218], Kalman filtering [32,377], and Bayesian algorithms [85,216,223,248,373,375,391,392], along with improved algorithms based on these approaches [143,217,376]; and (3) other numerous methods [52,53,79,196–198,203–205,207,208,210,211,213,219,220,227,308,311,381]. In addition to inversion methods, researchers have introduced several new strategies in areas such as sea clutter models, refractive index profiles, regional heterogeneity, and objective functions to improve inversion accuracy. In RFC technology, the PE method is typically employed to assess the intensity of radar sea clutter signals in a tropospheric duct. However, some studies also use the ray density of signals to represent signal strength [79,210,211]. To address the impact of grazing angle on sea clutter power modeling, researchers investigated incorporating the grazing angle information into the clutter model and proposed a clutter model based on multiple incident angles at each range [20,30]. In real atmospheric conditions, the *M* profile is often range-dependent. To reduce the degrees of freedom of the vertical *M* profile parameters at different ranges, researchers have explored various dimensionality reduction algorithms, including Markov models [372] and Karhunen–Loeve models [393]. The objective function used to assess the matching between measured

and simulated sea clutter is typically based on the least squares criterion [66]. Alternatively, some researchers have employed objective functions based on rank correlation methods [79,211]. More recently, an adaptive objective function with linear range weighting has been proposed, which reduces the contribution of sea clutter with high CNR at long ranges [162].

Moreover, researchers have proposed several innovative approaches to overcome the limitations of single data sources. These include the integration of sea clutter data from multiple frequencies [134,160,387,389], multiple elevation angles [19], and multiple antenna heights [47,97,134,159,184,197,207,209]. Researchers have refined the traditional PJ model by incorporating additional parameters to enhance its representational capacity, allowing for a more accurate description of complex *M* structures, with the two-piece modified model [317], three-parameter model [56], four-parameter model [161], and hybrid model [31]. In addition, the efficiency and accuracy of the inversion algorithm can be improved by pre-preparing a library of sea clutter under different ducting environments [52,309,310]. Meanwhile, incorporating prior meteorological information about the duct parameters [19,23,32,248,308] can further enhance its performance. As RFC technology continues to evolve, the range of signal sources used for inversion has become increasingly diverse. These sources now not only encompass traditional sea clutter signals but also extend to include Global Navigation Satellite System (GNSS) occultation signals [134,138,142,165,166,179,214,257,258,277,394–396], GNSS surface scattering signals [158,163,192,397], Automatic Identification System (AIS) signals [174,230,232,234,261,381,383,392], point-to-point (PTP) propagation measurements (PLs) [22,27,28,53,55,63,97,114,197,207,208,225,398,399], weather radar echoes [180,400], lidar signals [401–405], etc. Each signal source has a unique role and advantage in the process of atmospheric duct inversion, and can provide different types of information.

The rapid development and widespread application of AI have led to its integration in atmospheric duct inversion, improving both accuracy and efficiency. Internationally, Douvenot et al. [309,310,406–408] were among the pioneers in applying machine learning (ML) techniques from AI to the inversion of tropospheric refractivity profiles. In early work, Douvenot et al. [310] employed the least squares support vector machine (LS-SVM) method to invert the surface-based duct parameters. By utilizing a Gaussian kernel function and a pre-generated training database, the LS-SVM method significantly accelerated the inversion process. Although the accuracy was slightly lower than that of GA, the results demonstrated the feasibility of real-time inversion using the LS-SVM method. The results of the inversion of evaporation ducts indicate that, compared to quadratic regression, LS-SVM achieves similar prediction accuracy but offers greater reliability [309]. Douvenot et al. [407,408] also compared the performance of GA, LS, LSSVM and multi-task LSSVM (MuLS-SVM) in surface-based duct inversion. While GA achieved high accuracy, it required a longer inversion time. In contrast, the accuracy of LS, LS-SVM, and MuLS-SVM was sufficient for RFC applications. Therefore, Douvenot et al. [407,408] concluded that LS, LS-SVM and MuLS-SVM, when based on a pre-generated database, were more suitable for RFC. The advantage of MuLS-SVM over LS-SVM was its ability to retrieve all three parameters of the surface-based duct simultaneously. As a result, MuLS-SVM demonstrated higher efficiency than LS-SVM when applied to measured data. Later, Yang [409] compared the inversion performance of the relevance vector machine (RVM), radial basis function (RBF) network, and LS-SVM method for evaporation ducts. The inversion results show that the LS-SVM method has the highest accuracy, and the performance of the RVM is basically the same as that of the RBF network.

Recently, more researchers have turned to deep learning (DL) with unique architectures and high efficiency. Guo et al. [155] generated sea clutter and used it for retrieving

evaporation ducts and surface-based ducts using a deep neural network (DNN). Compared with GA and neural networks, the DNN has higher accuracy and efficiency. Subsequently, researchers began exploring and studying various artificial intelligence (AI)-based atmospheric duct inversion methods, including but not limited to artificial neural network (ANN) [329], random forest [410], K-nearest neighbor [410], and Multilayer Perceptron (MLP) [230,397]. To better adapt to diverse marine environments and inversion demands, researchers have innovatively refined traditional DL methods, resulting in novel inversion models. Before atmospheric duct parameter inversion, determining the duct type is crucial for accurate results. Han et al. [174] proposed a method combining AI and AIS signals for atmospheric duct classification and inversion, enabling a two-step process of classification followed by inversion. Subsequently, they observed that traditional DL loss functions use the same weight coefficients for different duct parameters. To address this, they introduced a weighted loss function and a method for determining coefficients based on the extended Fourier amplitude sensitivity [179]. Additionally, they developed a collaborative inversion model for duct parameters using GNSS occultation signals. Due to weak sea clutter at longer ranges, which is often overwhelmed by noise, inversion information is limited, while over-the-horizon target echoes have stronger power. To overcome this, Ji et al. [249] developed a joint inversion model for evaporation ducts using a dual-stream DNN architecture, combining sea clutter and target echoes, and significantly improving inversion accuracy. Considering the impact of range-dependent surface-based ducts on inversion, Wu et al. [256] first designed a one-dimensional residual dilated causal convolution autoencoder to extract feature representations from high-dimensional *M* profile parameters. They then proposed a fully coupled convolutional Transformer inversion model, enabling high-precision inversion of surface-based ducts. In 2025, Ji et al. [190] proposed a dual-stream Transformer and Gramian angular field (GAF) collaborative framework (termed RFCFormer, illustrated in Figure 14) to address the need for precise duct profile parameter characterization. This innovative approach transforms sea clutter data into sparse GAF matrices, which enhances the model's capability to identify latent patterns and improves the accuracy of feature-to-parameter mapping.

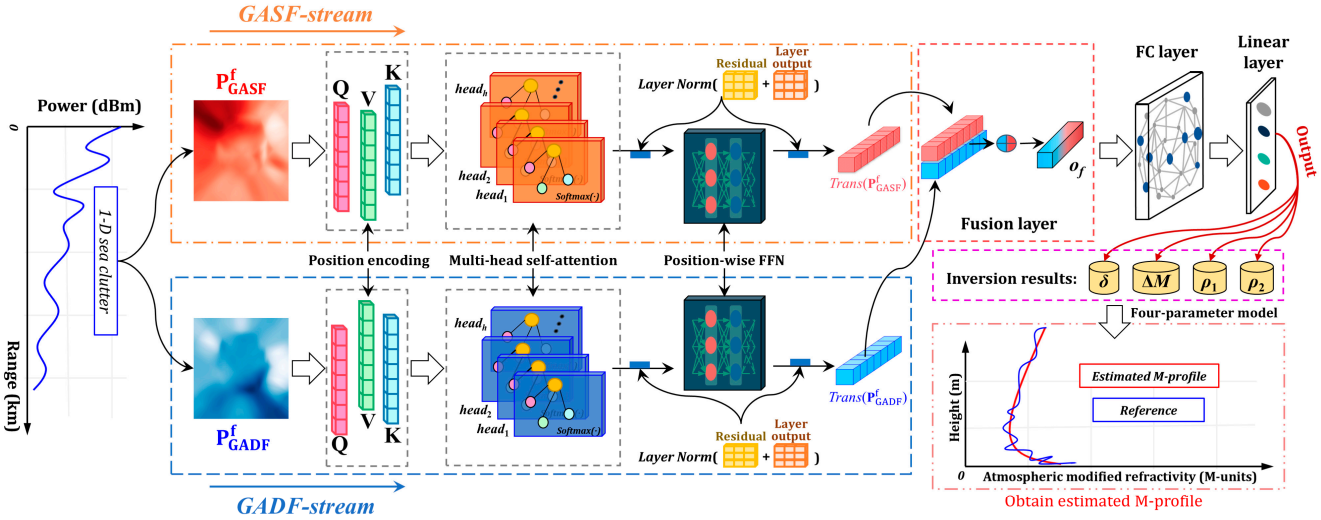


Figure 14. RFCFormer [190]. This model takes 1D radar sea clutter as input and transforms it into two spatially distributed 2D matrices ($\mathbf{P}^{f}_{GASF}$ and $\mathbf{P}^{f}_{GADF}$) using GAF-based Gramian Angular Sum Field (GASF) and Gramian Angular Difference Field (GADF). These matrices are processed through a dual-stream Transformer architecture, where positional encoding, multi-head attention mechanisms, and feedforward neural network (FFN) extract hierarchical features, followed by feature fusion in a

dedicated fusion layer. The fused features undergo high-order nonlinear transformation via fully connected (FC) layer, culminating in a linear output layer that predicts four duct parameters. These parameters are subsequently fed into a four-parameter evaporation duct model to reconstruct the duct profile.

4. Future Perspectives of Atmospheric Duct Sensing

4.1. Synergetic Observation with Multi-Source and Multi-Site Signals

Currently, with the continuous advancement in technology, various active atmospheric duct detection and monitoring methods have become increasingly mature and are constantly improving. These methods mainly include model estimation algorithms based on physical mechanisms and numerical weather prediction assimilation techniques relying on high-performance computing. Meanwhile, passive inversion methods have also made significant progress, especially the technology of inverting using multi-source signals obtained from distributed sensing station networks, including but not limited to radar sea clutter, GPS signals, AIS ship signals, etc. However, it should be noted that most existing studies focus on the independent application and optimization of a single technology. Although this research paradigm can deeply explore the potential of specific technologies, it inevitably has inherent methodological limitations. For example, model estimation methods are limited by the accuracy of initial and boundary conditions, numerical prediction methods have extremely high requirements for computing resources and have issues with prediction timeliness, and passive inversion methods are susceptible to observation environment noise and uneven distribution of signal sources. When these technologies develop to a certain stage, they will face insurmountable performance bottlenecks.

In previous studies, Ji et al. [249] proposed an evaporation duct inversion method utilizing radar sea clutter and target echoes. By integrating information from both sources, this approach significantly enhances inversion accuracy. Specifically, target echoes supplement additional data, mitigating the precision degradation caused by low signal-to-clutter ratios in sea clutter, thereby improving atmospheric duct retrieval performance compared to sea-clutter-only methods. Therefore, the future development direction should focus on the deep fusion and collaborative processing of multi-source heterogeneous data obtained from active detection and passive inversion. This fusion not only includes temporal–spatial registration and quality control at the data level but also requires innovative breakthroughs at the algorithm level such as feature extraction, information complementation, and uncertainty quantification. By constructing an active–passive collaborative three-dimensional sensing network, the complementary advantages of different technical means can be fully utilized, ultimately achieving a more comprehensive, accurate three-dimensional characterization and real-time monitoring of atmospheric duct structures. The practice of this collaborative sensing concept has important strategic value for improving the effectiveness of military applications.

4.2. Optimization of Regional Heterogeneous Atmospheric Duct Sensing

The intensity of tropospheric atmospheric ducts is quantified through the atmospheric refractive index, a parameter fundamentally governed by meteorological variables, including temperature, humidity, and pressure. Given the divergent atmospheric conditions over different oceanic regions, the spatial distribution of these physical parameters in the troposphere exhibits intrinsic inhomogeneity. Across vast marine areas, distinct climatic regimes—such as the humid tropics and arid subtropical highs—generate pronounced variations in background meteorological fields. This heterogeneity drives altitude- and range-dependent fluctuations in the refractive index, which collectively manifest as two defining characteristics of marine tropospheric ducts: (1) regionality, evidenced by system-

atic differences in duct occurrence frequency, intensity, and vertical structure; and (2) horizontal non-uniformity, where kilometer-scale refractivity gradients arise from mesoscale air–sea interactions. Microwave refractometer-derived atmospheric refractivity profiles from the Wallops '98 helicopter campaign are presented in Figure 15. The refractive index profile may demonstrate stratified gradients vertically while exhibiting front-like discontinuities horizontally, particularly across ocean current boundaries. These multidirectional variations constitute an inherent property of marine atmospheric ducts. Propagation loss patterns induced by inhomogeneous ducting exhibit distinct spatial variations compared to uniform ducts [350]. This necessitates studying radio wave propagation in such environments to evaluate radar performance, especially for detection range calibration and target localization in complex marine atmospheres.

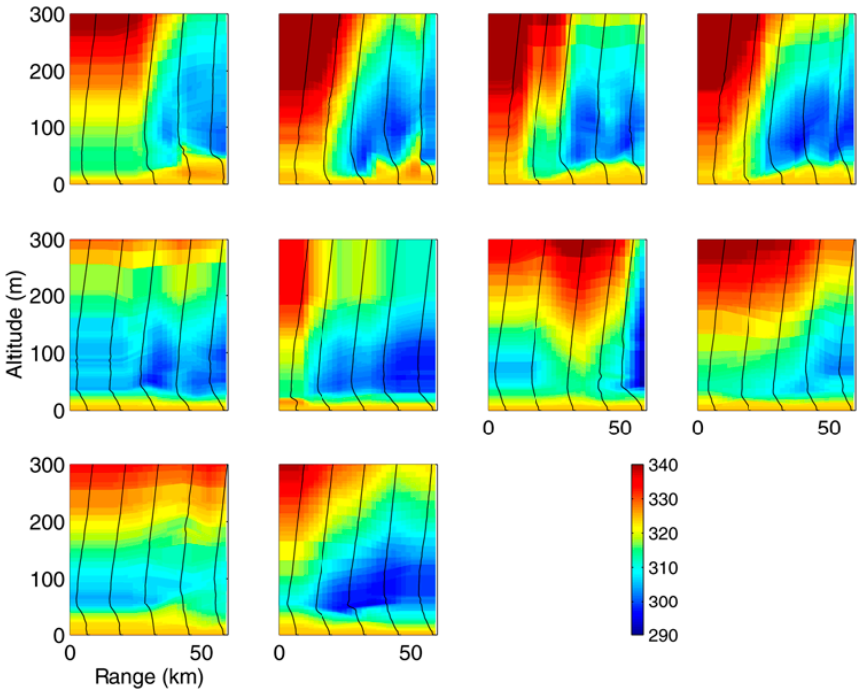


Figure 15. Chronologically ordered *M* profiles from Wallops '98 experiment. The first row is observed from 8:47 to 10:26 EST (08:47–09:05, 09:07–09:32, 09:33–09:57, and 09:58–10:26), the middle from 12:26 to 14:15 EST (12:26–12:50, 12:52–13:17, 13:19–13:49, and 13:51–14:14), and the bottom from 16:00 to 16:52 EST (15:59–16:27 and 16:29–16:52) [31].

Recent advances in marine EM wave propagation research underscore the critical impacts of atmospheric duct horizontal heterogeneity on communication/radar systems [363], driving significant scientific interest [129,411,412]. From a theoretical perspective, comprehensive characterization of the heterogeneous features of atmospheric ducts requires dense observational arrays in both horizontal and vertical dimensions, utilizing synchronized deployments of instruments such as radiosondes and microwave radiometers to acquire spatially distributed temperature, humidity, and pressure profiles. However, significant practical challenges persist in field implementation. Alternatively, two primary indirect sensing approaches exist: (1) inversion of inhomogeneous duct structures through radar-received EM signals [19,20,29,198,212,223,248,350], and (2) numerical modeling-based reconstruction leveraging reanalysis datasets or theoretical calculations to derive spatiotemporal characteristics of regional duct phenomena [106,107,125,129,344,347,411,412].

Both methodologies exhibit inherent limitations. For radar signal inversion, three primary constraints exist: (1) strong data dependency requiring high-quality radar echoes that are susceptible to marine environmental interference and sensitive to radar param-

eters (e.g., frequency, polarization), with inversion accuracy degrading significantly under low signal-to-noise ratio (SNR) conditions; (2) model simplification errors, where parametric duct assumptions (e.g., linear–log profiles) often neglect small-scale atmospheric perturbations, introducing systematic deviations from true duct structures; and (3) high computational complexity, with horizontally heterogeneous ducts demanding increased inversion parameters, exacerbating computational burdens, local optima traps, and real-time processing challenges. Regarding numerical modeling, key shortcomings include (1) initial field inaccuracies, with reliance on sparse marine meteorological observations (e.g., radiosondes, satellite data) reducing simulation fidelity in data-scarce regions; (2) over-simplified physics, with boundary-layer parameterizations (e.g., turbulence, moist processes) inadequately resolving fine-scale duct features; and (3) resolution constraints, where insufficient horizontal/vertical resolution fails to capture critical small-scale duct variability despite mesh-nesting advancements.

Therefore, future research should prioritize breakthroughs in high-precision sensing technologies for regionally inhomogeneous atmospheric ducts and establish a multi-source sensing fusion system. This system integrates satellite remote sensing (e.g., high-resolution microwave radiometers), UAV-mounted sensors (e.g., micro-sondes), and marine buoy arrays to achieve three-dimensional stereoscopic monitoring of atmospheric duct structures. For instance, GNSS radio occultation can retrieve vertical refractivity profiles, while UAV swarms conduct horizontal dense sampling to address spatial coverage limitations of traditional point-based observations. Concurrently, the development of low-power, highly integrated micro-meteorological sensors capable of synchronous multi-parameter measurements (temperature, humidity, pressure, and refractivity) is essential. Furthermore, machine learning algorithms should be incorporated to dynamically adjust sampling frequencies and observation locations based on duct evolution characteristics, enabling adaptive dense monitoring in critical zones such as land–sea interfaces and frontal activity regions.

4.3. Application of Large Weather Models

There have been some research advancements in marine atmospheric duct forecasting. However, existing forecasting methods still struggle to achieve comprehensive coverage and high accuracy. Moreover, the formation of atmospheric ducts is influenced by a complex interplay of various factors, such as the structure of the ocean–atmosphere boundary layer and air–sea interactions, making precise forecasting a challenging task. In recent years, the intersection of "AI + weather" has garnered significant attention, emerging as a pivotal approach to enhance both the accuracy and efficiency of weather forecasting. Large AI models, particularly those based on diverse deep learning architectures, leverage substantial computational resources and vast meteorological datasets [413], continuously refining their predictive capabilities during training. These deep learning models are adept at capturing intricate meteorological patterns and nonlinear relationships, offering distinct advantages in weather prediction. Unlike traditional numerical weather prediction models, AI-driven models can forecast without relying on conventional physical processes, instead utilizing data-driven methods [414]. This paradigm shift in weather forecasting represents a promising new frontier in meteorological science. Recent advancements in large weather models (LWMs), powered by DL, have significantly enhanced weather forecasting accuracy and efficiency. These models, such as FourCastNet [415], GraphCast [416], NowcastNet [417], Pangu Weather [418], FengWu (see Figure 16) [419], and Fuxi [420], underscore the transformative potential of deep learning in the atmospheric sciences. By leveraging vast amounts of meteorological data, these models are reshaping traditional forecasting techniques, enabling better predictive capabilities across both global and local

scales. Therefore, LWMs offer a novel and highly promising technological approach for the forecasting of marine atmospheric ducts.

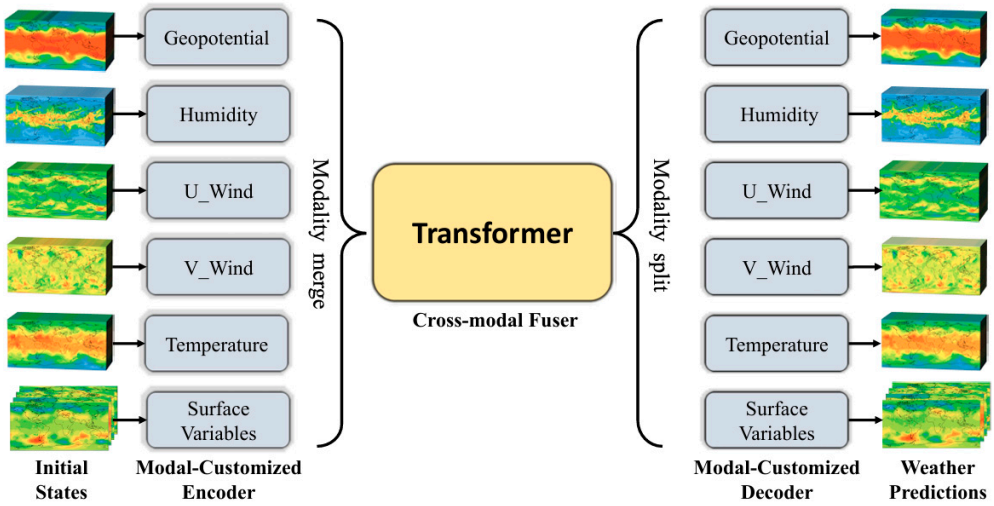


Figure 16. Overview of FengWu LWM [418].

4.4. Atmospheric Duct Interference Mitigation

Atmospheric ducts, as anomalous refractive structures in marine–air boundary layers, significantly alter electromagnetic wave propagation characteristics. They cause differential interference across radio systems, including radar detection, broadband wireless communication, and satellite navigation. Current research follows two parallel technical approaches: advancing duct sensing technologies to overcome spatiotemporal resolution limitations in refractive index retrieval under dynamic boundary layers, enabling precise acquisition of key atmospheric parameters; and developing adaptive interference mitigation solutions tailored to application-specific performance requirements against duct-induced system disturbances [421–423].

To enhance the anti-interference capability of radio equipment in atmospheric ducting environments and mitigate signal interruption or performance degradation, future research on ducting interference mitigation should prioritize the following directions: (1) Cognitive Radio-based Dynamic Frequency Selection: Current radar/communication systems often use fixed frequency bands vulnerable to ducting-induced interference. Implementing lightweight spectrum sensing modules can enable real-time identification of affected bands, dynamically switching to stable non-ducting-sensitive frequencies. This approach supports scenarios like coastal 6G networks and radar arrays. (2) AI-driven Antenna Parameter Optimization: Traditional fixed antenna configurations (height, beam elevation/azimuth) risk signal trapping in ducting layers. AI algorithms can integrate real-time ducting data to autonomously adjust antenna parameters, avoiding ducting-trapped elevation angles. This benefits shipborne radars, coastal base stations, and mobile offshore platforms. (3) Redundant Communication Link Pre-configuration: As a fail-safe solution for severe near-surface ducting, hybrid backup links (e.g., unmanned aerial vehicle relays, satellite communications, or near-vertical incidence skywave transmissions) should be established. With millisecond-level switching latency, critical services can maintain continuity when primary links fail.

5. Conclusions

As a special tropospheric structure, the marine atmospheric duct has attracted much attention due to its significant influence on EM wave propagation and marine detection and

communication systems. In recent years, with the rapid development of ocean observation technologies and the continuous progress of numerical simulation methods, remarkable advances have been made in the research of marine atmospheric ducts. This paper reviews the status and progress of research on the observation of marine atmospheric ducts, with a focus on analyzing the sensing and research methods for three main types: evaporation ducts, elevated ducts, and surface ducts. In the study of evaporation ducts, the development of diagnostic models based on similarity theory and their regional adaptability research have become hot topics. In the research of elevated ducts and surface ducts, the application of mesoscale numerical models has significantly improved the simulation accuracy of atmospheric ducts during specific weather processes, providing an important basis for further analyzing their occurrence patterns and climatic causes. With continuous technological advancements, remote sensing retrieval methods have progressively emerged as a dominant approach in atmospheric duct detection, demonstrating increasingly extensive applications within this field. Looking ahead, the ongoing optimization of remote sensing algorithms will further amplify the pivotal role of these retrieval methods in atmospheric duct characterization. In addition, by combining AI technology, researchers have gradually achieved high-precision quantitative research on marine atmospheric ducts. In the future, with the further development of AI, the internet of things, and autonomous sensing systems, the research on marine atmospheric ducts will place more emphasis on the integration and intelligent analysis of multi-source data, aiming to provide more scientific support for marine environmental monitoring, communication system optimization, and climate change research.

Author Contributions: Conceptualization, H.-J.J.; methodology, J.-P.Z.; formal analysis, Y.-J.L.; investigation, H.-Y.P.; resources, X.-M.G.; data curation, Y.-S.Z.; writing—original draft preparation, J.-P.Z.; writing—review and editing, H.-J.J.; visualization, H.-Y.P.; project administration, Y.-J.L.; funding acquisition, J.-P.Z. All authors have read and agreed to the published version of the manuscript.

Funding: This work was supported in part by the National Natural Science Foundation of China (Grant Nos. 625B2136, 62231021, U254120011, U21A20457), in part by the National Key Laboratory Foundation of Electromagnetic Wave Propagation (Grant No. 6142403240201), and in part by the Stabled-Support Scientific Project of China Research Institute of Radiowave Propagation (Grant No. A132301214).

Data Availability Statement: No new data were created or analyzed in this study. Data sharing is not applicable to this article.

Acknowledgments: The authors hereby express profound respect to all researchers dedicated to tropospheric ducting sensing studies. We are deeply grateful for the unwavering support and generous assistance from colleagues during the preparation of this work. Special acknowledgment is extended to scholars whose foundational research—whether directly or indirectly referenced—has contributed essential theoretical frameworks to this study. Should any relevant publications have been inadvertently overlooked in our citations, we sincerely apologize to the affected researchers. We also extend heartfelt gratitude to the peer reviewers for their invaluable critiques and time invested in evaluating this manuscript.

Conflicts of Interest: The authors declare no conflicts of interest.

References

1. Hitney, H.V.; Richter, J.H.; Pappert, R.A.; Anderson, K.D.; Baumgartner, G.B. Tropospheric radio propagation assessment. *Proc. IEEE* **1985**, *73*, 265–283. [CrossRef]
2. Turton, J.D.; Bennetts, D.A.; Farmer, S.F.G. An introduction to radio ducting. *Meteorol. Mag.* **1988**, *117*, 245–254.
3. Kerr, D.E. *Propagation of Short Radio Waves*; McGraw-Hill: London, UK; New York, NY, USA, 1951.

4. Du Castel, F.; Sofaer, E.; Wait, J.R. *Tropospheric Radiowave Propagation Beyond the Horizon*; Pergamon Press: New York, NY, USA; Oxford, UK, 1966.
5. Paulus, R.A. VOCAR: An Experiment in Variability of Coastal Atmospheric Refractivity. In Proceedings of the IGARSS '94—1994 IEEE International Geoscience and Remote Sensing Symposium, Pasadena, CA, USA, 8–12 August 1994; Volume 1, pp. 386–388.
6. Katzin, M.; Bauchman, R.W.; Binnian, W. 3- and 9-Centimeter Propagation in Low Ocean Ducts. *Proc. IRE* **1947**, *35*, 891–905. [CrossRef]
7. Baumgartner, G.B.J.; Hitney, H.V.; Pappert, R.A. Duct Propagation Modelling for the Integrated-Refractive-Effects Prediction System (IREPS). *IEE Proc. F Commun. Radar Signal Process.* **1983**, *130*, 630–642. [CrossRef]
8. Patterson, W.L.; Hattan, C.P.; Hitney, H.V.; Paulus, R.A.; Lindem, G.E. Engineer's Refractive Effects Prediction System (EREPS) Version 3.0. NASA STI/Recon Technical Report. 1994, p. 95. Available online: https://api.semanticscholar.org/CorpusID:108549202 (accessed on 1 May 1994).
9. Rogers, L.T.; Anderson, K.D. *Evaporation Duct Communication: Measurement Results*; Naval Command, Control and Ocean Surveillance Center, RDT&E Division: San Diego, CA, USA, 1993. Available online: https://api.semanticscholar.org/CorpusID:108271386(1993) (accessed on 20 May 2026).
10. Anderson, K.D. Radar Detection of Low-Altitude Targets in a Maritime Environment. *IEEE Trans. Antennas Propag.* **1995**, *43*, 609–613. [CrossRef]
11. Patterson, W.L. Advanced Refractive Effects Prediction System (AREPS). In Proceedings of the 2007 IEEE Radar Conference, Waltham, MA, USA, 17–20 April 2007; pp. 891–895.
12. Kang, S.; Zhang, Y.; Wang, H. *Tropospheric Duct*; Science Press: Beijing, China, 2014.
13. Vilar, E.; Austin, J.; Tawfik, A.N.; Wan, K.W.; Lam, W.K.; Shen, X. Narrow and Wide Band Transhorizon Propagation Studies at X Band. In Proceedings of the 1993 International Symposium on Radio Propagation (ISRP'93), Beijing, China, 18–21 August 1993; pp. 89–92.
14. Haddad, H.; Chang, D.C. Transient Electromagnetic Field Generated by a Vertical Electric Dipole on the Surface of a Dissipative Earth. *Radio Sci.* **1981**, *16*, 169–177. [CrossRef]
15. Battaglia, M.R. *Modelling the Radar Evaporative Duct*; Weapons Systems Research Laboratory, Defence Science and Technology Organization: Edinburgh, Australia, 1984. Available online: https://api.semanticscholar.org/CorpusID:129285486 (accessed on 1 April 1985).
16. Heemskerk, H.J.M.; Boekema, R.B. The Influence of Evaporation Duct on the Propagation of Electromagnetic Waves Low above the Sea Surface at 3–94 GHz. In Proceedings of the Eighth International Conference on Antennas and Propagation, Edinburgh, UK, 30 March–2 April 1993; pp. 348–351.
17. Sarma, S.B.S.S.; Reddy, B.M. Development and Evaluation of Airborne Microwave Refractometer for Studies on Atmospheric Tropical Boundary Layer Radiorefractive Index. *Ann. Geophys.* **1994**, *12*, 785–793. [CrossRef]
18. Yardim, C.; Gerstoft, P.; Hodgkiss, W.S.; Rogers, T. Statistical Estimation of Refractivity from Radar Sea Clutter. In Proceedings of the 2007 IEEE Radar Conference, Waltham, MA, USA, 17–20 April 2007; pp. 938–943.
19. Gerstoft, P.; Rogers, L.T.; Hodgkiss, W.S.; Wagner, L.J. Refractivity Estimation Using Multiple Elevation Angles. *IEEE J. Ocean. Eng.* **2003**, *28*, 513–525. [CrossRef]
20. Karimian, A.; Yardim, C.; Hodgkiss, W.S.; Gerstoft, P.; Barrios, A.E. Estimation of Radio Refractivity Using a Multiple Angle Clutter Model. *Radio Sci.* **2012**, *47*, RS0M07. [CrossRef]
21. Karimian, A.; Yardim, C.; Haack, T.; Gerstoft, P.; Hodgkiss, W.S.; Rogers, T. Toward the Assimilation of the Atmospheric Surface Layer Using Numerical Weather Prediction and Radar Clutter Observations. *J. Appl. Meteorol. Climatol.* **2013**, *52*, 2345–2355. [CrossRef]
22. Gerstoft, P.; Gingras, D.F.; Rogers, L.T.; Hodgkiss, W.S. Estimation of Radio Refractivity Structure Using Matched-Field Array Processing. *IEEE Trans. Antennas Propag.* **2000**, *48*, 345–356. [CrossRef] [PubMed]
23. Yardim, C.; Gerstoft, P.; Hodgkiss, W.S. Sensitivity Analysis and Performance Estimation of Refractivity from Clutter Techniques. *Radio Sci.* **2009**, *44*, RS1008. [CrossRef]
24. Brooks, I.M. Air-Sea Interaction and Spatial Variability of the Surface Evaporation Duct in a Coastal Environment. *Geophys. Res. Lett.* **2001**, *28*, 2009–2012. [CrossRef]
25. Yardim, C. Statistical Estimation and Tracking of Refractivity from Radar Clutter. Ph.D. Thesis, University of California, San Diego, CA, USA, 2007.
26. Brooks, I.M.; Goroch, A.K.; Rogers, D.P. Observations of Strong Surface Radar Ducts over the Persian Gulf. *J. Appl. Meteorol.* **1999**, *38*, 1293–1310. [CrossRef]
27. Wagner, M.; Gerstoft, P.; Rogers, T. Estimating Refractivity from Propagation Loss in Turbulent Media. *Radio Sci.* **2016**, *51*, 1876–1894. [CrossRef]
28. Matsko, I.J.; Hackett, E.E. Impact of Radar Data Sampling on the Accuracy of Atmospheric Refractivity Inversions Over Marine Surfaces. *Radio Sci.* **2019**, *54*, 704–714. [CrossRef]

29. Karimian, A.; Yardim, C.; Gerstoft, P.; Hodgkiss, W.S.; Barrios, A.E. Multiple Grazing Angle Sea Clutter Modeling. *IEEE Trans. Antennas Propag.* **2012**, *60*, 4408–4417. [CrossRef]
30. Gerstoft, P.; Rogers, L.T.; Krolik, J.L.; Hodgkiss, W.S. Inversion for Refractivity Parameters from Radar Sea Clutter. *Radio Sci.* **2003**, *38*, 8053. [CrossRef]
31. Yardim, C.; Gerstoft, P.; Hodgkiss, W.S. Tracking Refractivity from Clutter Using Kalman and Particle Filters. *IEEE Trans. Antennas Propag.* **2008**, *56*, 1058–1070. [CrossRef]
32. Karimian, A.; Yardim, C.; Gerstoft, P.; Hodgkiss, W.S.; Barrios, A.E. Refractivity Estimation from Sea Clutter: An Invited Review. *Radio Sci.* **2011**, *46*, RS6013. [CrossRef]
33. Babin, S.M.; Miller, R.E.; Rowland, J.R. A High-Power, Dual-Frequency Monostatic Acoustic Sounder for Studying the Atmospheric Boundary Layer. *J. Atmos. Ocean. Technol.* **1993**, *10*, 486–492. [CrossRef]
34. Babin, S.M. Development and Experimental Evaluation of Oceanic Evaporation Duct Models Based on the LKB Approach. Master's Thesis, University of Maryland, College Park, MD, USA, 2001. Available online: https://api.semanticscholar.org/CorpusID:27933845 (accessed on 30 September 1999).
35. Babin, S.M.; Rowland, J.R. Observation of a Strong Surface Radar Duct Using Helicopter Acquired Fine-Scale Radio Refractivity Measurements. *Geophys. Res. Lett.* **1992**, *19*, 917–920. [CrossRef]
36. Rowland, J.R.; Babin, S.M. Fine-Scale Measurements of Microwave Refractivity Profiles with Helicopter and Low-Cost Rocket Probes. *Johns Hopkins APL Tech. Dig.* **1987**, *8*, 413–417.
37. Babin, S.M.; Dockery, G.D. LKB-Based Evaporation Duct Model Comparison with Buoy Data. *J. Appl. Meteorol.* **2002**, *41*, 434–446. [CrossRef]
38. Babin, S.M.; Young, G.S.; Carton, J.A. A New Model of the Oceanic Evaporation Duct. *J. Appl. Meteorol.* **1997**, *36*, 193–204. [CrossRef]
39. Joseph, R.I.; Smith, G.D. Propagation in an Evaporation Duct: Results in Some Simple Analytic Models. *Radio Sci.* **1972**, *7*, 433–441. [CrossRef]
40. Goldhirsh, J.; Dockery, G.D. Propagation Measurements and Modeling at C Band for Over-the-Water, Line-of-Sight Propagation Links in the Mid-Atlantic Coast. *Radio Sci.* **1991**, *26*, 671–690. [CrossRef]
41. Goldhirsh, J.; Musiani, B.H. Signal Level Statistics and Case Studies for an Over-the-Horizon Mid-Atlantic Coastal Link Operating at C-Band. *Radio Sci.* **1999**, *34*, 355–370. [CrossRef]
42. Pidgeon, V.W. Frequency Dependence of Radar Ducting. *Radio Sci.* **1970**, *5*, 541–549. [CrossRef]
43. Babin, S.M. A Case Study of Subrefractive Conditions at Wallops Island, Virginia. *J. Appl. Meteorol.* **1995**, *34*, 1028–1038. [CrossRef]
44. Reilly, J.P.; Dockery, G.D. Influence of Evaporation Ducts on Radar Sea Return. *IEE Proc. F Radar Signal Process.* **1990**, *137*, 80–88. [CrossRef]
45. Compaleo, J.; Yardim, C.; Xu, L. Refractivity-From-Clutter Capable, Software-Defined, Coherent-on-Receive Marine Radar. *Radio Sci.* **2021**, *56*, e2020RS007173. [CrossRef]
46. Xu, L.; Yardim, C.; Haack, T. Evaluation of COAMPS Boundary Layer Refractivity Forecast Accuracy for 2–40 GHz Electromagnetic Wave Propagation. *Radio Sci.* **2022**, *57*, e2021RS007404. [CrossRef]
47. Pozderac, J.; Johnson, J.; Yardim, C.; Merrill, C.; de Paolo, T.; Terrill, E.; Ryan, F.; Frederickson, P. X-Band Beacon-Receiver Array Evaporation Duct Height Estimation. *IEEE Trans. Antennas Propag.* **2018**, *66*, 2545–2556. [CrossRef]
48. Wang, Q.; Burkholder, R.J.; Yardim, C.; Xu, L.; Pozderac, J.; Christman, A.; Fernando, H.; Alappattu, D.P.; Wang, Q. Range and Height Measurement of X-Band EM Propagation in the Marine Atmospheric Boundary Layer. *IEEE Trans. Antennas Propag.* **2019**, *67*, 4880–4893. [CrossRef]
49. Sit, H.; Earls, C.J. Deep Learning for Classifying and Characterizing Atmospheric Ducting within the Maritime Setting. *Comput. Geosci.* **2021**, *157*, 104919. [CrossRef]
50. Sit, H.; Earls, C.J. Gaussian Process Regression for Estimating EM Ducting within the Marine Atmospheric Boundary Layer. *Radio Sci.* **2020**, *55*, e2019RS006890.
51. Sit, H.; Earls, C.J. Characterizing Evaporation Ducts within the Marine Atmospheric Boundary Layer Using Artificial Neural Networks. *Radio Sci.* **2019**, *54*, 1181–1191. [CrossRef]
52. Fountoulakis, V.; Earls, C. Duct Heights Inferred from Radar Sea Clutter Using Proper Orthogonal Bases. *Radio Sci.* **2016**, *51*, 1614–1626. [CrossRef]
53. Fountoulakis, V.; Earls, C. Inverting for Maritime Environments Using Proper Orthogonal Bases from Sparsely Sampled Electromagnetic Propagation Data. *IEEE Trans. Geosci. Remote Sens.* **2016**, *54*, 7166–7176. [CrossRef]
54. Gilles, M.A.; Earls, C.; Bindel, D. A Subspace Pursuit Method to Infer Refractivity in the Marine Atmospheric Boundary Layer. *IEEE Trans. Geosci. Remote Sens.* **2019**, *57*, 5606–5617. [CrossRef]
55. Penton, S.E.; Hackett, E.E. Rough Ocean Surface Effects on Evaporative Duct Atmospheric Refractivity Inversions Using Genetic Algorithms. *Radio Sci.* **2018**, *53*, 804–819. [CrossRef]

56. Saeger, J.T.; Grimes, N.G.; Rickard, H.E.; Hackett, E.E. Evaluation of Simplified Evaporation Duct Refractivity Models for Inversion Problems. *Radio Sci.* **2015**, *50*, 1110–1130. [CrossRef]
57. Pastore, D.M.; Greenway, D.P.; Stanek, M.J.; Wessinger, S.E.; Haack, T.; Wang, Q.; Hackett, E.E. Comparison of Atmospheric Refractivity Estimation Methods and Their Influence on Radar Propagation Predictions. *Radio Sci.* **2021**, *56*, e2020RS007244. [CrossRef]
58. Lentini, N.E.; Hackett, E.E. Global Sensitivity of Parabolic Equation Radar Wave Propagation Simulation to Sea State and Atmospheric Refractivity Structure. *Radio Sci.* **2015**, *50*, 1027–1049. [CrossRef]
59. Pastore, D.M.; Yamaguchi, R.T.; Wang, Q.; Hackett, E.E. On the Variability of In Situ Surface Layer Refractivity Measurements. *Atmosphere* **2023**, *14*, 1085. [CrossRef]
60. Stanek, M.J.; Pastore, D.M.; Hackett, E.E. A Novel Near-Surface Wave-Coherent Instantaneous Profiling System for Atmospheric Measurements. *Sensors* **2023**, *23*, 4099. [CrossRef] [PubMed]
61. Greenway, D.P.; Haack, T.; Hackett, E.E. Fusing Numerical Weather Prediction Ensembles with Refractivity Inversions during Surface Ducting Conditions. *J. Appl. Meteorol. Climatol.* **2023**, *62*, 1333–1346. [CrossRef]
62. Wessinger, S.E.; Greenway, D.P.; Haack, T.; Hackett, E.E. Near-Surface Thermodynamic Influences on Evaporation Duct Shape. *Atmosphere* **2024**, *15*, 718. [CrossRef]
63. Pastore, D.M.; Wessinger, S.E.; Greenway, D.P.; Stanek, M.J.; Burkholder, R.J.; Haack, T.; Wang, Q.; Hackett, E.E. Refractivity Inversions from Point-to-Point X-Band Radar Propagation Measurements. *Radio Sci.* **2022**, *57*, e2021RS007345. [CrossRef]
64. Franklin, K.B.; Wang, Q.; Jiang, Q.; Shen, L. Understanding Evaporation Duct Variabilities on Turbulent Eddy Scales. *J. Geophys. Res. Atmos.* **2022**, *127*, e2022JD036434. [CrossRef]
65. Wang, Q.; Alappattu, D.P.; Billingsley, S.; Blomquist, B.; Burkholder, R.J.; Christman, A.J.; Creegan, E.D.; de Paolo, T.; Eleuterio, D.P.; Fernando, H.J.S.; et al. CASPER: Coupled Air–Sea Processes and Electromagnetic Ducting Research. *Bull. Am. Meteorol. Soc.* **2018**, *99*, 1449–1474. [CrossRef]
66. Rogers, L.T.; Hattan, C.P.; Stapleton, J.K. Estimating Evaporation Duct Heights from Radar Sea Echo. *Radio Sci.* **2000**, *35*, 955–966. [CrossRef]
67. Paulus, R.A. Practical Application of an Evaporation Duct Model. *Radio Sci.* **1985**, *20*, 887–896. [CrossRef]
68. Hitney, H.V. Evaporation Duct Assessment from Meteorological Buoys. *Radio Sci.* **2002**, *37*, 1–7. [CrossRef]
69. Cook, J. A Sensitivity Study of Weather Data Inaccuracies on Evaporation Duct Height Algorithms. *Radio Sci.* **1991**, *26*, 731–746. [CrossRef]
70. Pappert, R.A.; Goodhart, C.L. Case Studies of Beyond-the-Horizon Propagation in Tropospheric Ducting Environments. *Radio Sci.* **1977**, *12*, 75–87. [CrossRef]
71. Pappert, R.A.; Paulus, R.A.; Tappert, F.D. Sea Echo in Tropospheric Ducting Environments. *Radio Sci.* **1992**, *27*, 189–209. [CrossRef]
72. Jiang, Q.; Wang, Q.; Gaberšek, S. Mesoscale Variability of Surface Ducts During Santa Ana Wind Episodes. *J. Geophys. Res. Atmos.* **2022**, *127*, e2022JD036698. [CrossRef]
73. Rogers, L.T.; Jablecki, M.; Gerstoft, P. Posterior Distributions of a Statistic of Propagation Loss Inferred from Radar Sea Clutter. *Radio Sci.* **2005**, *40*, RS6005. [CrossRef]
74. Haack, T.; Wang, C.; Garrett, S.; Glazer, A.; Mailhot, J.; Marshall, R. Mesoscale Modeling of Boundary Layer Refractivity and Atmospheric Ducting. *J. Appl. Meteorol. Climatol.* **2010**, *49*, 2437–2457. [CrossRef]
75. Burk, S.D.; Haack, T.; Rogers, L.T.; Wagner, L.J. Island Wake Dynamics and Wake Influence on the Evaporation Duct and Radar Propagation. *J. Appl. Meteorol.* **2003**, *42*, 349–367. [CrossRef]
76. Haack, T.; Burk, S.D. Summertime Marine Refractivity Conditions along Coastal California. *J. Appl. Meteorol.* **2001**, *40*, 673–687. [CrossRef]
77. Thompson, W.T.; Haack, T. An Investigation of Sea Surface Temperature Influence on Microwave Refractivity: The Wallops-2000 Experiment. *J. Appl. Meteorol. Climatol.* **2011**, *50*, 2319–2337. [CrossRef]
78. Lefurjah, G.; Marshall, R.; Casey, T.S.; Haack, T.; De Forest Boyer, D. Synthesis of Mesoscale Numerical Weather Prediction and Empirical Site-Specific Radar Clutter Models. *IET Radar Sonar Navig.* **2010**, *4*, 747–754. [CrossRef]
79. Barrios, A. Estimation of Surface-Based Duct Parameters from Surface Clutter Using a Ray Trace Approach. *Radio Sci.* **2004**, *39*, RS6013. [CrossRef]
80. Patterson, W.L. Comparison of Evaporation Duct and Path Loss Models. *Radio Sci.* **1985**, *20*, 1061–1068. [CrossRef]
81. Hitney, H.V.; Pappert, R.A.; Hattan, C.P.; Goodhart, C.L. Evaporation Duct Influences on Beyond-the-Horizon High Altitude Signals. *Radio Sci.* **1978**, *13*, 669–675. [CrossRef]
82. Alappattu, D.P.; Wang, Q.; Kalogiros, J. Anomalous Propagation Conditions over Eastern Pacific Ocean Derived from MAGIC Data. *Radio Sci.* **2016**, *51*, 1142–1156. [CrossRef]
83. Hitney, H.V. Whispering gallery effects in the troposphere. *Radio Sci.* **1992**, *27*, 893–898. [CrossRef]
84. Schleher, J.S. Tilted refractive surfaces at Eglin Air Force Base, Florida. *Radio Sci.* **1982**, *17*, 1281–1284. [CrossRef]

85. Rogers, L.T. Likelihood estimation of tropospheric duct parameters from horizontal propagation measurements. *Radio Sci.* **1997**, *32*, 79–92. [CrossRef]
86. Hitney, H.V.; Hitney, L.R. Frequency diversity effects of evaporation duct propagation. *IEEE Trans. Antennas Propag.* **1990**, *38*, 1694–1700. [CrossRef]
87. Alappattu, D.P.; Wang, Q.; Yamaguchi, R.T.; Haack, T.; Ulate, M.; Fernando, H.J.; Frederickson, P. Electromagnetic Ducting in the Near-Shore Marine Environment: Results From the CASPER-East Field Experiment. *J. Geophys. Res. Atmos.* **2022**, *127*, e2022JD037423. [CrossRef]
88. Anderson, K.D. Radar measurements at 16.5 GHz in the oceanic evaporation duct. *IEEE Trans. Antennas Propag.* **1989**, *37*, 100–106. [CrossRef]
89. Anderson, K.; Brooks, B.; Caffrey, P.; Clarke, A.; Cohen, L.; Crahan, K.; Davidson, K.; De Jong, A.; De Leeuw, G.; Dion, D.; et al. The RED Experiment: An Assessment of Boundary Layer Effects in a Trade Winds Regime on Microwave and Infrared Propagation over the Sea. *Bull. Am. Meteorol. Soc.* **2004**, *85*, 1355–1365. [CrossRef]
90. Richter, J.H. High Resolution Tropospheric Radar Sounding. *Radio Sci.* **1969**, *4*, 1261–1268. [CrossRef]
91. Burk, S.D.; Thompson, W.T. Mesoscale Modeling of Summertime Refractive Conditions in the Southern California Bight. *J. Appl. Meteorol.* **1997**, *36*, 22–31. [CrossRef]
92. Hodur, R.M. The Naval Research Laboratory's Coupled Ocean/Atmosphere Mesoscale Prediction System (COAMPS). *Mon. Weather Rev.* **1997**, *125*, 1414–1430. [CrossRef]
93. Zhao, Q.; Haack, T.; Rogers, T.; Gordon, N.; Will, I. Ensemble prediction of atmospheric refractivity conditions for EM propagation. In Proceedings of the 2015 USNC-URSI Radio Science Meeting (Joint with AP-S Symposium), Vancouver, BC, Canada, 19–24 July 2015; p. 249.
94. Zhao, Q.; Haack, T.; McLay, J.; Reynolds, C. Ensemble Prediction of Atmospheric Refractivity Conditions for EM Propagation. *J. Appl. Meteorol. Climatol.* **2016**, *55*, 2113–2130. [CrossRef]
95. Ulate, M.; Wang, Q.; Haack, T.; Holt, T.; Alappattu, D.P. Mean Offshore Refractive Conditions during the CASPER East Field Campaign. *J. Appl. Meteorol. Climatol.* **2019**, *58*, 853–874. [CrossRef]
96. Cook, J.; Burk, S. Potential refractivity as a similarity variable. *Bound.-Layer Meteorol.* **1992**, *58*, 151–159. [CrossRef]
97. Gingras, D.F.; Gerstoft, P.; Gerr, N.L. Electromagnetic matched-field processing: Basic concepts and tropospheric simulations. *IEEE Trans. Antennas Propag.* **1997**, *45*, 1536–1545. [CrossRef]
98. von Engeln, A.; Nedoluha, G.; Teixeira, J. An analysis of the frequency and distribution of ducting events in simulated radio occultation measurements based on ECMWF fields. *J. Geophys. Res. Atmos.* **2003**, *108*, 4669. [CrossRef]
99. Yan, X.; Yang, K.; Ma, Y. Calculation Method for Evaporation Duct Profiles Based on Artificial Neural Network. *IEEE Antennas Wirel. Propag. Lett.* **2018**, *17*, 2274–2278. [CrossRef]
100. Shi, Y.; Zhang, Q.; Wang, S.; Yang, K.; Yang, Y.; Ma, Y. Impact of Typhoon on Evaporation Duct in the Northwest Pacific Ocean. *IEEE Access* **2019**, *7*, 109111–109119. [CrossRef]
101. Wang, S.; Yang, K.; Shi, Y.; Zhang, H.; Yang, F.; Hu, D.; Dong, G.; Shu, Y. Long-term over-the-horizon microwave channel measurements and statistical analysis in evaporation ducts over the Yellow Sea. *Front. Mar. Sci.* **2023**, *10*, 1077470. [CrossRef]
102. Wang, S.; Yang, K.; Shi, Y.; Yang, F. Observations of Anomalous Over-the-Horizon Propagation in the Evaporation Duct Induced by Typhoon Kompasu (202118). *IEEE Antennas Wirel. Propag. Lett.* **2022**, *21*, 963–967. [CrossRef]
103. Wang, S.; Yang, K.; Shi, Y.; Yang, F.; Zhang, H. Impact of Evaporation Duct on Electromagnetic Wave Propagation During a Typhoon. *J. Ocean Univ. China* **2022**, *21*, 1069–1083. [CrossRef]
104. Yang, K.; Yang, F.; Wang, S.; Shi, Y.; Zhang, H. The Observed Effects of a Cold Wave on Over-the-horizon Propagation in Evaporation Ducts across Multiple Sea Areas. *IEEE Trans. Antennas Propag.* **2023**, *72*, 852–861.
105. Wang, S.; Yang, K.; Shi, Y.; Yang, F.; Zhang, H. Observed Over-the-Horizon Propagation Characteristics and Evaporation Duct Inversion During the Entire Process of Tropical Cyclone Mulan (202207). *IEEE Trans. Antennas Propag.* **2023**, *71*, 5322–5334. [CrossRef]
106. Yang, K.; Zhang, Q.; Shi, Y. Interannual variability of the evaporation duct over the South China Sea and its relations with regional evaporation. *J. Geophys. Res. Ocean.* **2017**, *122*, 6698–6713. [CrossRef]
107. Yang, K.D.; Ma, Y.L.; Shi, Y. Spatio-temporal distributions of evaporation duct for the West Pacific Ocean. *Acta Phys. Sin.* **2009**, *58*, 7339–7350. (In Chinese) [CrossRef]
108. Shi, Y.; Yang, K.; Yang, Y.; Ma, Y. A New Evaporation Duct Climatology over the South China Sea. *J. Meteorol. Res.* **2015**, *29*, 764–778. [CrossRef]
109. Yang, K.; Zhang, Q.; Shi, Y.; He, Z.; Lei, B.; Han, Y. On analyzing space-time distribution of evaporation duct height over the global ocean. *Acta Oceanol. Sin.* **2016**, *35*, 20–29. [CrossRef]
110. Zhang, Q.; Yang, K.; Shi, Y. Spatial and temporal variability of the evaporation duct in the Gulf of Aden. *Tellus A Dyn. Meteorol. Oceanogr.* **2016**, *68*, 29792. [CrossRef]

111. Yang, S.; Kun-De, Y.; Yi-Xin, Y.; Yuan-Liang, M. Influence of obstacle on electromagnetic wave propagation in evaporation duct with experiment verification. *Chin. Phys. B* **2015**, *24*, 323–328. [CrossRef]
112. Duan, R.; Yang, K.; Ma, Y.; Chapman, N.R. A simple expression for sound attenuation due to surface duct energy leakage in low-latitude oceans. *J. Acoust. Soc. Am.* **2016**, *139*, EL118–EL123. [CrossRef] [PubMed]
113. Zhang, Q.; Yang, K.; Yang, Q. Statistical Analysis of the Quantified Relationship between Evaporation Duct and Oceanic Evaporation for Unstable Conditions. *J. Atmos. Ocean. Technol.* **2017**, *34*, 2489–2497. [CrossRef]
114. Zhang, Q.; Yang, K. Study on evaporation duct estimation from point-to-point propagation measurements. *IET Sci. Meas. Technol.* **2018**, *12*, 456–460. [CrossRef]
115. Shi, Y.; Zhang, Q.; Wang, S.; Yang, K.; Yang, Y.; Yan, X.; Ma, Y. A Comprehensive Study on Maximum Wavelength of Electromagnetic Propagation in Different Evaporation Ducts. *IEEE Access* **2019**, *7*, 82308–82319. [CrossRef]
116. Yan, X.; Yang, K. Influence of wind speed on electromagnetic wave propagation under evaporation duct condition based on sea surface model. *Oceanol. Limnol. Sin.* **2020**, *51*, 13–19. (In Chinese)
117. Hu, D.; Yang, K.; Zhang, H.; Wang, S.; Yang, F.; Dong, G.; Shi, Y. Observed Diurnal Variations of Over-the-horizon Propagation Loss in Evaporation Duct Over the South China Sea. *IEEE Antennas Wirel. Propag. Lett.* **2023**, *22*, 1060–1064.
118. Wang, S.; Yang, K.; Shi, Y.; Yang, F.; Zhang, H.; Ma, Y. Prediction of Over-the-Horizon Electromagnetic Wave Propagation in Evaporation Ducts Based on the Gated Recurrent Unit Network Model. *IEEE Trans. Antennas Propag.* **2023**, *71*, 3485–3496. [CrossRef]
119. Shi, Y.; Wang, S.; Yang, F.; Yang, K. Statistical Analysis of Hybrid Atmospheric Ducts over the Northern South China Sea and Their Influence on Over-the-Horizon Electromagnetic Wave Propagation. *J. Mar. Sci. Eng.* **2023**, *11*, 669. [CrossRef]
120. Yang, F.; Yang, K.; Shi, Y.; Wang, S.; Zhang, H.; Zhao, Y. The Effects of Rainfall on Over-the-Horizon Propagation in the Evaporation Duct over the South China Sea. *Remote Sens.* **2022**, *14*, 4787. [CrossRef]
121. Yang, K.D.; Shi, Y.; Ma, Y.L.; Zhang, Q. *Theoretical Models and Characteristics of Evaporation Duct Near Sea Surface*; Science Press: Beijing, China, 2022. (In Chinese)
122. Yang, F.; Wang, S.; Yang, K.; Shu, Y.; Shi, Y. Marine High-Speed Over-the-Horizon Communications and Channel Sensing in Evaporation Ducts Over the South China Sea. *IEEE Antennas Wirel. Propag. Lett.* **2024**, *23*, 2870–2874. [CrossRef]
123. Yang, F.; Yang, K.; Shi, Y.; Wang, S.; Shu, Y. Inversions of the Evaporation Duct Heights Utilizing Opportunistic Signals of Navigation Radar. *IEEE Trans. Antennas Propag.* **2024**, *72*, 8647–8654. [CrossRef]
124. Shu, Y.; Wang, S.; Yang, K.; Yang, F.; Zhang, T.; Shi, Y.; Feng, C. Atmospheric Stability-Dependent Performance of Evaporation Duct Models: Experimental Validation Through Over-the-Horizon Propagation in the South China Sea. *IEEE Trans. Antennas Propag.* **2026**, *74*, 873–884. [CrossRef]
125. Shi, Y.; Yang, K.D.; Yang, Y.X.; Ma, Y.L. Experimental verification of effect of horizontal inhomogeneity of evaporation duct on electromagnetic wave propagation. *Chin. Phys. B* **2015**, *9*, 054101. [CrossRef]
126. Zhao, W.; Zhao, J.; Li, J.; Zhao, D.; Huang, L.; Zhu, J.; Lu, J.; Wang, X. An Evaporation Duct Height Prediction Model Based on a Long Short-Term Memory Neural Network. *IEEE Trans. Antennas Propag.* **2021**, *69*, 7795–7804. [CrossRef]
127. Liao, Q.; Mai, Y.; Sheng, Z.; Wang, Y.; Ni, Q.; Zhou, S. The Comparison of Long Short-Term Memory Neural Network and Deep Forest for the Evaporation Duct Height Prediction. *IEEE Trans. Antennas Propag.* **2023**, *71*, 4444–4450. [CrossRef]
128. Chai, X.; Li, J.; Zhao, J.; Hu, Y.; Zhao, X. NWPP-EDH: Numerical weather prediction products evaporation duct regional prediction model. *Front. Earth Sci.* **2023**, *10*, 1031186. [CrossRef]
129. Zhao, X.; Yang, P.; Zhou, F.; Zhou, Z. Comparison of Evaporation Duct Height Statistics Based on Surface Bulk Measurements Over Yongxing Island. *IEEE Antennas Wirel. Propag. Lett.* **2023**, *22*, 1306–1310. [CrossRef]
130. Zhu, X.; Li, J.; Zhu, M.; Jiang, Z.; Li, Y. An Evaporation Duct Height Prediction Method Based on Deep Learning. *IEEE Geosci. Remote Sens. Lett.* **2018**, *15*, 1307–1311. [CrossRef]
131. Zhao, W.P.; Li, J.; Zhao, J.; Zhao, D.; Lu, J.; Wang, X. XGB Model: Research on Evaporation Duct Height Prediction Based on XGBoost Algorithm. *Radioengineering* **2020**, *29*, 81–93. [CrossRef]
132. Mai, Y.; Sheng, Z.; Shi, H.; Li, C.; Liao, Q.; Bao, J. A New Short-Term Prediction Method for Estimation of the Evaporation Duct Height. *IEEE Access* **2020**, *8*, 136036–136045. [CrossRef]
133. Zhao, W.; Li, J.; Zhao, J.; Zhao, D.; Zhu, X. PDD_GBR: Research on Evaporation Duct Height Prediction Based on Gradient Boosting Regression Algorithm. *Radio Sci.* **2019**, *54*, 949–962. [CrossRef]
134. Liao, Q.; Sheng, Z.; Shi, H.; Zhang, L.; Zhou, L.; Ge, W.; Long, Z. A Comparative Study on Evolutionary Multi-objective Optimization Algorithms Estimating Surface Duct. *Sensors* **2018**, *18*, 4428. [CrossRef] [PubMed]
135. Ding, J.; Fei, J.; Huang, X.; Cheng, X.; Liang, Z. Validation of Evaporation Duct Model in Coastal Regions with ASIT Data. *J. Coast. Res.* **2020**, *99*, 270. [CrossRef]
136. Mai, Y.; Sheng, Z.; Shi, H.; Li, C.; Liu, L.; Liao, Q.; Zhang, W.; Zhou, S. A New Diagnostic Model and Improved Prediction Algorithm for the Heights of Evaporation Ducts. *Front. Earth Sci.* **2020**, *8*, 102. [CrossRef]

137. Zhao, W.; Li, J.; Zhao, J.; Jiang, T.; Zhu, J.; Zhao, D.; Zhao, J. Research on evaporation duct height prediction based on back propagation neural network. *IET Microw. Antennas Propag.* **2020**, *14*, 1547–1554. [CrossRef]
138. Liao, Q.; Sheng, Z.; Shi, H.; Xiang, J.; Yu, H. Estimation of Surface Duct Using Ground-Based GPS Phase Delay and Propagation Loss. *Remote Sens.* **2018**, *10*, 724. [CrossRef]
139. Huang, L.; Zhao, X.; Liu, Y.; Yang, P.; Ding, J.; Zhou, Z. The Diurnal Variation of the Evaporation Duct Height and Its Relationship with Environmental Variables in the South China Sea. *IEEE Trans. Antennas Propag.* **2022**, *70*, 10865–10875. [CrossRef]
140. Huang, L.; Zhao, X.; Liu, Y. The Statistical Characteristics of Atmospheric Ducts Observed Over Stations in Different Regions of American Mainland Based on High-Resolution GPS Radiosonde Soundings. *Front. Environ. Sci.* **2022**, *10*, 946226. [CrossRef]
141. Huang, L.; Zhao, X.; Liu, Y.; Yang, P. Analysis of the Atmospheric Duct Existence Factors in Tropical Cyclones Based on the SHAP Interpretation of Extreme Gradient Boosting Predictions. *Remote Sens.* **2022**, *14*, 3952. [CrossRef]
142. Liao, Q.; Zhou, S.; Shi, H.; Shi, W. Parameter Estimation of Nonlinear Systems by Dynamic Cuckoo Search. *Neural Comput.* **2017**, *29*, 1103–1123. [CrossRef] [PubMed]
143. Wang, Y.; Huang, S.X.; Xiang, J. Study on Abelian inversion of refractive index based on Bayesian algorithm. *Chin. J. Geophys.* **2019**, *62*, 4506–4512. (In Chinese)
144. Jia, W.; Zhang, W.; Zhu, J.; Sun, J. The Effect of Boreal Summer Intraseasonal Oscillation on Evaporation Duct and Electromagnetic Propagation over the South China Sea. *Atmosphere* **2020**, *11*, 1298. [CrossRef]
145. Liao, Q.; Sheng, Z.; Shi, H. Joint Inversion of Atmospheric Refractivity Profile Based on Ground-Based GPS Phase Delay and Propagation Loss. *Atmosphere* **2016**, *7*, 12. [CrossRef]
146. Liang, Z.; Ding, J.; Fei, J.; Cheng, X.; Huang, X. Maintenance and Sudden Change of a Strong Elevated Ducting Event Associated with High Pressure and Marine Low-Level Jet. *J. Meteorol. Res.* **2020**, *34*, 1287–1298. [CrossRef]
147. Ding, J.; Fei, J.; Huang, X.; Cheng, X.; Hu, X. Observational Occurrence of Tropical Cyclone Ducts from GPS Dropsonde Data. *J. Appl. Meteorol. Climatol.* **2013**, *52*, 1221–1236. [CrossRef]
148. Mai, Y.; Shi, H.; Liao, Q.; Sheng, Z.; Zhao, S.; Ni, Q.; Zhang, W. Using the Decomposition-Based Multi-Objective Evolutionary Algorithm with Adaptive Neighborhood Sizes and Dynamic Constraint Strategies to Retrieve Atmospheric Ducts. *Sensors* **2020**, *20*, 2230. [CrossRef] [PubMed]
149. Mai, Y.; Sheng, Z.; Shi, H.; Liao, Q.; Zhang, W. Spatiotemporal Distribution of Atmospheric Ducts in Alaska and Its Relationship with the Arctic Vortex. *Int. J. Antennas Propag.* **2020**, *2020*, 9673289. [CrossRef]
150. Chai, X.; Li, J.; Zhao, J.; Wang, W.; Zhao, X. LGB-PHY: An Evaporation Duct Height Prediction Model Based on Physically Constrained LightGBM Algorithm. *Remote Sens.* **2022**, *14*, 3448. [CrossRef]
151. Liu, Q.; Zhao, X.; Zou, J.; Li, Y.; Qiu, Z.; Hu, T.; Wang, B.; Li, Z. Development of a Numerical Prediction Model for Marine Lower Atmospheric Ducts and Its Evaluation across the South China Sea. *J. Mar. Sci. Eng.* **2024**, *12*, 141. [CrossRef]
152. Wang, J.; Zhao, X.; Zou, J.; Yang, P.; Wang, B.; Yang, S.; Qiu, Z.; Li, Z.; Hu, T.; Song, M. Investigating the Temporal and Spatial Characteristics of Lower Atmospheric Ducts in the Arctic via Long-Term Numerical Simulations. *Atmosphere* **2024**, *16*, 11. [CrossRef]
153. Liu, Q.; Zhao, X.; Zou, J.; Hu, T.; Qiu, Z.; Wang, B.; Li, Z.; Cui, C.; Cao, R. Investigating the spatio-temporal characteristics of lower atmospheric ducts across the China seas by performing a long-term simulation using the WRF model. *Front. Mar. Sci.* **2024**, *11*, 1332805. [CrossRef]
154. Cheng, Z.; Li, J.; Zhao, J.; Zhao, J.; Zhang, P. TCN-GRU: A Diagnostic Model for the Evaporation Duct Height. *IEEE Trans. Antennas Propag.* **2025**, *73*, 10571–10585. [CrossRef]
155. Guo, X.; Wu, J.; Zhang, J.; Han, J. Deep learning for solving inversion problem of atmospheric refractivity estimation. *Sustain. Cities Soc.* **2018**, *43*, 524–531. [CrossRef]
156. Han, J.; Wu, J.; Zhu, Q.; Wang, H.; Zhou, Y.; Jiang, M.; Zhang, S.; Wang, B. Evaporation Duct Height Nowcasting in China's Yellow Sea Based on Deep Learning. *Remote Sens.* **2021**, *13*, 1577. [CrossRef]
157. Yang, C.; Zhang, J.; Guo, L. Investigation on the Inversion of the Atmospheric Duct Using the Artificial Bee Colony Algorithm Based on Opposition-Based Learning. *Int. J. Antennas Propag.* **2016**, *2016*, 2749035. [CrossRef]
158. Liu, X.; Cao, Y.; Wu, Z.; Wang, H. Inversion for Inhomogeneous Surface Duct without a Base Layer Based on Ocean-Scattered Low-Elevation BDS Signals. *Remote Sens.* **2021**, *13*, 3914. [CrossRef]
159. Zhang, J.; Wu, Z.; Zhang, Y.; Wang, B. Evaporation Duct Retrieval Using Changes in Radar Sea Clutter Power Versus Receiving Height. *Prog. Electromagn. Res.* **2012**, *126*, 555–571. [CrossRef]
160. Zhang, J.; Wu, Z.; Hu, R. Combined Estimation of Low-Altitude Radio Refractivity Based on Sea Clutters from Multiple Shipboard Radars. *J. Electromagn. Waves Appl.* **2011**, *25*, 1201–1212. [CrossRef]
161. Zhang, J.P.; Wu, Z.S.; Zhu, Q.L.; Wang, B. A Four-Parameter M-Profile Model for the Evaporation Duct Estimation from Radar Clutter. *Prog. Electromagn. Res.* **2011**, *114*, 353–363. [CrossRef]
162. Zhang, J.; Wu, Z.; Wang, B. An Adaptive Objective Function for Evaporation Duct Estimations from Radar Sea Echo. *Chin. Phys. Lett.* **2011**, *28*, 034301. [CrossRef]

163. Wang, B.; Wu, Z.; Zhao, Z.; Wang, H. A Passive Technique to Monitor Evaporation Duct Height Using Coastal GNSS-R. *IEEE Geosci. Remote Sens. Lett.* **2011**, *8*, 587–591. [CrossRef]
164. Wang, B.; Wu, Z.; Zhao, Z.; Wang, H. Retrieving evaporation duct heights from radar sea clutter using particle swarm optimization (PSO) algorithm. *Prog. Electromagn. Res. M* **2009**, *9*, 79–91. [CrossRef]
165. Wang, H.; Wu, Z.; Kang, S.; Zhao, Z. Monitoring the Marine Atmospheric Refractivity Profiles by Ground-Based GPS Occultation. *IEEE Geosci. Remote Sens. Lett.* **2013**, *10*, 962–965. [CrossRef]
166. Wang, H.G.; Wu, Z.S.; Lin, L.K.; Kang, S.F.; Zhao, Z. Retrieving evaporation duct heights from power of ground-based GPS occultation signal. *Prog. Electromagn. Res. M* **2013**, *30*, 183–194. [CrossRef]
167. Yang, C.; Guo, L.; Wu, Z. Investigation on global positioning system signal scattering and propagation over the rough sea surface. *Chin. Phys. B* **2010**, *19*, 241–249. [CrossRef]
168. Liu, C.G.; Huang, J.Y.; Jiang, C.Y.; Lin, F.J. Modeling Evaporation Duct over Sea with Pseudo-Refractivity and Similarity Theory. *Acta Electron. Sin.* **2001**, *29*, 970–972. (In Chinese)
169. Hao, X.; Li, Q.; Guo, L.; Lin, L.; Ding, Z.; Zhao, Z.; Yi, W. Digital Maps of Atmospheric Refractivity and Atmospheric Ducts Based on a Meteorological Observation Datasets. *IEEE Trans. Antennas Propag.* **2022**, *70*, 2873–2883. [CrossRef]
170. Hao, X.J.; Li, Q.L.; Guo, L.X.; Guo, X.M. A Preliminary Study on Inversion Method of Trapping Duct Based on Meteorological Satellite Data in China Coastal Areas. *Acta Electron. Sin.* **2019**, *47*, 600–605. (In Chinese)
171. Zhao, X.; Huang, J.; Gong, S. Modeling on multi-eigenpath channel in marine atmospheric duct. *Radio Sci.* **2009**, *44*, RS1009. [CrossRef]
172. Wei, Y.; Gao, M.; Tian, D.; Guo, L.; Li, J.; Yang, L.; Guo, X. A Model for Calculating Electromagnetic Scattering from Target in Evaporation Duct. *IEEE Antennas Wirel. Propag. Lett.* **2022**, *21*, 2312–2316. [CrossRef]
173. Wang, N.; Guo, L.X.; Zhao, Z.W.; Ding, Z.H.; Lin, L.K. Primary exploration of the algorithm of retrieving troposphere abnormal structure in the southeast coast of China. *J. Remote Sens.* **2017**, *21*, 948–954. (In Chinese) [CrossRef]
174. Han, J.; Wu, J.; Zhang, L.; Wang, H.; Zhu, Q.; Zhang, C.; Zhao, H.; Zhang, S. A Classifying-Inversion Method of Offshore Atmospheric Duct Parameters Using AIS Data Based on Artificial Intelligence. *Remote Sens.* **2022**, *14*, 3197. [CrossRef]
175. Yang, K.; Wu, Z.; Guo, X.; Wu, J.; Cao, Y.; Qu, T.; Xue, J. Estimation of co-channel interference between cities caused by ducting and turbulence. *Chin. Phys. B* **2022**, *31*, 024102. [CrossRef]
176. Zhang, J.; Wu, Z.; Zhao, Z.; Zhang, Y.; Wang, B. Propagation modeling of ocean-scattered low-elevation GPS signals for maritime tropospheric duct inversion. *Chin. Phys. B* **2012**, *21*, 014101. [CrossRef]
177. Zhang, J.; Wu, Z.; Wang, B.; Wang, H.; Zhu, Q. Modeling low elevation GPS signal propagation in maritime atmospheric ducts. *J. Atmos. Sol.-Terr. Phys.* **2012**, *80*, 12–20. [CrossRef]
178. Yang, C.; Guo, L.X.; Li, H.Q.; Wu, Z.S. Study on the Propagation Characteristics of Electromagnetic Waves in Atmospheric Ducts. *J. Xidian Univ.* **2009**, *36*, 1097–1102. (In Chinese)
179. Han, J.; Wu, J.; Wang, H.; Zhu, Q.; Zhang, L.; Zhang, C.; Wang, Q.; Zhao, H. Weight Loss Function for the Cooperative Inversion of Atmospheric Duct Parameters. *Atmosphere* **2022**, *13*, 338. [CrossRef]
180. Liu, X.; Wu, Z.; Wang, H. Inversion Method of Regional Range-Dependent Surface Ducts with a Base Layer by Doppler Weather Radar Echoes Based on WRF Model. *Atmosphere* **2020**, *11*, 754. [CrossRef]
181. Zhao, X.L.; Huang, J.Y.; Gong, S.H. Statistical Analysis of an Over-the-Sea Experimental Transhorizon Communication at X-band in China. *J. Electromagn. Waves Appl.* **2008**, *22*, 1430–1439. [CrossRef]
182. Cheng, Y.H.; Peng, S.B.; Zhao, B.B.; Wang, H.G.; Zhang, Y.S.; Hao, X.J. Estimation of Two Reanalysis Datasets on the Application to Atmospheric Refractive Environment over the Global Sea. *Chin. J. Radio Sci.* **2023**, *38*, 491–501. (In Chinese)
183. Liu, C.G.; Huang, J.Y.; Jiang, C.Y. Occurrence Law of Tropospheric Duct Structure in Southeast Coastal Areas of China. *Chin. J. Radio Sci.* **2002**, *17*, 509–513. (In Chinese)
184. Zhang, J.P.; Wu, Z.S.; Zhao, Z.W.; Wang, B. Evaporation Duct Inversion Based on Radar Sea Clutters from Different Antenna Heights. *Chin. J. Radio Sci.* **2011**, *26*, 422–430. (In Chinese)
185. Liu, C.G.; Huang, J.Y.; Jiang, C.Y.; Pan, Z.W.; Lin, F.J.; Zhang, Y.S. Study on the Environmental Characteristics of Tropospheric Ducts in China. *J. Xidian Univ.* **2002**, *29*, 119–123. (In Chinese)
186. Guo, L. Hybrid GRU–Random Forest Model for Accurate Atmospheric Duct Detection with Incomplete Sounding Data. *Remote Sens.* **2024**, *16*, 4308. [CrossRef]
187. Ji, H.; Guo, L.; Zhang, J.; Wei, Y.; Guo, X.; Zhang, Y.; Nie, T.; Feng, J. IPILT–OHPL: An Over-the-Horizon Propagation Loss Prediction Model Established by Incorporating Prior Information Into the LSTM–Transformer Structure. *IEEE J. Sel. Top. Appl. Earth Obs. Remote Sens.* **2024**, *17*, 10067–10082. [CrossRef]
188. Ji, H.; Wei, Y.; Zhao, Q.; Guo, L.; Zhang, J. EKDInformer-LTEDH: An Informer-Based Environmental Knowledge-Driven Prediction Model for Long-Term Evaporation Duct Height. *IEEE Geosci. Remote Sens. Lett.* **2024**, *21*, 1003905. [CrossRef]
189. Ji, H.; Guo, L.; Zhang, J.; Wei, Y.; Guo, X.; Zhang, Y. EDH-STNet: An Evaporation Duct Height Spatiotemporal Prediction Model Based on Swin-Unet Integrating Multiple Environmental Information Sources. *Remote Sens.* **2024**, *16*, 4227. [CrossRef]

190. Ji, H.; Zhang, J.; Guo, L.; Wei, Y.; Guo, X.; Zhang, Y. RFCFormer: A Dual-Stream Transformer Architecture Integrating Gramian Angular Field Representations for Retrieving Evaporation Duct Refractivity From Radar Sea Clutter. *IEEE Trans. Geosci. Remote Sens.* **2025**, *63*, 2001718. [CrossRef]
191. Gao, Q.; Gong, S.; Duan, Y.; Liu, Z. Real-time inversion method of uneven atmospheric ducts in actual environments via refraction propagation law. *IEEE Trans. Geosci. Remote Sens.* **2026**, *64*, 2001319. [CrossRef]
192. Ji, H.; Zhang, J.; Guo, L.; Wei, Y.; Leng, J.; Zhang, Y.; Li, Q.; Guo, X.; Zhang, Y. DenseRefrception: A Densely Connected Perception Framework for Passive Retrieval of Ocean Refractive Environments via GPS Scattered Signals. *IEEE Trans. Geosci. Remote Sens.* **2026**, *64*, 2001719. [CrossRef]
193. Wang, B.; Wu, Z.S.; Zhao, Z.W.; Wang, H.G. Improved method to retrieve low altitude atmospheric refractivity profiles from radar clutter. *Syst. Eng. Electron.* **2010**, *32*, 1234–1238. (In Chinese)
194. Ji, H.; Zhang, J.; Wei, Y.; Li, Q.; Guo, X.; Zhang, Y.; Zhang, Y.; Guo, L. Explainable Deep Learning-Based Prediction of Radar Wave Propagation Loss in Evaporation Ducts and Exploration of Driving Factors. *IEEE Antennas Wirel. Propag. Lett.* **2025**, *24*, 2432–2436. [CrossRef]
195. Zhao, X.F.; Huang, S.X.; Wang, D.X. Using particle filter to track horizontal variations of atmospheric duct structure from radar sea clutter. *Atmos. Meas. Tech.* **2012**, *5*, 2859–2866. [CrossRef]
196. Zhao, X.F.; Huang, S.X. Refractivity from Clutter by Variational Adjoint Approach. *Prog. Electromagn. Res. B* **2011**, *33*, 153–174. [CrossRef]
197. Zhao, X.; Huang, S.; Du, H. Theoretical analysis and numerical experiments of variational adjoint approach for refractivity estimation. *Radio Sci.* **2011**, *46*, RS1006. [CrossRef]
198. Zhao, X.F. Refractivity-from-Clutter Based on Local Empirical Refractivity Model. *Chin. Phys. B* **2018**, *27*, 550–554. [CrossRef]
199. Ding, J.L.; Fei, J.F.; Huang, X.G.; Cheng, X.P.; Hu, X.H.; Liang, J.I. Development and Validation of an Evaporation Duct Model. Part II: Evaluation and Improvement of Stability Functions. *J. Meteorol. Res.* **2015**, *29*, 482–495. [CrossRef]
200. Ding, J.; Fei, J.; Huang, X.; Cheng, X.; Hu, X.; Liang, J. Development and Validation of an Evaporation Duct Model. Part I: Model Establishment and Sensitivity Experiments. *J. Meteorol. Res.* **2015**, *29*, 467–481. [CrossRef]
201. Zhao, X.; Yardim, C.; Wang, D.; Howe, B.M. Estimating Range-Dependent Evaporation Duct Height. *J. Atmos. Ocean. Technol.* **2017**, *34*, 1113–1123. [CrossRef]
202. Zhao, X.; Yang, P. A Simple Two-Dimensional Ray-Tracing Visual Tool in the Complex Tropospheric Environment. *Atmosphere* **2017**, *8*, 35. [CrossRef]
203. Zhao, X.; Wang, D.; Huang, S. Atmospheric duct estimation from multi-source radar sea clutter returns: Theoretical framework and preliminary numerical results. *Chin. Sci. Bull.* **2014**, *59*, 4899–4906. [CrossRef]
204. Zhao, X.; Huang, S. Estimation of Atmospheric Duct Structure Using Radar Sea Clutter. *J. Atmos. Sci.* **2012**, *69*, 2808–2818. [CrossRef]
205. Zhao, X.; Huang, S. Atmospheric Duct Estimation Using Radar Sea Clutter Returns by the Adjoint Method with Regularization Technique. *J. Atmos. Ocean. Technol.* **2014**, *31*, 1250–1262. [CrossRef]
206. Zhao, X.; Wang, D.; Huang, S.; Huang, K.; Chen, J. Statistical estimations of atmospheric duct over the South China Sea and the Tropical Eastern Indian Ocean. *Chin. Sci. Bull.* **2013**, *58*, 2794–2797. [CrossRef]
207. Zhao, X. Evaporation Duct Height Estimation and Source Localization From Field Measurements at an Array of Radio Receivers. *IEEE Trans. Antennas Propag.* **2012**, *60*, 1020–1025. [CrossRef]
208. Zhao, X.F.; Huang, S.X. Remote Sensing of Atmospheric Refractivity from Field Measurements of Vertical Receiver Array. *Acta Phys. Sin.* **2011**, *60*, 119203. [CrossRef]
209. Zhao, X.F.; Huang, S.X.; Xiang, J.; Shi, W.L. Remote Sensing of Atmospheric Duct Parameters Using Simulated Annealing. *Chin. Phys. B* **2011**, *20*, 468–475. [CrossRef]
210. Zhao, X.; Huang, S. Refractivity estimations from an angle-of-arrival spectrum. *Chin. Phys. B* **2011**, *20*, 029201. [CrossRef]
211. Zhao, X.; Huang, S.; Sheng, Z. Ray tracing/correlation approach to estimation of surface-based duct parameters from radar clutter. *Chin. Phys. B* **2010**, *19*, 49201. [CrossRef]
212. Huang, S.X.; Zhao, X.F.; Sheng, Z. Refractivity Estimation from Radar Sea Clutter. *Chin. Phys. B* **2009**, *18*, 5084–5090. [CrossRef]
213. Sheng, Z.; Huang, S.X.; Zhao, X.F. The Determination of Observation Weight in Inversion of Oceanic Duct Using Radar Clutter. *Acta Phys. Sin.* **2009**, *58*, 6627–6632. (In Chinese) [CrossRef]
214. Fang, H.X.; Sheng, Z. Monitoring of Ducting by Using a Ground-Based GPS Receiver. *Chin. Phys. B* **2013**, *22*, 055701. [CrossRef]
215. Sheng, Z.; Huang, S.X. Ocean Duct Inversion Using Radar Clutter and Its Noise Restraining Ability. *Acta Phys. Sin.* **2009**, *58*, 4328–4334. [CrossRef]
216. Sheng, Z.; Huang, S.X.; Zeng, G.D. Ocean Duct Inversion from Radar Clutter Using Bayesian-Markov Chain Monte Carlo Method. *Acta Phys. Sin.* **2009**, *58*, 4335–4341. [CrossRef]
217. Sheng, Z. Tracking Refractivity from Radar Clutter Using Extended Kalman Filter and Unscented Kalman Filter. *Acta Phys. Sin.* **2011**, *60*, 812–818. [CrossRef]

218. Sheng, Z.; Chen, J.Q.; Xu, R.H. Tracking Refractivity from Radar Clutter Using Particle Filter. *Acta Phys. Sin.* **2012**, *61*, 523–528. [CrossRef]
219. Sheng, Z.; Huang, S.X. Ocean Duct Inversion from Radar Clutter Using Variation Adjoint and Regularization Method (I): Theoretical Part. *Acta Phys. Sin.* **2010**, *59*, 1734–1739. [CrossRef]
220. Sheng, Z.; Huang, S.X. Ocean Duct Inversion from Radar Clutter Using Variation Adjoint and Regularization Method (II): Inversion Experiment. *Acta Phys. Sin.* **2010**, *59*, 3912–3916. [CrossRef]
221. Fang, H.X.; Sheng, Z. Inversion for Atmosphere Duct Parameters Using Real Radar Sea Clutter. *Chin. Phys. B* **2012**, *21*, 618–623. [CrossRef]
222. He, R.; Huang, S.X.; Zhou, C.T.; Jiang, Z.H. Genetic Algorithm with Regularization Method to Retrieve Ocean Atmosphere Duct. *Acta Phys. Sin.* **2012**, *61*, 504–511. [CrossRef]
223. Sheng, Z. The estimation of lower refractivity uncertainty from radar sea clutter using the Bayesian-MCMC method. *Chin. Phys. B* **2013**, *22*, 580–585. [CrossRef]
224. Zhang, Z.; Sheng, Z.; Shi, H. Parameter estimation of atmospheric refractivity from radar clutter using the particle swarm optimization via Lévy flight. *J. Appl. Remote Sens.* **2015**, *9*, 095998. [CrossRef]
225. Zhang, Z.; Sheng, Z.; Shi, H.; Fan, Z. Inversion for Refractivity Parameters Using a Dynamic Adaptive Cuckoo Search with Crossover Operator Algorithm. *Comput. Intell. Neurosci.* **2016**, *2016*, 3208724. [CrossRef] [PubMed]
226. Zhao, X.F.; Huang, S.X. Radar Sea Clutter Power Modeling under the Atmospheric Duct Propagation Conditions. *Acta Phys. Sin.* **2013**, *62*, 540–546. [CrossRef]
227. He, M.Y.; Du, H.D.; Long, Z.Y.; Huang, S.X. Selection of Regularization Parameters Using an Atmospheric Retrievable Index in a Retrieval of Atmospheric Profile. *Acta Phys. Sin.* **2012**, *61*, 289–295. (In Chinese) [CrossRef]
228. Ding, J.L.; Fei, J.F.; Huang, X.G.; Zhang, X.; Zhou, X.; Tian, B. Comparative Analysis of Evaporation Duct Occurrence Law in the South China Sea and East China Sea. *Chin. J. Radio Sci.* **2009**, *24*, 1018–1023. (In Chinese)
229. Zhao, X. Theoretical and Algorithmic Investigations on the Atmospheric Duct Inversion by the Radar Data. Ph.D. Thesis, PLA University of Science and Technology, Nanjing, China, 2010. (In Chinese)
230. Tang, W.; Cha, H.; Wei, M.; Tian, B.; Ren, X. An atmospheric refractivity inversion method based on deep learning. *Results Phys.* **2019**, *12*, 582–584. [CrossRef]
231. Tian, B.; Liu, Q.; Lu, J.; He, X.; Zeng, G.; Teng, L. The influence of seasonal and nonreciprocal evaporation duct on electromagnetic wave propagation in the Gulf of Aden. *Results Phys.* **2020**, *18*, 103181. [CrossRef]
232. Tang, W.; Cha, H.; Wei, M.; Tian, B. Estimation of surface-based duct parameters from automatic identification system using the Levy flight quantum-behaved particle swarm optimization algorithm. *J. Electromagn. Waves Appl.* **2019**, *33*, 827–837. [CrossRef]
233. Tang, W.; Cha, H.; Wei, M.; Tian, B. The effect of atmospheric ducts on the propagation of AIS signals. *Aust. J. Electr. Electron. Eng.* **2019**, *16*, 111–116. [CrossRef]
234. Tang, W.; Cha, H.; Wei, M.; Tian, B.; Ren, X. Atmospheric refractivity estimation from AIS signal power using the quantum-behaved particle swarm optimization algorithm. *Open Geosci.* **2019**, *11*, 542–548. [CrossRef]
235. Zuo, L.; Cha, H.; Zhou, M.; Tu, Y. Inversion for evaporation duct from radar sea clutter based on immune algorithm. *Acta Electron. Sin.* **2011**, *39*, 2382–2386.
236. Zuo, L.; Gu, X.F.; Shao, W.; Tu, Y.J. Experimental Analysis of Inversion of Atmospheric Refractive Index Profile Using Radar Sea Clutter. *J. Huazhong Univ. Sci. Technol.* **2012**, *40*, 75–77. (In Chinese)
237. Tian, B.; Cha, H.; Li, J.; Liu, C.G. Comparison of Characteristics between PJ Model and Pseudo-Refractivity Model. *J. Huazhong Univ. Sci. Technol.* **2009**, *37*, 29–32. (In Chinese)
238. Zuo, L.; Cha, H.; Tian, B.; Tian, S.S. A Preliminary Study on the Applicability of Paulus-Jeske Model of Evaporation Duct in China Seas. *Acta Electron. Sin.* **2009**, *37*, 1100–1103. (In Chinese)
239. Tian, B.; Cui, M.D.; Ren, X.C.; Ge, Y.J.; Zeng, G.D.; Song, W. Influence of Seasonal Variation of Evaporation Duct on Electromagnetic Wave Propagation in the Gulf of Aden. *J. Harbin Eng. Univ.* **2018**, *39*, 2054–2063. (In Chinese)
240. Tian, B.; Ge, Y.J.; Li, H.Z.; Yu, P.; Cui, Y.J. Study on the Influence of Evaporation Duct on Electromagnetic Wave Propagation in the Western Indian Ocean Fjord Area. *Adv. Eng. Sci.* **2017**, *49*, 104–110. (In Chinese)
241. Liu, A.G.; Cha, H.; Li, Z.M. Detection Range Prediction Method for Shore-Based Microwave Over-the-Horizon Radar. *J. Huazhong Univ. Sci. Technol.* **2014**, *42*, 96–100. (In Chinese)
242. Song, W.; Tian, B.; Zhou, M.; Li, M.L. Research on Evaporation Duct Prediction Model. *J. Huazhong Univ. Sci. Technol.* **2013**, *41*, 52–56. (In Chinese)
243. Wang, L.D.; Wang, J.A.; Chen, D. Principle and Experimental Analysis of Laser Detection of Evaporation Duct. *J. Huazhong Univ. Sci. Technol.* **2012**, *40*, 80–83. (In Chinese)
244. Ren, X.C.; Wang, J.A.; Wu, R.H. Aerosol Scattering Characteristics Based on Evaporation Duct. *J. Huazhong Univ. Sci. Technol.* **2010**, *38*, 129–132. (In Chinese)

245. Tian, B.; Cha, H.; Zhou, M.; Song, W.; Zhang, N. Adaptability Study of Analytical MGB Model for Evaporation Duct. *Acta Armamentarii* **2010**, *31*, 796–801. (In Chinese)
246. Liu, A.G.; Cha, H. Study of the Microwave OTH Radar Maximum Detection Range of Ships. *J. Xidian Univ.* **2009**, *36*, 741–745. (In Chinese)
247. Tian, B.; Cha, H.; Zhang, Y.S.; Ding, J.L.; Jiang, H.J. Adaptability Study of Evaporation Duct A Model in China Seas. *Chin. J. Radio Sci.* **2009**, *24*, 556–561. (In Chinese)
248. Zhang, J.P.; Zhang, Y.S.; Wu, Z.S.; Zhang, Y.S.; Hu, R.X. Inversion of Regional Range-Dependent Evaporation Duct from Radar Sea Clutter. *Acta Phys. Sin.* **2015**, *64*, 136–146. [CrossRef]
249. Ji, H.; Yin, B.; Zhang, J.; Zhang, Y. Joint Inversion of Evaporation Duct Based on Radar Sea Clutter and Target Echo Using Deep Learning. *Electronics* **2022**, *11*, 2157. [CrossRef]
250. Guo, X.; Zhao, D.; Zhang, L.; Wang, H.; Kang, S. A Comparison Study of Sensitivity on PJ and NPS Models in China Seas. *J. Ocean Univ. China* **2019**, *18*, 1022–1030. [CrossRef]
251. Guo, X.; Li, Q.; Zhao, Q.; Kang, S.; Wei, Y.; Yang, L. A Comparative Study of Rough Sea Surface and Evaporation Duct Models on Radio Wave Propagation. *IEEE Trans. Antennas Propag.* **2023**, *71*, 6060–6071. [CrossRef]
252. Guo, X.; Zhao, D.; Zhang, L.; Wang, H.; Kang, S.; Lin, L. C band transhorizon signal characterisations in evaporation duct propagation environment over Bohai Sea of China. *IET Microw. Antennas Propag.* **2019**, *13*, 407–413. [CrossRef]
253. Zhang, Y.S.; Guo, X.M.; Zhao, Q.; Zhao, Z.W.; Kang, S.F. Research Status and Thinking of Atmospheric Duct. *Chin. J. Radio Sci.* **2020**, *35*, 813–831. (In Chinese)
254. Ji, H.; Yin, B.; Zhang, J.; Zhang, Y.; Li, Q.; Hou, C. Multiscale Decomposition Prediction of Propagation Loss for EM Waves in Marine Evaporation Duct Using Deep Learning. *J. Mar. Sci. Eng.* **2022**, *11*, 51. [CrossRef]
255. Wu, J.; Wei, Z.; Zhang, J.; Guo, X.; Jia, D.; Xu, J.; Zhang, Y.; Li, Q.; Zhou, H. Environmental Knowledge-Driven Over-the-Horizon Propagation Loss Prediction Based on Short- and Long- Parallel Double-Flow TrellisNets. *IEEE Trans. Antennas Propag.* **2023**, *71*, 9799–9813. [CrossRef]
256. Wu, J.; Wei, Z.; Zhang, J.; Zhang, Y.; Jia, D.; Yin, B.; Yu, Y. Full-Coupled Convolutional Transformer for Surface-Based Duct Refractivity Inversion. *Remote Sens.* **2022**, *14*, 4385. [CrossRef]
257. Lin, L.; Zhao, Z.; Zhu, Q.; Zhang, Y. Profiling tropospheric refractivity in real time, based on a relevance vector machine and single ground-based GPS receiver. *Int. J. Remote Sens.* **2012**, *33*, 4044–4058. [CrossRef]
258. Lin, L.K.; Zhao, Z.W.; Zhang, Y.R.; Zhu, Q.L. Tropospheric refractivity profiling based on refractivity profile model using single ground-based global positioning system. *IET Radar Sonar Navig.* **2011**, *5*, 7–11. [CrossRef]
259. Chen, L.; Gao, S.H.; Kang, S.F.; Zhang, Y.S.; Wu, Z.M. Analysis of Synoptic Characteristics of Low-Altitude Atmospheric Duct in Local Coastal Waters of China. *Acta Electron. Sin.* **2010**, *38*, 1997–2002. (In Chinese)
260. Zhang, L.J.; Wang, H.G.; Li, J.R.; Zhang, C.; Han, J.; Wang, Q.N.; Zhu, Q.L. Experimental Analysis of Low-Altitude Atmospheric Duct Monitoring Based on AIS Signals. *Chin. J. Radio Sci.* **2023**, *38*, 108–113. (In Chinese)
261. Huang, L.; Liu, C.; Wu, Z.; Zhang, L.; Wang, H.; Zhu, Q.; Han, J.; Sun, M. Comparative Analysis of Intelligent Optimization Algorithms for Atmospheric Duct Inversion Using Automatic Identification System Signals. *Remote Sens.* **2023**, *15*, 3577. [CrossRef]
262. Lin, L.K.; Zhang, Y.R.; Zhao, Z.W.; Wang, B. Relevance Vector Machine Algorithm for Atmospheric Profile Detection Using Microwave Radiometer. *Chin. J. Radio Sci.* **2009**, *24*, 90–94. (In Chinese)
263. Wu, J.; Wei, Z.; Zhang, J.; Xu, J.; Jia, D.; Ji, H. Trends and frontiers of atmospheric duct research based on CiteSpace and deep learning. *Environ. Sci. Pollut. Res.* **2022**, *29*, 82336–82350. [CrossRef] [PubMed]
264. Lin, F.J.; Wang, H.G.; Lin, L.K.; Ni, H.W. Study on the Influence of Wind Direction on the Environmental Characteristics of Evaporation Duct. *Chin. J. Radio Sci.* **2007**, *22*, 410–413. (In Chinese)
265. Lin, F.J.; Liu, C.G.; Cheng, S.; Yang, Y.P. Statistical Analysis of Marine Atmospheric Duct. *Chin. J. Radio Sci.* **2005**, *20*, 64–68. (In Chinese)
266. Lin, F.J.; Liu, C.G.; Pan, Z.W. Detection of Atmospheric Duct near Sea Surface and Comparison with Other Research Results. *Chin. J. Radio Sci.* **2002**, *17*, 269–281. (In Chinese)
267. Zhang, Y.S.; Han, J.; Guo, X.M.; Hao, X.J.; Kang, S.F. Research on Trapping Duct Prediction Based on Wet Potential Vorticity Field. *Chin. J. Radio Sci.* **2011**, *26*, 610–614. (In Chinese)
268. Zhang, Y.S.; Kang, S.F.; Zhao, Z.W.; Han, J.; Guo, X.M.; Cheng, Y.H. Simulation Analysis of Correlation between Atmospheric Duct and Meteorological Physical Quantity Fields. *Chin. J. Radio Sci.* **2009**, *24*, 742–747. (In Chinese)
269. Chen, L. Statistical Analysis of Atmospheric Duct Characteristics in China's Coastal Waters and Numerical Study of Evolution Mechanism. Ph.D. Thesis, Ocean University of China, Qingdao, China, 2010. (In Chinese)
270. Guo, X.M.; Kang, S.F.; Han, J.; Zhang, Y.S.; Wang, H.G.; Zhang, S.B. Evaporation Duct Database and Statistical Analysis for the Chinese Sea Areas. *Chin. J. Radio Sci.* **2013**, *28*, 1147–1152. (In Chinese)
271. Pan, Z.W.; Liu, C.G.; Guo, L. Prediction Method of Duct Structure in Southeast Coastal Areas. *Chin. J. Radio Sci.* **1996**, *11*, 58–64. (In Chinese)

272. Liu, C.G.; Pan, Z.W. Limiting Frequency and Penetration Angle of Low-Altitude Atmospheric Duct in China. *J. China Inst. Commun.* **1998**, *19*, 12–18. (In Chinese)
273. Huang, L.; Liu, C.; Wang, H.; Zhu, Q.; Zhang, L.; Han, J.; Zhang, Y.; Wang, Q. Experimental Analysis of Atmospheric Ducts and Navigation Radar Over-the-Horizon Detection. *Remote Sens.* **2022**, *14*, 2588. [CrossRef]
274. Zhao, Z. Statistical Analysis of Atmospheric Ducts in the Yellow and Bohai Seas of China and Study of Their Electromagnetic Wave Propagation Characteristics. *Atmosphere* **2024**, *15*, 1041. [CrossRef]
275. Gao, Y.; Zhang, Y.; Zhao, X.; Shi, Y.; Guo, X.; Wang, B. Evaporation Duct Anomalies Caused by Mesoscale Eddies in the Kuroshio Extension. *Geophys. Res. Lett.* **2024**, *51*, e2024GL108404. [CrossRef]
276. Chen, L.; Gao, S.H.; Kang, S.F.; Zhang, Y.S.; Wu, Z.M. Spatiotemporal Characteristics of Atmospheric Duct in China's Coastal Waters. *Chin. J. Radio Sci.* **2009**, *24*, 702–708. (In Chinese)
277. Dong, X.; Sun, F.; Zhu, Q.; Lin, L.; Zhao, Z.; Zhou, C. Tropospheric Refractivity Profile Estimation by GNSS Measurement at China Big-Triangle Points. *Atmosphere* **2021**, *12*, 1468. [CrossRef]
278. Wu, J.; Wei, Z.; Liu, C.; Ma, Q.; Wei, Z.; Cui, T.; Li, Q.; Wu, X.; Ye, J.; Wu, S.; et al. Ad-SACNet: Spatial Attention Compression Network for Atmospheric duct inversion with Radar Sea Clutter Data. *IEEE Trans. Antennas Propag.* 2026, *early access*. [CrossRef]
279. Koshel, K.V.; Shishkarev, A.A. Influence of layer and anisotropic fluctuations of the refractive index on the beyond-the-horizon SHF propagation in the troposphere over the sea when there is an evaporation duct. *Waves Random Media* **1993**, *3*, 25–38. [CrossRef]
280. Strelkov, G.M. Propagation of narrow radiobeam in an evaporation duct: A numerical experiment. *J. Commun. Technol. Electron.* **1996**, *41*, 1199–1205.
281. Lytaev, M.S. Discretize-Then-Optimize Approach to Real-Time Tropospheric Refractivity Inversion. *IEEE Antennas Wirel. Propag. Lett.* **2025**, *24*, 1919–1923. [CrossRef]
282. Lytaev, M.S. Tropospheric Refractivity Estimation Using DeepONet. *IEEE Antennas Wirel. Propag. Lett.* **2025**, *24*, 3794–3798. [CrossRef]
283. Lytaev, M.S. Numerical method-informed DeepONet for refractivity inversion in waveguides. *J. Comput. Sci.* **2026**, *94*, 102788. [CrossRef]
284. Pasricha, P.K.; Prasad, M.V.S.N.; Sarkar, S.K. Comparison of evaporation duct models to compute duct height over Arabian sea and Bay of Bengal. *Indian J. Radio Space Phys.* **2002**, *31*, 155–158.
285. Sarma, S.B.S.S. High resolution radio refractive index studies in India using airborne microwave refractometers. *J. Earth Syst. Sci.* **1991**, *100*, 145–154. [CrossRef]
286. Venkiteshwaran, S.P.; Narayanan, G.C.V.S.; Sinha, H.S.S. Radio Refractivity Profile Over India. *IETE J. Res.* **1969**, *15*, 395–410. [CrossRef]
287. Basha, G.; Venkat Ratnam, M.; Manjula, G.; Chandra Sekhar, A.V. Anomalous propagation conditions observed over a tropical station using high-resolution GPS radiosonde observations. *Radio Sci.* **2013**, *48*, 42–49. [CrossRef]
288. Kulessa, A.S.; Woods, G.S.; Piper, B.; Heron, M.L. Line-of-sight EM propagation experiment at 10.25 GHz in the tropical ocean evaporation duct. *IEE Proc. Microw. Antennas Propag.* **1998**, *145*, 65–69. [CrossRef]
289. Kulessa, A.S.; Barrios, A.; Claverie, J.; Garrett, S.; Haack, T.; Hacker, J.M.; Hansen, H.J.; Horgan, K.; Hurtaud, Y.; Lemon, C.; et al. The Tropical Air-Sea Propagation Study (TAPS). *Bull. Am. Meteorol. Soc.* **2017**, *98*, 517–537. [CrossRef]
290. Salamon, S.J.; Hansen, H.J.; Abbott, D. Modelling radio refractive index in the atmospheric surface layer. *Electron. Lett.* **2015**, *51*, 1119–1121. [CrossRef]
291. von Engeln, A.; Teixeira, J. A ducting climatology derived from the European Centre for Medium-Range Weather Forecasts global analysis fields. *J. Geophys. Res. Atmos.* **2004**, *109*, D18104. [CrossRef]
292. Jeske, H. State and Limits of Prediction Methods of Radar Wave Propagation Conditions Over Sea. In *Modern Topics in Microwave Propagation and Air-Sea Interaction*; Zancla, A., Ed.; Springer: Dordrecht, The Netherlands, 1973; pp. 130–148.
293. Jin, T.; Cho, J.; Jang, D.; Choo, H. Prediction of Atmospheric Duct Conditions from a Clutter Power Spectrum Using Deep Learning. *Remote Sens.* **2024**, *16*, 674. [CrossRef]
294. Heo, J.; Jang, D.; Choo, H.; Na, D.; Park, Y.B. Real-Time Duct Prediction and Propagation Analysis Using Genetic Algorithm-Based RFC and Parabolic Equation Method. *IEEE Access* **2025**, *13*, 471–479. [CrossRef]
295. Jang, B.; Heo, J.; Park, Y.B.; Na, D. NWP-based Atmospheric Refractivity Modeling and Fast & Stable Non-uniform Plane Wave Ray-Tracing Simulations for LEO Link Analysis. *IEEE Antennas Wirel. Propag. Lett.* **2026**, *25*, 1847–1851. [CrossRef]
296. Heo, J.; Yang, J.; Kim, J.; Na, D.; Park, Y.B. Propagation Analysis Using Discrete Mixed Fourier Transform-Based Parabolic Equation Method for Long Range Radar Detection Error Correction. *IEEE Access* **2023**, *11*, 119436–119445. [CrossRef]
297. Jin, T.; Jang, D.; Choo, H. Prediction of Atmospheric Refractivity From Clutter Power Images Using a Convolutional Neural Network and a Trilinear Atmospheric Model. *IEEE Access* **2025**, *13*, 35567–35573. [CrossRef]
298. Keun, J.; Jang, D.; Choo, H. Analysis of LEO Satellite Detection Errors Considering Atmospheric Environment. *IEEE Open J. Antennas Propag.* **2025**, *6*, 1708–1716. [CrossRef]

299. Wang, C.; Wilson, D.; Haack, T.; Clark, P.; Lean, H.; Marshall, R. Effects of Initial and Boundary Conditions of Mesoscale Models on Simulated Atmospheric Refractivity. *J. Appl. Meteorol. Climatol.* **2012**, *51*, 115–132. [CrossRef]
300. Gunashekar, S.D.; Warrington, E.M.; Siddle, D.R. Long-term statistics related to evaporation duct propagation of 2 GHz radio waves in the English Channel. *Radio Sci.* **2010**, *45*, RS6010. [CrossRef]
301. Gunashekar, S.D.; Warrington, E.M.; Siddle, D.R.; Valtr, P. Signal strength variations at 2 GHz for three sea paths in the British Channel Islands: Detailed discussion and propagation modeling. *Radio Sci.* **2007**, *42*, RS4020. [CrossRef]
302. Atkinson, B.W.; Li, J.G.; Plant, R.S. Numerical Modeling of the Propagation Environment in the Atmospheric Boundary Layer over the Persian Gulf. *J. Appl. Meteorol.* **2001**, *40*, 586–603. [CrossRef]
303. Zhu, M.; Atkinson, B.W. Simulated climatology of atmospheric ducts over the Persian Gulf. *Bound.-Layer Meteorol.* **2005**, *115*, 433–452. [CrossRef]
304. Atkinson, B.W.; Zhu, M. Coastal effects on radar propagation in atmospheric ducting conditions. *Meteorol. Appl.* **2006**, *13*, 53–62. [CrossRef]
305. Lee, Y.H.; Dong, F.; Meng, Y.S. Near Sea-Surface Mobile Radiowave Propagation at 5 GHz: Measurements and Modeling. *Radioengineering* **2014**, *23*, 824–830.
306. Lee, Y.H.; Meng, Y.S. Empirical Modeling of Ducting Effects on a Mobile Microwave Link Over a Sea Surface. *Radioengineering* **2012**, *21*, 1054–1059.
307. Lee, Y.H.; Meng, Y.S.; Yao, Y. Key Considerations in the Modeling of Tropical Maritime Microwave Attenuations. *Int. J. Antennas Propag.* **2015**, *2015*, 246793. [CrossRef]
308. Douvenot, R.; Fabbro, V.; Gerstoft, P.; Bourlier, C.; Saillard, J. Real time refractivity from clutter using a best fit approach improved with physical information. *Radio Sci.* **2010**, *45*, RS1007. [CrossRef]
309. Douvenot, R.; Fabbro, V.; Bourlier, C.; Saillard, J.; Fuchs, H.; Essen, H.; Foerster, J. Retrieve the evaporation duct height by least-squares support vector machine algorithm. *J. Appl. Remote Sens.* **2009**, *3*, 33503. [CrossRef]
310. Douvenot, R.; Fabbro, V.; Gerstoft, P.; Bourlier, C.; Saillard, J. A duct mapping method using least squares support vector machines. *Radio Sci.* **2008**, *43*, RS6005. [CrossRef]
311. Douvenot, R.; Fabbro, V. On the knowledge of radar coverage at sea using real time refractivity from clutter. *IET Radar Sonar Navig.* **2010**, *4*, 293–301. [CrossRef]
312. Mesnard, F.; Sauvageot, H. Climatology of Anomalous Propagation Radar Echoes in a Coastal Area. *J. Appl. Meteorol. Climatol.* **2010**, *49*, 2285–2300. [CrossRef]
313. Musson Genon, L.; Gauthier, S.; Bruth, E. A simple method to determine evaporation duct height in the sea surface boundary layer. *Radio Sci.* **1992**, *27*, 635–644. [CrossRef]
314. Isaakidis, S.A.; Xenos, T.D.; Dris, N.A. Tropospheric ducting phenomena over the Hellenic region. *Int. J. Commun. Syst.* **2004**, *17*, 337–346. [CrossRef]
315. Isaakidis, S.A.; Dimou, I.N.; Xenos, T.D.; Dris, N.A. An artificial neural network predictor for tropospheric surface duct phenomena. *Nonlinear Process. Geophys.* **2007**, *14*, 569–573. [CrossRef]
316. Isaakidis, S.A.; Xenos, T.D. Ten years analysis of Tropospheric refractivity variations. *Ann. Geophys.* **2004**, *47*, 1234–1245. [CrossRef]
317. Ivanov, V.K.; Shalyapin, V.N.; Levadnyi, Y. Determination of the evaporation duct height from standard meteorological data. *Izv. Atmos. Ocean. Phys.* **2007**, *43*, 36–44. [CrossRef]
318. Ivanov, V.K.; Shalyapin, V.N.; Levadny, Y.V. Microwave scattering by tropospheric fluctuations in an evaporation duct. *Radiophys. Quantum Electron.* **2009**, *52*, 277–286. [CrossRef]
319. Levadnyi, Y.V.; Ivanov, V.K.; Shalyapin, V.N. Simulation of centimeter wave propagation in evaporation duct over the rough sea surface. *Telecommun. Radio Eng.* **2010**, *69*, 773–784. [CrossRef]
320. Sirkova, I. Revisiting Enhanced AIS Detection Range under Anomalous Propagation Conditions. *J. Mar. Sci. Eng.* **2023**, *11*, 1838. [CrossRef]
321. Sirkova, I.; Hernandez-Figueroa, H.E. Local transparent boundary condition applied to the modeling of tropospheric ducting propagation. *Microw. Opt. Technol. Lett.* **1999**, *21*, 343–346. [CrossRef]
322. Sirkova, I.D. Comparison between a local and a nonlocal transparent boundary condition applied to the tropospheric ducting propagation problem. *Microw. Opt. Technol. Lett.* **2000**, *25*, 44–47. [CrossRef]
323. Sirkova, I. Brief review on PE method application to propagation channel modeling in sea environment. *Cent. Eur. J. Eng.* **2012**, *2*, 19–38. [CrossRef]
324. Sirkova, I.; Mikhalev, M. Parabolic Wave Equation Method Applied to the Tropospheric Ducting Propagation Problem: A Survey. *Electromagnetics* **2006**, *26*, 155–173. [CrossRef]
325. Sirkova, I.; Mikhalev, M. Parabolic-equation-based study of ducting effects on microwave propagation. *Microw. Opt. Technol. Lett.* **2004**, *42*, 390–394. [CrossRef]

326. Ozgun, O.; Sahin, V.; Erguden, M.E.; Apaydin, G.; Yilmaz, A.E.; Kuzuoglu, M.; Sevgi, L. PETOOL v2.0: Parabolic Equation Toolbox with evaporation duct models and real environment data. *Comput. Phys. Commun.* **2020**, *256*, 107454. [CrossRef]
327. Ozgun, O.; Apaydin, G.; Kuzuoglu, M.; Sevgi, L. PETOOL: MATLAB-based one-way and two-way split-step parabolic equation tool for radiowave propagation over variable terrain. *Comput. Phys. Commun.* **2011**, *182*, 2638–2654. [CrossRef]
328. Mentes, S.S.; Kaymaz, Z. Investigation of Surface Duct Conditions over Istanbul, Turkey. *J. Appl. Meteorol. Climatol.* **2007**, *46*, 318–337. [CrossRef]
329. Tepecik, C.; Navruz, I. A novel hybrid model for inversion problem of atmospheric refractivity estimation. *Int. J. Electron. Commun.* **2018**, *84*, 258–264. [CrossRef]
330. Ao, C.O. Effect of ducting on radio occultation measurements: An assessment based on high-resolution radiosonde soundings. *Radio Sci.* **2007**, *42*, RS2008. [CrossRef]
331. Sokolovskiy, S.; Schreiner, W.; Zeng, Z.; Hunt, D.; Lin, Y.C.; Kuo, Y.H. Observation, analysis, and modeling of deep radio occultation signals: Effects of tropospheric ducts and interfering signals. *Radio Sci.* **2014**, *49*, 954–970. [CrossRef]
332. Lee, H.; Lee, T.; Chun, J.; Lee, J. Target Positioning with Surveillance Radar by the Estimation of Atmospheric Refractivity Profile. *IEEE Trans. Aerosp. Electron. Syst.* **2020**, *56*, 2245–2255. [CrossRef]
333. Yang, C.; Wang, J. The Investigation of Cooperation Diversity for Communication Exploiting Evaporation Ducts in the South China Sea. *IEEE Trans. Antennas Propag.* **2022**, *70*, 8337–8347. [CrossRef]
334. Yang, C.; Wang, J.; Ma, J. Exploration of X-Band Communication for Maritime Applications in the South China Sea. *IEEE Antennas Wirel. Propag. Lett.* **2022**, *21*, 481–485. [CrossRef]
335. Yang, C.; Shi, Y.; Wang, J.; Feng, F. Regional Spatiotemporal Statistical Database of Evaporation Ducts Over the South China Sea For Future Long-Range Radio Application. *IEEE J. Sel. Top. Appl. Earth Obs. Remote Sens.* **2022**, *15*, 6432–6444. [CrossRef]
336. Hong, F.; Zhang, Q. Time Series Analysis of Evaporation Duct Height over South China Sea: A Stochastic Modeling Approach. *Atmosphere* **2021**, *12*, 1663. [CrossRef]
337. Ijioma, B.A.; Akpan, A.E. Radio Duct Estimation in Some Selected Areas of the Gulf of Guinean Troposphere. *J. Sci. Technol. Res.* **2022**, *4*, 171–178.
338. Qin, T.; Su, B.; Chen, L.; Yang, J.; Sun, H.; Ma, J.; Yu, W. Arctic Atmospheric Ducting Characteristics and Their Connections with Arctic Oscillation and Sea Ice. *Atmosphere* **2022**, *13*, 2119. [CrossRef]
339. Zhang, Q.; Chen, X.; Yin, F.; Hong, F. Analysis and Research on Chaotic Dynamics of Evaporation Duct Height Time Series with Multiple Time Scales. *Atmosphere* **2022**, *13*, 2072. [CrossRef]
340. Zhou, Y.; Liu, Y.; Qiao, J.; Li, J.; Zhou, C. Statistical Analysis of the Spatiotemporal Distribution of Lower Atmospheric Ducts over the Seas Adjacent to China, Based on the ECMWF Reanalysis Dataset. *Remote Sens.* **2022**, *14*, 4864. [CrossRef]
341. Cheng, Y.; Zhou, S.; Wang, D.; Lu, Y.; Huang, K.; Yao, J.; You, X. Characteristics of the atmospheric ducts over the South China Sea pre- and post-monsoon onset in 1998. *Chin. J. Oceanol. Limnol.* **2016**, *34*, 619–628.
342. Geernaert, G.L. On the Evaporation Duct for Inhomogeneous Conditions in Coastal Regions. *J. Appl. Meteorol. Climatol.* **2007**, *46*, 538–543. [CrossRef]
343. Yang, S.; Li, X.; Wu, C.; He, X.; Zhong, Y. Application of the PJ and NPS evaporation duct models over the South China Sea (SCS) in winter. *PLoS ONE* **2017**, *12*, e0172284. [CrossRef]
344. Zhang, C.; Qiu, Z.; Fan, C.; Song, G.; Wang, B.; Hu, T.; Zou, J.; Li, Z.; Wu, S. Research on a Multimodel Fusion Diagnosis Method for Evaporation Ducts in the East China Sea. *Sensors* **2023**, *23*, 8786. [CrossRef] [PubMed]
345. Wang, Q.; Li, X.; Li, H.; Yang, S.; Yang, S.; Ma, L.; Zhao, J. A Novel System for the Measurement of an Evaporation Duct Using the Magnetic Coupling Principle for Power Feeding and Data Transmission. *Sensors* **2022**, *22*, 7376. [CrossRef] [PubMed]
346. Qiu, Z.; Zhang, C.; Wang, B.; Hu, T.; Zou, J.; Li, Z.; Chen, S.; Wu, S. Analysis of the accuracy of using ERA5 reanalysis data for diagnosis of evaporation ducts in the East China Sea. *Front. Mar. Sci.* **2023**, *9*, 1108600. [CrossRef]
347. Cheng, Y.; Zha, M.; You, Z.; Zhang, Y. Duct climatology over the South China Sea based on European Center for Medium Range Weather Forecast reanalysis data. *J. Atmos. Sol.-Terr. Phys.* **2021**, *222*, 105720. [CrossRef]
348. Skolnik, M.I. *Introduction to Radar Systems*; McGraw-Hill: New York, NY, USA, 1962.
349. Bean, B.R.; Dutton, E.J. *Radio Meteorology*; Dover Publications: New York, NY, USA, 1968.
350. Zhang, J.P. Research on Inversion Methods of Tropospheric Duct Using Radar Sea Clutter/GPS Signals. Ph.D. Thesis, Xidian University, Xi'an, China, 2013. (In Chinese)
351. Pham, C.C.; Nguyen, X.A. Determination of radio wave propagation conditions in the atmosphere of Hanoi using the radiosonde data of balloons. *ICT Express* **2022**, *8*, 611–617. [CrossRef]
352. Bussey, H.; Birnbaum. Measurement of variations in atmospheric refractive index with an airborne microwave refractometer. *J. Res. Int. Bur. Stand.* **1953**, *51*, 171. [CrossRef]
353. Stapleton, J.K.; Wiss, V.R.; Marshall, R.E. Measured Anomalous Radar Propagation and Ocean Backscatter in the Virginia Coastal Region. In Proceedings of the 31st International Conference on Radar Meteorology, Seattle, WA, USA, 6–12 August 2003.

354. Essen, H.; Fuchs, H.; Pagels, A. Radar propagation in coastal environments: Vampira results. In Proceedings of the SPIE Environmental Remote Sensing, 2006, Stockholm, Sweden, 11–14 September 2006; Volume 6364.
355. Cook, D.; Garrett, S. The Seabreeze 2009 experiment: Investigating the impact of ocean and atmospheric processes on radar performance in the Bay of Plenty, New Zealand. *N. Z. Clim. Weather* **2011**, *31*, 82–100.
356. Babin, S.M. Surface Duct Height Distributions for Wallops Island, Virginia, 1985–1994. *J. Appl. Meteorol.* **1996**, *35*, 86–93. [CrossRef]
357. Sarma, S. Elevated Duct Effects on Radar Ranges Using an Airborne Microwave Refractometer. *Aust. J. Phys.* **1990**, *43*, 99–106. [CrossRef]
358. Leontakianakos, A.N. S-band clear air propagation and ducting in coastal West Africa. *Microw. Opt. Technol. Lett.* **1997**, *15*, 102–106. [CrossRef]
359. Foken, T. 50 years of the Monin-Obukhov similarity theory. *Bound.-Layer Meteorol.* **2006**, *119*, 431–447. [CrossRef]
360. Liu, W.T.; Katsaros, K.B.; Businger, J.A. Bulk Parameterization of Air-Sea Exchanges of Heat and Water Vapor Including the Molecular Constraints at the Interface. *J. Atmos. Sci.* **1979**, *36*, 1722–1735. [CrossRef]
361. Liu, W.T.; Blanc, T.V. *The Liu, Katsaros, and Businger (1979) Bulk Atmospheric Flux Computational Iteration Program in FORTRAN and BASIC*; Naval Research Laboratory: Washington, DC, USA, 1984. Available online: https://api.semanticscholar.org/CorpusID:93902184 (accessed on 8 May 1984).
362. Fairall, C.W.; Bradley, E.F.; Hare, J.E.; Grachev, A.A.; Edson, J.B. Bulk Parameterization of Air–Sea Fluxes: Updates and Verification for the COARE Algorithm. *J. Clim.* **2003**, *16*, 571–591. [CrossRef]
363. Ji, H.; Guo, L.; Zhang, Y.; Nie, T.; Wei, Y.; Zhang, J.; Li, Q.; Guo, X.; Zhang, Y. Numerical modeling of electromagnetic wave propagation in spatially-varying evaporation duct conditions via 3D parabolic equation method. *Front. Mar. Sci.* **2025**, *12*, 1611884. [CrossRef]
364. Babin, S.M. A New Model of the Oceanic Evaporation Duct and Its Comparison with Current Models. Ph.D. Thesis, University of Maryland, College Park, MD, USA, 1996.
365. Qiu, Z.; Hu, T.; Wang, B.; Zou, J.; Li, Z. Selection Optimal Method of Evaporation Duct Model Based on Sensitivity Analysis. *J. Atmos. Ocean. Technol.* **2022**, *39*, 941–957. [CrossRef]
366. Zhang, Y.S. Case Study of Synoptic Situation Related to Atmospheric Duct Structure. *Chin. J. Radio Sci.* **2004**, *19*, 227–229. (In Chinese)
367. Grell, G.A.; Dudhia, J.; Stauffer, D.R. *A Description of the Fifth-Generation Penn State/NCAR Mesoscale Model (MM5)*; National Center for Atmospheric Research: Boulder, CO, USA, 1994. Available online: https://api.semanticscholar.org/CorpusID:130948085(1994) (accessed on 20 May 2026).
368. Skamarock, W.C.; Klemp, J.B.; Dudhia, J.; Gill, D.O.; Powers, J.G. *A Description of the Advanced Research WRF Version 3*; National Center for Atmospheric Research: Boulder, CO, USA, 2008.
369. Wang, S.; Gao, S. An Ensemble Diagnosis Method for Evaporation Duct and Its Application in Numerical Prediction. *Acta Electron. Sin.* **2019**, *47*, 1049–1057. (In Chinese)
370. Krolik, J.L.; Tabrikian, J.; Vasudevan, A.; Rogers, L.T. Using radar sea clutter to estimate refractivity profiles associated with the capping inversion of the marine atmospheric boundary layer. In Proceedings of the 1999 IEEE International Geoscience and Remote Sensing Symposium, Hamburg, Germany, 28 June–2 July 1999; pp. 649–651.
371. Rogers, L.T.; Hattan, C.P.; Krolik, J.L. Using radar sea echo to estimate surface layer refractivity profiles. In Proceedings of the IEEE 1999 International Geoscience and Remote Sensing Symposium, Hamburg, Germany, 28 June–2 July 1999; pp. 658–662.
372. Vasudevan, S.; Krolik, J.L. Refractivity estimation from radar clutter by sequential importance sampling with a Markov model for microwave propagation. In Proceedings of the 2001 IEEE International Conference on Acoustics, Speech, and Signal Processing, Salt Lake City, UT, USA, 7–11 May 2001; pp. 2905–2908.
373. Vasudevan, S.; Anderson, R.H.; Kraut, S.; Gerstoft, P.; Rogers, L.T.; Krolik, J.L. Recursive Bayesian electromagnetic refractivity estimation from radar sea clutter. *Radio Sci.* **2007**, *42*, RS2014. [CrossRef]
374. Gerstoft, P.; Hodgkiss, W.S.; Rogers, L.T.; Jablecki, M. Probability distribution of low-altitude propagation loss from radar sea clutter data. *Radio Sci.* **2004**, *39*, RS6006. [CrossRef]
375. Yardim, C.; Gerstoft, P.; Hodgkiss, W.S. Estimation of radio refractivity from Radar clutter using Bayesian Monte Carlo analysis. *IEEE Trans. Antennas Propag.* **2006**, *54*, 1318–1327. [CrossRef]
376. Yardim, C.; Gerstoft, P.; Hodgkiss, W.S. Statistical maritime radar duct estimation using hybrid genetic algorithm–Markov chain Monte Carlo method. *Radio Sci.* **2007**, *42*, RS3014. [CrossRef]
377. Yardim, C.; Gerstoft, P.; Hodgkiss, W.S. Tracking atmospheric ducts using radar clutter: Evaporation duct tracking using kalman filters. In Proceedings of the 2007 IEEE Antennas and Propagation Society International Symposium, Honolulu, HI, USA, 9–15 June 2007; pp. 4609–4612.
378. Jang, D.; Kim, J.; Park, Y.B.; Choo, H. Study of an Atmospheric Refractivity Estimation from a Clutter Using Genetic Algorithm. *Appl. Sci.* **2022**, *12*, 8566. [CrossRef]

379. Cui, Y.; Hu, T.; Qi, K.; Qiu, Z.; Zou, J.; Li, Z.; Wang, B. Research on Optimization Method of Evaporation Duct Prediction Model. *Mathematics* **2024**, *12*, 205. [CrossRef]
380. Cheng, R.; Liu, C.; Cao, L.; Xiao, T.; Tang, G.; Huang, L.; Wang, H. The Influence of PE Initial Field Construction Method on Radio Wave Propagation Loss and Tropospheric Duct Inversion. *Atmosphere* **2023**, *15*, 46. [CrossRef]
381. Wang, B.; Wu, Z.; Zhao, Z. Performance Comparison of GA, PSO, and DE Approaches in Estimating Low Atmospheric Refractivity Profiles. *Wuhan Univ. J. Nat. Sci.* **2010**, *15*, 433–439. [CrossRef]
382. Tang, W.; Liu, S.; Hu, H.; Liu, L.; Xie, Y. Atmospheric Ducts Inversion with Over-the-Horizon Propagation of Automatic Identification System Signals. *APSIPA Trans. Signal Inf. Proc.* **2024**, *13*, 1–14. [CrossRef]
383. Tang, W.; Hu, H.; Liu, S.; Tian, B. Validation of Atmospheric Ducts Inversion Using Automatic Identification System Signals at Sea. *IET Microw. Antennas Propag.* **2025**, *19*, e70051. [CrossRef]
384. Yang, C. Estimation of the Atmospheric Duct from Radar Sea Clutter Using Artificial Bee Colony Optimization Algorithm. *Prog. Electromagn. Res.* **2013**, *135*, 183–199. [CrossRef]
385. Wang, B.; Wu, Z.; Zhao, Z.; Wang, H. Retrieving Evaporation Duct from Radar Sea Clutter Based on Ant Colony Algorithm. *Chin. J. Radio Sci.* **2009**, *24*, 598–603. (In Chinese)
386. Yang, C.; Guo, L. Inferring the Atmospheric Duct from Radar Sea Clutter Using the Improved Artificial Bee Colony Algorithm. *Int. J. Microw. Wirel. Technol.* **2018**, *10*, 437–445. [CrossRef]
387. Zhou, W.; Shen, M.; Zhang, Y.; Wu, D.; Zhu, D. Offshore Surface Evaporation Duct Joint Inversion Algorithm Using Measured Dual-Frequency Sea Clutter. *IEEE J. Sel. Top. Appl. Earth Obs. Remote Sens.* **2022**, *15*, 6382–6390. [CrossRef]
388. Yang, C.; Wang, Y. Inversion of the Surface Duct from Radar Sea Clutter Using the Improved Whale Optimization Algorithm. *Electromagnetics* **2019**, *39*, 611–627. [CrossRef]
389. Wang, B.; Zhao, Z.W.; Wu, Z.S.; Wang, H.G. Study on Inversion of Atmospheric Duct Using Multi-Band Radar Clutter. *Chin. J. Radio Sci.* **2010**, *25*, 865–870. (In Chinese)
390. Zhou, M.; Zuo, L.; Wang, C.; Jin, D.; Wang, Y.; Feng, C. Inversion of Evaporation Duct Based on Genetic/Simulated Annealing Hybrid Algorithm. *Chin. J. Radio Sci.* **2014**, *29*, 122–128. (In Chinese)
391. Ji, H.; Guo, L.; Zhang, J.; Wei, Y.; Li, Q.; Guo, X.; Zhang, Y. A Bayesian Fusion Framework for Characterizing Marine Ducts Using Multisource Prior Constraints. *IEEE Geosci. Remote Sens. Lett.* **2025**, *22*, 3505105. [CrossRef]
392. Wang, H.; Zhang, L.; Han, J.; Huang, L.; Zhu, Q. Estimation of surface duct parameters using AIS data based on Bayesian inversion method. *Front. Mar. Sci.* **2025**, *12*, 1639777. [CrossRef]
393. Kraut, S.; Anderson, R.H.; Krolik, J.L. A generalized Karhunen-Loeve basis for efficient estimation of tropospheric refractivity using radar clutter. *IEEE Trans. Signal Process.* **2004**, *52*, 48–60. [CrossRef]
394. Lowry, A.R.; Rocken, C.; Sokolovskiy, S.V.; Anderson, K.D. Vertical profiling of atmospheric refractivity from ground-based GPS. *Radio Sci.* **2002**, *37*, 13-1–13-19. [CrossRef]
395. Zuffada, C.; Hajj, G.A.; Kursinski, E.R. A novel approach to atmospheric profiling with a mountain-based or airborne GPS receiver. *J. Geophys. Res. Atmos.* **1999**, *104*, 24435–24447. [CrossRef]
396. Wu, Y.Y.; Hong, Z.J.; Guo, F.; Zheng, J. Simulation of Atmospheric Refractive Profile Retrieving from Low-Elevation Ground-Based GPS Observation. *Chin. J. Geophys.* **2010**, *53*, 1085–1090. [CrossRef]
397. Cui, M.; Zhang, Y. Deep Learning Method for Evaporation Duct Inversion Based on GPS Signal. *Atmosphere* **2022**, *13*, 2091. [CrossRef]
398. Tabrikian, J.; Krolik, J.L. Theoretical performance limits on tropospheric refractivity estimation using point-to-point microwave measurements. *IEEE Trans. Antennas Propag.* **1999**, *47*, 1727–1734. [CrossRef]
399. Valtr, P.; Pechac, P.; Kvicera, V.; Grabner, M. Estimation of the Refractivity Structure of the Lower Troposphere From Measurements on a Terrestrial Multiple-Receiver Radio Link. *IEEE Trans. Antennas Propag.* **2011**, *59*, 1707–1715. [CrossRef]
400. López, R.; Río, V. High Temporal Resolution Refractivity Retrieval from Radar Phase Measurements. *Remote Sens.* **2018**, *10*, 896. [CrossRef]
401. Hallen, H.; Philbrick, C.R. Raman lidar measurements for boundary layer gradients and atmospheric refraction of millimeter-wave signals. In Proceedings of the Laser Radar Technology and Applications Conference, Online, 22–26 June 2020; pp. 123–130.
402. Agnew, J.; Twort, K. A Raman backscattering lidar system for radio refractivity determination. In Proceedings of the 21st ILRC Conference, Quebec City, QC, Canada, 8–12 July 2002; pp. 713–716.
403. Willitsford, A.; Philbrick, C.R. Lidar description of the evaporative duct in ocean environments. In Proceedings of the SPIE Optics + Photonics, San Diego, CA, USA, 31 July–1 August 2005; Voume 5885, pp. 140–147.
404. Philbrick, C.R.; Blood, D.W. Lidar measurements of refractive propagation effects. In *Propagation Assessment in Coastal Environments*; AGARD: Neuilly-sur-Seine, France, 1995; pp. 1–13.
405. Gibson, A.I.; Craig, K.H.; Yilmaz, U.M. Remote sensing of radio refractivity by lidar. In Proceedings of the Tenth International Conference on Antennas and Propagation, Edinburgh, UK, 14–17 April 1997; pp. 234–237.

406. Douvenot, R.; Fabbro, V.; Fuchs, H.H.; Essen, H.; Bourlier, C.; Saillard, J.; Hurtaud, Y. Retrieving evaporation duct heights from measured propagation factors. In Proceedings of the 2007 IET International Conference on Radar Systems, Edinburgh, UK, 15–18 October 2007; pp. 1–5.
407. Douvenot, R.; Fabbro, V.; Bourlier, C.; Saillard, J.; Fuchs, H.H.; Essen, H. Refractivity from sea clutter applied on VAMPIRA and Wallops' 98 data. In Proceedings of the 2008 International Conference on Radar, Adelaide, SA, Australia, 2–5 September 2008; pp. 482–487.
408. Douvenot, R.; Fabbro, V.; Bourlier, C.; Saillard, J. Inverse methods for Refractivity From Clutter. In Proceedings of the 2008 International Conference on Radar, Adelaide, SA, Australia, 2–5 September 2008; pp. 488–491.
409. Yang, C. A Comparison of the Machine Learning Algorithm for Evaporation Duct Estimation. *Radioengineering* **2013**, *22*, 657–661.
410. Yang, C.; Wang, Y.; Zhang, A.; Fan, H.; Guo, L. A Random Forest Algorithm Combined with Bayesian Optimization for Atmospheric Duct Estimation. *Remote Sens.* **2023**, *15*, 4296. [CrossRef]
411. Yang, N.; Song, D.; Su, D.; Lu, T.; Sun, L.; Wang, T. The Influence of Sea Surface Temperature from ECMWF Reanalysis Data on the Nonuniformity of Evaporation Duct. *IEEE Geosci. Remote Sens. Lett.* **2024**, *21*, 1503805. [CrossRef]
412. Yang, N.; Su, D.; Sun, L.; Lu, T.; Song, D.; Wang, T. The Horizontal Inhomogeneity of the Evaporation Duct Based on Surface Bulk Measurements Over the South China Sea. *IEEE Trans. Antennas Propag.* **2024**, *72*, 7916–7926. [CrossRef]
413. Rasp, S.; Hoyer, S.; Merose, A.; Langmore, I.; Battaglia, P.; Russell, T.; Sanchez-Gonzalez, A.; Yang, V.; Carver, R.; Agrawal, S.; et al. WeatherBench 2: A Benchmark for the Next Generation of Data-Driven Global Weather Models. *J. Adv. Model. Earth Syst.* **2024**, *16*, e2023MS004019. [CrossRef]
414. Nguyen, T.; Brandstetter, J.; Kapoor, A.; Gupta, J.K.; Grover, A. ClimaX: A foundation model for weather and climate. *arXiv* **2023**, arXiv:2301.10343.
415. Pathak, J.; Subramanian, S.; Harrington, P.; Raja, S.; Chattopadhyay, A.; Mardani, M.; Kurth, T.; Hall, D.; Li, Z.; Azizzadenesheli, K.; et al. FourCastNet: A Global Data-driven High-resolution Weather Model using Adaptive Fourier Neural Operators. *arXiv* **2022**, arXiv:2202.11214.
416. Lam, R.; Sanchez-Gonzalez, A.; Willson, M.; Wirnsberger, P.; Fortunato, M.; Alet, F.; Ravuri, S.; Ewalds, T.; Eaton-Rosen, Z.; Hu, W.; et al. Learning skillful medium-range global weather forecasting. *Science* **2023**, *382*, 1416–1421. [CrossRef] [PubMed]
417. Zhang, Y.; Long, M.; Chen, K.; Xing, L.; Jin, R.; Jordan, M.I.; Wang, J. Skilful nowcasting of extreme precipitation with NowcastNet. *Nature* **2023**, *619*, 526–532. [CrossRef] [PubMed]
418. Bi, K.; Xie, L.; Zhang, H.; Chen, X.; Gu, X.; Tian, Q. Author Correction: Accurate medium-range global weather forecasting with 3D neural networks. *Nature* **2023**, *621*, E45. [CrossRef] [PubMed]
419. Chen, K.; Han, T.; Gong, J.; Bai, L.; Ling, F.; Luo, J.J.; Chen, X.; Ma, L.; Zhang, T.; Su, R.; et al. FengWu: Pushing the Skillful Global Medium-range Weather Forecast beyond 10 Days Lead. *arXiv* **2023**, arXiv:2304.02948.
420. Chen, L.; Zhong, X.; Zhang, F.; Cheng, Y.; Xu, Y.; Qi, Y.; Li, H. FuXi: A cascade machine learning forecasting system for 15-day global weather forecast. *npj Clim. Atmos. Sci.* **2023**, *6*, 111–190. [CrossRef]
421. Muralitharan, R.; Jayasinghe, U.; Ragel, R.G.; Lee, G.M. Machine learning and deep learning-based atmospheric duct interference detection and mitigation in TD-LTE networks †. *Future Internet* **2025**, *17*, 237. [CrossRef]
422. Perera, P.L.; Xia, K.; Wang, T.; Xiaoyu, C.; Li, W.; Zhiwei, Z.; Shrui, F.; Yassine, J.; Yveline, M.A.M. Optimized deep learning for reliable atmospheric duct interference prediction in radar and communication system. *Int. J. Commun. Syst.* **2025**, *38*, e70290. [CrossRef]
423. Zhou, T.; Sun, T.; Hu, H.; Xu, H.; Yang, Y.; Harjula, I.; Koucheryavy, Y. Analysis and prediction of 100 km-scale atmospheric duct interference in TD-LTE networks. *J. Commun. Inf. Netw.* **2017**, *2*, 66–80. [CrossRef]

Disclaimer/Publisher's Note: The statements, opinions and data contained in all publications are solely those of the individual author(s) and contributor(s) and not of MDPI and/or the editor(s). MDPI and/or the editor(s) disclaim responsibility for any injury to people or property resulting from any ideas, methods, instructions or products referred to in the content.